IMMOBILIZATION OF ENZYMES ON INORGANIC NANOPARTICLES

A Dissertation

Presented to the Faculty of the Graduate School

of Cornell University

In Partial Fulfillment of the Requirements for the Degree of

Doctor of Philosophy

by

Nikolaos Chalkias

January 2007

IMMOBILIZATION OF ENZYMES ON INORGANIC NANOPARTICLES

Nikolaos Chalkias, Ph. D.

Cornell University 2007

Immobilization of avidinylated enzymes (Glucose Oxidase or GOx and Horseradish Peroxidase or HRP) on inorganic particles was accomplished utilizing the affinity of avidin for biotin. We have synthesized biotinylated oxides (layered silicates and iron oxides) via a condensation reaction, and through a simple one step process, we have immobilized enzymes improving their thermal behavior, storage stability and behavior in different pH environments.

Furthermore, a profound catalytic activity increase per mass (30-fold) was observed for HRP when immobilized on magnetic iron oxide particles (magnetite particles). This phenomenon proved to be independent of the immobilization steps and was observed even when particles and HRP were simply suspended together in a buffer solution. The activity increase was reversible and could be turned on and off with the addition and subtraction of the magnetic particles (with a Nd magnet). The results were reproduced using different activity assays and different batches of enzyme. Activity assays using particles with increasing magnetic properties showed a proportional increase on the enzymatic activity. The results suggest that the randomly distributed magnetic particles affect the paramagnetic species found in the catalytic cycle of HRP, changing the overall reaction rate.

On a different approach modified silicates with immobilized gramicidin were evaluated as delivery vehicles for gramicidin to *E. coli* bacteria. Also a fluorescent

protein immobilized on a biotinylated layered silicate was used to track the uptake of modified silicates to mammalian 9L Glioma cells.

Finally, layered silicates and amphiphilic molecules were combined to develop a synthetic biomimetic membrane. The biomimetic membrane has the characteristics of a lipid bilayer membrane with similar thermotropic transitions. To evaluate the membrane's sensing capability, a sensing platform was developed that utilized the biomimetic membrane as the recognition element. The sensing capability was evaluated using saccharin as the analyte, a suspected carcinogen molecule already proven to interact with lipid bilayer membranes in a sensor setup.

BIOGRAPHICAL SKETCH

Nikolaos Chalkias (pronounced Nikolas Halkias) was born to parents Giorgo and Niki Chalkia in Thessaloniki, Greece on July 30th, 1978. He is the third child of the family and has two older sisters, Matina and Tzela. The family is originally from the coastal region of Sithonia in Chalkidiki, Greece where both Nikolas' parents were born and raised. Nikolas grew up in Thessaloniki in the northern region of Greece but he always considered home the family house near the sea at Chalkidiki where he spent all his summers. The curiosity that drove him all the way to the other side of the Atlantic was born there, where Nikolas through his parents would get exposed to the sea and to the olive trees. Through the little projects around the house that his father would take him along, Nikolas' curiosity for 'how things work' was slowly born. In high school Nikolas loved only mathematics, physics and chemistry, he had a scornful attitude towards literature and all the 'unimportant classes'; an attitude that later in his life would give way to his love for poetry and history. Nikolas graduated from the 1996 senior class of the 2nd High School of Thessaloniki with honors. Immediately after graduation, he successfully passed the entrance examination for the Chemical Engineering Department of the Aristotle University of Thessaloniki. During the five years of the curriculum, Nikolas was exposed to science and engineering and spent the summer of 1999 in Brussels as an intern. In Brussels he worked on a scanning tunneling microscope (STM) investigating carbon Nanotubes, an experience that strengthened his interest in research. For his undergraduate thesis, Nikolas worked with Prof. Michael Stoukides; using a solid state proton (H^+)-conducting cell-reactor he experimented on the dehydrogenation of methane and the deposition of carbon under an AC voltage. During the summer of 2000, Nikolas started searching for his next education adventure. Driven by his wander and curiosity, he left home and engaged in a new search for knowledge. In August of 2001, Nikolas got accepted into

the Ph.D. program of the department of Chemical and Biomolecular Engineering of Cornell University in Ithaca NY. Ithaca became his home for the next 5 years where he worked with the Giannelis research group under the supervision of Prof. E. P. Giannelis. In Ithaca he met interesting people and learned the strength of the 'scientific method'. During his stay in Ithaca, Nikolas serendipitously found out that one of the inspiring figures of his youth, Dr. Carl Sagan, spent most of his life in Cornell as a Professor. The experience of studying and living in Cornell was extraordinary. In a way Nikolas' arrival to 'Ithaca' marked the beginning of the journey not the ultimate objective, as Kavafis' famous poem proclaims.

To my beloved Father, Mother and Sisters

ACKNOWLEDGMENTS

This dissertation was a five-year process and involved the input of numerous people. First, I would like to thank the members of my advising committee, Professor E. P. Giannelis, Professor P. Clancy, and Professor A. J. Baeumner, for their support in the completion of this dissertation. I would also like to thank the Cornell University Nanobiotechnology Center (NBTC) for providing the funding and the resources for my research endeavors. In addition I would like to thank the Cornell Nanoscale Science and Technology Facility (CNF) and the Cornell Center for Materials Research (CCMR) for the use of their resources and facilities. My thanks also extend to various people whose enthusiasm, advice, and scrutiny, helped me in many important ways. These include Dr. Magnus Bergkvist from the NBTC, Dr. Daniel Schimdt, Dr. Deepak Shah, and generally the past and present members of the Giannelis group that helped me during these past years.

However, the most important support I have received, during the 5 years of scientific and personal search, was the emotional support. First and foremost I want to thank my friend and brother, Giorgo Vakalopoulo. We have started together the Ph. D. journey in Ithaca and Paris and his support all these years maintained my sanity. Through the endless hours on the phone, we shared moments, fears and words that only we can speak of, understand of, and endure.

Equally I want to acknowledge the inspiration and support I received from my family, my father, my mother, and my two sisters, who gave me the hope and motivation to succeed and persist in finishing my degree. This work is dedicated to them.

I also want to thank all the friends, only some of which, I name below, and express my gratitude for their love, friendship, and support. Some of them who are in Thessaloniki like Dimitri, Thodoro, Sotiri, Damiano, Giorgo, Mario, Yianni, Katerina

for their love and support all these years. All my friends in Ithaca Christina, Pano, Petro, Stathi, and my classmates Alejandro, Yong-Min, Cormac, Rafael for all the times we shared and helped me keep going everyday in Ithaca. All my friends in Boston, Mari, Niki and Aristeidi who supported me during my escapes from Ithaca and for all the amazing moments we shared in ‘our’ Boston.

Finally, I want to thank my companion Dr. Maria Nikolou who was the most important person during the last year of my degree. She has given me the love, support and courage to push forward; without her, the next pages would not be possible.

TABLE OF CONTENTS

LIST OF FIGURES

LIST OF TABLES

LIST OF EQUATIONS

INTRODUCTION

Enzymes in their native form have been used for centuries in the food industry and their use is vital to different technologies of the human species. Two historically key processes such as bread-making and wine-making are based in enzymatic reactions that occur inside eukaryotic organisms (yeast).[1-4] More recently enzymes have found applications in the chemical and pharmaceutical industries as well as many other innovating areas of technology such as sensing applications, biotechnology and organic synthesis.[5-9]

In 1998, Uhlig[10] compiled a summary of the major uses of enzymes in an industrial scale. Specifically, Uhlig discussed the use of enzymes in food industry processes such as flour processing, baking, alcohol production, brewing, dairy production and meat processing. Another area where enzymatic processes have an important role is molecular biology and biotechnology. In general, the technology advancements in the biosciences rely heavily in the specificity and availability of enzymes. For example Polymerase Chain Reaction (PCR), a commonly used lab technique for the amplification of DNA nucleotides, is based on specialty enzymes (i.e DNA polymerases).[11] Lysing enzymes (lyases) is another category of enzymes that find numerous applications in molecular biology along with transferases.[12]

In the early 20th century attention was focused to 'insoluble enzymatic molecules' and the first attempt to immobilize enzymes was via a physical adsorption mechanism.[13,14] There was little progress for the next decades and only in mid-1960s, interest was once again turned to the technology of immobilizing enzymes rendering them insoluble recyclable reagents. In 1963 Bernfeld et al. were successful in entrapping various enzymes and antigens in a polymeric matrix[15] while Silman and Katchalski set the foundations of what we know today as 'enzyme immobilization' in a review article describing the four main techniques of immobilization.[16]

During the next decade the first industrial applications using immobilized enzymes were reported.[7] In 1970 Carrington et al. developed columns of immobilized *Asperigillus oryzae* aminocylase for the resolution of synthetic, racemic D,L-amino acids into the corresponding, optically active, enantiomers.[7,17] Since then the interest and the applications of immobilized enzymes grew rapidly and nowadays enzymatic processes are an important tool from food industry to molecular biology and renewable energy sources.[18] Specifically for the latter, industrial biotechnology and enzymes in particular have evolved in a hopeful promise for today's growing energy problems.[18-20]

However, all the above applications relative to enzymes have been already realized without ever dealing with immobilization. What are the advantages of enzyme immobilization? The advantages of using immobilized enzymes instead of their soluble counterparts are[8] enhanced stability, repeated or continuous use, easy separation from the reaction mixture, possible modulation of the catalytic properties, contamination prevention in the product and easier prevention of microbial contaminations. It is thus apparent, that enzyme immobilization can have immediate effects on the cost of a process or the quality of a product. Furthermore, it is the potential tuning of enzyme properties through immobilization that has promise. For example, choosing an immobilization method that can improve the thermal behavior of an enzyme could potentially extend the operating capabilities of a process and allow a reactor to operate into higher temperatures, hence increasing the reaction rates and product yields.

The potential applications and technological improvements are endless and even though enzymes, as catalysts, have the capability to operate in multiple cycles, in practice they are widely treated as one-time-use reagent. The reason for the one-time use lies in the multiple complications that immobilization steps introduce. One of the

most common disadvantages often encountered is the partial loss of enzymatic activity, either during the process of immobilization or due to denaturation at the final immobilized enzyme conformation. Harsh chemical conditions during the immobilization process usually affect irreversibly the native tertiary structure of enzymes leading to loss of activity and deactivation.[5]

Nevertheless, in the last few decades the field of enzyme immobilization has made significant advances.[9,21-23] In the last few years, methods of immobilization were devised where the immobilized enzyme suffered minimal loss of enzymatic activity when compared to its native soluble form,[5,24-26] but commercialization of immobilized enzymes is yet to be realized in a large scale and only a few examples exist (i.e. Amberzyme® by Rohm and Haas).

In the literature, enzyme immobilization processes fall into four main categories, each of them with unique advantages and disadvantages; these are[8,16] non-covalent adsorption or deposition, covalent attachment or carrier binding, entrapment in a gel, matrix or membrane and cross-linking.

In this work, a versatile immobilization scheme is presented that takes advantage of the affinity between biotin and avidin. The immobilization is realized by combining biotinylated oxides (iron oxides, layered silicates) and avidinylated enzymes that are commercially available. This approach could potentially serve as a generic method for the immobilization of a variety of avidinylated enzymes on biotinylated oxides as the universal insoluble host.

This approach is simple and leads to immobilized enzymes with improved behavior (i.e. thermal and storage stability) and minimal activity loss. Furthermore, immobilization on magnetic iron oxides can offer a quick separation method in a magnetic field, hence avoiding expensive separation processes like filtration and centrifugation.

In addition, results are presented indicating that the immobilization of, at least one, heme-containing enzyme (Horseradish Peroxidase) on magnetic particles resulted to an increase of its catalytic activity and turnover rate. The investigation was extended to probe the origin of the observed effect and initial results showed a correlation between the magnetic properties of the iron oxide and the rate of catalysis for Horseradish Peroxidase.

Finally, enzyme immobilization on oxides is extended to a drug delivery application. A biotinylated silicate with an attached fluorescent protein (avidin) is evaluated as a drug delivery vehicle. In the final chapter, results for the immobilization and delivery of an antibiotic protein to *E. coli* bacteria are presented. The approach is based on integrating gramicidin into the inter-layer galleries of a silicate and delivering the particles to *E. coli*.

REFERENCES

1. Martinez Anaya, M. A. Enzymes and Bread Flavor. *Journal of Agricultural and Food Chemistry* **44**, 2469-2480 (1996).

2. Colagrande, O., Silva, A. & Fumi, M. D. Recent Applications of Biotechnology in Wine Production. *Biotechnology Progress* **10**, 2-18 (1994).

3. Amerine, M. A. & Kunkee, R. E. Microbiology of Winemaking. *Annual Review of Microbiology* **22**, 323-& (1968).

4. Pretorius, I. S. Tailoring Wine Yeast for the New Millennium: Novel Approaches to the Ancient Art of Winemaking. *Yeast* **16**, 675-729 (2000).

5. Brena, B. M. & Batista-Viera, F. Immobilization of Enzymes: A Literature Survey. *Methods in Biotechnology* **22**, 15 (2006).

6. Kirk, O., Borchert, T. V. & Fuglsang, C. C. Industrial Enzyme Applications. *Current Opinion in Biotechnology* **13**, 345-351 (2002).

7. Katchalski-Katzir, E. Immobilized Enzymes - Learning from Past Successes and Failures. *Trends in Biotechnology* **11**, 471 (1993).

8. Bornscheuer, U. T. Immobilizing Enzymes: How to Create More Suitable Biocatalysts. *Angewandte Chemie-International Edition in English* **42**, 3336-3337 (2003).

9. Cao, L. Q. Immobilised Enzymes: Science or Art? *Current Opinion in Chemical Biology* **9**, 217-226 (2005).

10. Uhlig, H. *Industrial Enzymes and Their Applications* (J. Wiley, New York, 1998).

11. McPherson, M. J. & Møller, S. G. *PCR* (Taylor & Francis, New York; Abingdon [England], 2006).

12. Bryant, J. A. *Molecular Biology* (Academic Press, San Diego, 1997).

13. Nelson, J. M. & Griffin, E. G. Adsorption of Invertase. *Journal of the American Chemical Society* **38**, 1109-1115 (1916).

14. Nelson, J. M. & Hitchcock, D. I. The Activity of Adsorbed Invertase. *Journal of the American Chemical Society* **43**, 1956-1961 (1921).

15. Bernfeld, P. & Wan, J. Antigens and Enzymes Made Insoluble by Entrapping Them into Lattices of Synthetic Polymers. *Science* **142**, 678-& (1963).

16. Silman, I. H. & Katchalski, E. Water-Insoluble Derivatives of Enzymes Antigens and Antibodies. *Annual Review of Biochemistry* **35**, 873-& (1966).

17. Carrington, T. R. Development of Commercial Processes for Production of 6-Aminopenicillanic Acid (6-APA). *Proceedings of the Royal Society of London Series B-Biological Sciences* **179**, 321-& (1971).

18. Herrera, S. Industrial Biotechnology - a Chance at Redemption. *Nature Biotechnology* **22**, 671-675 (2004).

19. Kourkoutas, Y., Bekatorou, A., Banat, I. M., Marchant, R. & Koutinas, A. A. Immobilization Technologies and Support Materials Suitable in Alcohol Beverages Production: A Review. *Food Microbiology* **21**, 377-397 (2004).

20. Nagashima, M., Azuma, M. & Noguchi, S. Technology Developments in Biomass Alcohol Production in Japan - Continuous Alcohol Production with Immobilized Microbial-Cells. *Annals of the New York Academy of Sciences* **413**, 457-468 (1983).

21. Cao, L. *Carrier-Bound Immobilized Enzymes: Principles, Applications and Design* (Wiley-VCH, Weinheim, 2005).

22. Hou, C. T. *Handbook of Industrial Biocatalysis* (Taylor & Francis/CRC, Boca Raton, FL, 2005).

23. Taylor, R. F. *Protein Immobilization: Fundamentals and Applications* (M. Dekker, New York, 1991).

24. Luckarift, H. R., Spain, J. C., Naik, R. R. & Stone, M. O. Enzyme Immobilization in a Biomimetic Silica Support. *Nature Biotechnology* **22**, 211-213 (2004).

25. Lei, C. H., Shin, Y. S., Liu, J. & Ackerman, E. J. Entrapping Enzyme in a Functionalized Nanoporous Support. *Journal of the American Chemical Society* **124**, 11242-11243 (2002).

26. Dyal, A., Loos, K., Noto, M., Chang, S. W., Spagnoli, C., Shafi, K. V. P. M., Ulman, A., Cowman, M. & Gross, R. A. Activity of Candida Rugosa Lipase Immobilized on Gamma-Fe_2O_3 Magnetic Nanoparticles. *Journal of the American Chemical Society* **125**, 1684-1685 (2003).

CHAPTER 1: ACTIVITY INCREASE OF HORSERADISH PEROXIDASE IN THE PRESENCE OF MAGNETIC PARTICLES

INTRODUCTION

Magnetic fields have long been suspected to have an effect in biological systems. For instance, the magnetic sense of higher animals, particularly of birds, is well documented but still awaits a conclusive mechanistic explanation.[1-3] During the past twenty years, the relationship between magnetic fields and enzymatic reactions has been also recognized and explanations have been provided in the context of the radical recombination theory.[4] The existing experimental evidence is based mainly on the effects of uniform external magnetic fields with intensities ranging from a few hundred to a few thousand Gauss. However, strong magnetic fields are rare in the biological world (the geomagnetic field is around 0.5 Gauss) and evidence of such magnetic field effects are yet to be confirmed.[5] Here, for the first time, evidence for the effect of very low magnetic fields on a biological reaction is presented. The presence of magnetite particles (with permanent magnetic moment of 1 emu/g) in the assay led to a 30-fold increase on the rate of reaction of Horseradish Peroxidase. The activity of this enzyme was evaluated with two chromogen systems and the apparent Michaelis-Menten kinetic parameters were extracted.

Magnetic field effects (MFE) on enzymatic reactions were investigated as early as the 1960s and most of the experiments carried out initially showed no effects on the reaction rates.[6-10] In the mid 1980s, focus was turned to radical pairs and the effect of magnetic fields on radical reactions.[4,11] Later, and in the context of the newly suggested radical pair recombination theory, magnetic field effects on biological reactions involving radicals and paramagnetic species were studied.[4-6,12,13] In particular, a number of publications examined the effect of an external magnetic field

and that of spin-orbit coupling (SOC) on the kinetics of enzymatic reactions.[9,10,14-19] Currently, magnetic field dependence of enzymatic reactions has evolved into an area of research that has generated promising results in catalysis, a field of great scientific, commercial and economic importance. Molin et al. have reported that the rate of O_2 evolution in H_2O_2 decomposition catalyzed by the heme enzyme Catalase is increased by 20 % in a magnetic field of 8000 G.[20] In 1994, Harkins and Grissom showed that an external magnetic field affected the kinetics of ethanolamine catalysis by B_{12} Ethanolamine Ammonia Lyase, a reaction that involves a radical pair recombination step.[21-23] The same group also reported the dependence of electron transfer in the case of Horseradish Peroxidase (HRP) on an external magnetic field.[15] These authors reported a 15 % decrease in the relative rate of conversion of Compound I to Compound II states of HRP and 35 % decrease in the conversion of Compound II back to native ferric HRP at 750 G (see Figure 1.1).

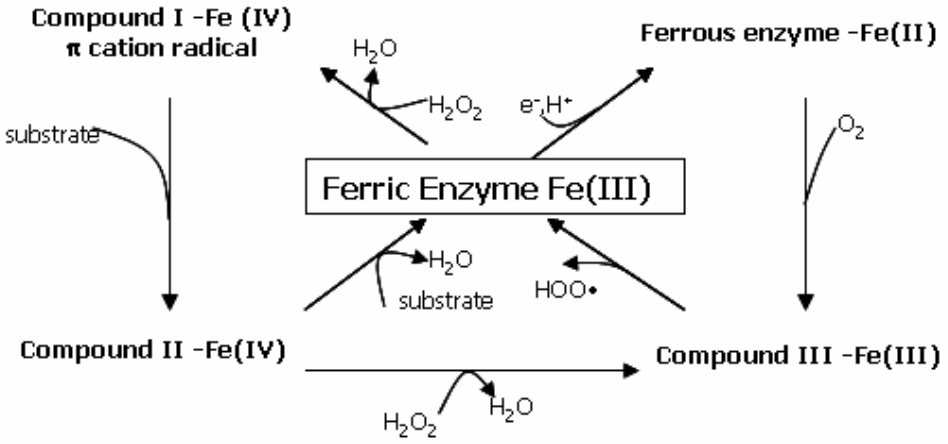

Figure 1.1: The five oxidation states of Horseradish Peroxidase. Berglund et al.[24]

In 2006, Jones et al. revisited the experiment to investigate the effect of low intensity magnetic fields on HRP kinetics, but were unable to reproduce the findings.[25] These authors pointed out the lack of evidence for a radical pair recombination step on

the second reductive half-reaction of HRP and discussed problems in the initial fitting analysis of Taraban et al.[15]

Enzyme catalysis is an active field and the complexity of the underlying physics is not yet fully understood in many cases.[26-29] The discussion for magnetic field effects on biological systems is somewhat controversial and the debate is still active. Nevertheless, there are a few enzyme systems known to have magnetic field dependence. From the literature a magnetosensitive step in the catalytic cycle of HRP appears to exist even though is not fully isolated and understood.[30-32] The experiments presented here are the first ones to report changes on the reaction rate of a heme-containing enzyme (HRP) in the presence of iron oxide (Fe_3O_4) magnetic particles.

MATERIALS AND METHODS

Materials.

Two different batches of Peroxidase from Horseradish, Catalase from Bovine liver, Chloroperoxidase (CPO) from *Caldariomyces fumago*, Glucose oxidase (GOx) from *Aspergillus Niger* and Cytochrome C from Equine Heart, were obtained from Sigma Aldrich and Fisher Scientific as lyophilized powders. Phenol and 4-aminoantipyrine (AAP) were obtained from Sigma as solids (98% purity). 2,2´-Azino-di-(3-ethyl-benzthiazoline-6-sulphonic acid) (ABTS) was obtained in pellets from Sigma. Sodium phosphate buffer (PBS) pH 7.4 and 67mM was purchased from Invitrogen, deionized water (DI) with a minimum resistivity of 18MΩcm was used throughout the experiments. Amine-terminated iron oxide super-paramagnetic particles (SPM), hydrogen peroxide, $FeCl_2$, and $FeCl_3$ were also obtained from Sigma Aldrich and all other reagents used were ACS grade.

Synthesis of magnetic iron oxide particles.

Magnetite Fe_3O_4 particles were synthesized by co-precipitation of Fe^{2+} and Fe^{3+} in a basic solution under nitrogen. A 25 mL solution containing 5.2 g of $FeCl_3 \cdot 6H_2O$, 2 g of $FeCl_2 \cdot 4H_2O$ and 1 mL of 12 N HCl was added dropwise to 250 mL of 1.5 M NaOH under bubbling nitrogen. All solutions were bubbled with nitrogen for 15 minutes prior to reaction in order to eliminate any oxygen present. Once the Fe^{2+} and Fe^{3+} ions were in the sodium hydroxide solution a black precipitate formed. The precipitate was separated with a neodymium magnet from the reaction solution and consecutively resuspended and precipitated in water multiple times until the pH of the suspension reached 8. Thereafter, 100 mL of 0.01 M HCl were added to the precipitate to neutralize the anionic charges on the particles. Finally, the particles were separated two more times with a neodymium magnet to separate the larger magnetic particles from any smaller paramagnetic particles formed.

Characterization of iron oxide particles.

The magnetic properties of the iron oxide particles were evaluated in an MPMS XL® (Quantum Design) magnetometer utilizing Superconducting Quantum Interference Device (SQUID) technology. Magnetization hysteresis curves were obtained at 300 K and the applied magnetic field was varied between 40 Oe and 50 kOe. From the hysteresis curves we evaluated the saturation magnetization of the samples (M_s), the coercive field (H_c) and the remanence (M_R).

To evaluate the size distribution of the iron oxide particles in the samples we have utilized a Dynamic Light Scattering (DLS) apparatus from Malvern Instruments (Zetasizer Nano Series). The medium used during the measurement was DI water with a very dilute concentration of particles in the measurement cuvette. Monochromatic light was emitted on the test volume and the light scattered at an angle of 173 degrees

was measured by a detector. The correlation of the intensity at successive time intervals was measured and the signal was then converted to a size distribution for the sample through the Stokes-Einstein equation.

Powder X-Ray Diffraction (PXRD) spectra were collected on a Scintag Inc θ-θ diffractometer using CuK_α radiation and equipped with a germanium detector.

UV/vis analysis.

The concentration of HRP stock solutions were determined from the absorbance at 403 nm with a Spectrophotometer (SpectraMax Plus^{384}, Molecular Devices, Sunnyvale, CA) based on an extinction coefficient of 102 $mM^{-1}cm^{-1}$.[33]

The enzymatic activity of Horseradish Peroxidase was evaluated using a phenol/4-aminoantipyrine (AAP) chromogen assay.[34] The assay solution contained 80 mM phenol, 13 mM AAP and 5 mM hydrogen peroxide in 67 mM phosphate buffer (pH 7.4). Using an extinction coefficient of 7100 $M^{-1}cm^{-1}$ for the red product of the reaction (quinoneimine), the rate of absorbance increase was monitored at 510 nm.[35] The above protocol was also used to generate plots of activity with varying amounts of substrate (Michaelis-Menten plots). Data were obtained using 96-well plates. The 96-wells of each plate were prepared with the same concentrations of phenol, AAP and phosphate buffer as described above. The molarities of hydrogen peroxide were varied between 0.01 mM and 0.5 M. The enzyme solution was added last, using a multipipettor to minimize the time for adding the enzyme and assure minimal error between the multiple measured activities in the wells. The plate was mixed between every reading to assure uniformity of the solutions. Software was used to calculate the 1 cm optical path length equivalent absorbance independently of the amount of liquid in the well via a patented PathCheck® sensor technology. The rate of absorbance increase at 510 nm was obtained for the initial linear range of the response and the

activity of the enzyme was calculated using the extinction coefficient of the chromogen.

2,2´-Azino-di-(3-ethyl-benzthiazoline-6-sulphonic acid) (ABTS) was also used in the assay as another chromogen substrate. In this assay 15 mM of ABTS and 67 mM of phosphate buffer (pH 7.4) were used. The amount of hydrogen peroxide was varied again to obtain activity plots as a function of peroxide concentration. The activity was calculated by measuring the rate of absorbance change at 414 nm during the first few seconds of the reaction. The extinction coefficient at 414 nm for the oxidized ABTS is 36000 $M^{-1}cm^{-1}$.[36]

Fitting of Michaelis-Menten equation to experimental data.

Fitting of a modified Michaelis-Menten Equation to the data was performed with Origin® 7.5 software using a non-linear least squares fit (NLSF) routine weighting the data according to the standard deviation of the multiple repetitions of each experimental point. To obtain an initial set of parameters for the NLSF routine we evaluated the V_{max} in all cases through a Lineweaver-Burk graph using only the values of relatively small substrate concentrations where inhibition is negligible. Since the inhibition term depends on the square of the substrate concentration (see Equation 1.3) this term can be ignored for small concentrations to obtain a rather accurate estimate of V_{max} from a Lineweaver-Burk representation of the data.

RESULTS AND DISCUSSION

During the catalytic cycle, native HRP, Compounds I, II and the oxidized substrate radicals generated in the process are all paramagnetic. A combination of any two can constitute a paramagnetic (radical) pair that can undergo spin selective processes.[15,33] The presence of randomly distributed magnetic particles in the assay is likely to have an effect on the spin states of geminate pairs (G-pairs) and on random

encounter diffusing radicals (F-pairs) via an accelerated intersystem crossing (ISC) mechanism that can alter the overall kinetics of the enzyme reaction.[13,23] Most of the existing literature has utilized external magnetic fields in the order of 500 G and higher; however, it was recently shown that even weak magnetic fields less than 20 G can affect radical pairs and their recombination rates.[1,4,37]

In this work, iron oxide (magnetite) particles with different magnetic properties were used. B3 and B4 represent different samples of iron oxide with different magnetic properties. B3 particles were synthesized at room temperature (25 ºC) and under nitrogen; B4 was synthesized similarly to B3 except that the temperature during synthesis was elevated to 90 ºC. The higher temperature resulted in a higher crystallinity, which in turn resulted in higher magnetic moment magnetite particles.

Properties of the iron oxide particles used

Various techniques such as Superconducting Quantum Interference Device (SQUID, Figure 1.2), Dynamic Light Scattering (DLS, Figure 1.3) and Powder X-Ray Diffraction (PXRD, Figure 1.4) were used to characterize the particles used in this work. Table 1.1 summarizes the characteristic properties for the iron oxide particles.

Saturation magnetization (M_S) as well as remanence (M_R) decreased with decreased average crystallite size of particles and the values shown in Table 1.1 are in agreement with similar published results.[38]

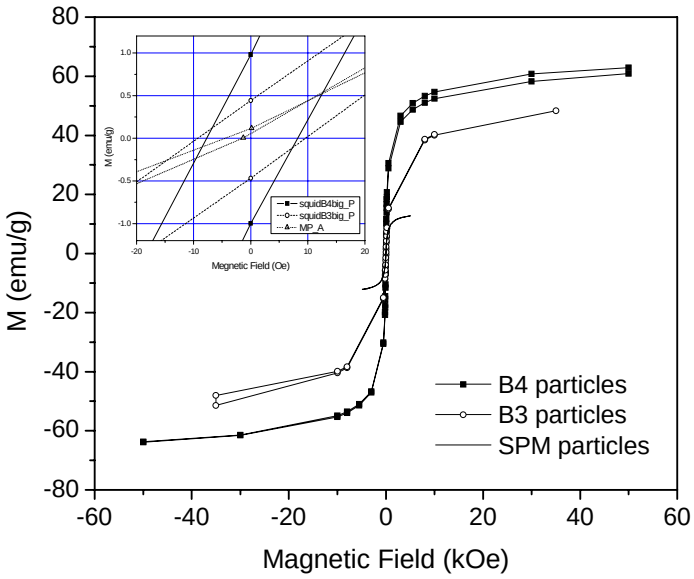

Figure 1.2: Hysteresis curves of the iron oxide particles used (B3, B4 and SPM). The inset graph is an enlargement showing differences in magnetic remanence (M_R) of three batches of particles.

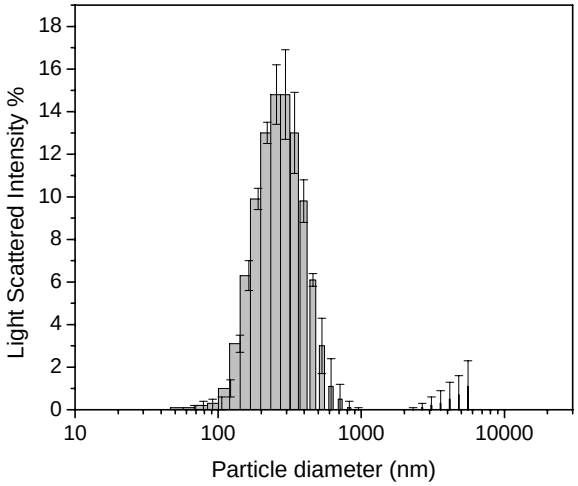

Figure 1.3: Dynamic light scattering measurements. Diameter distribution of the B4 particles population.

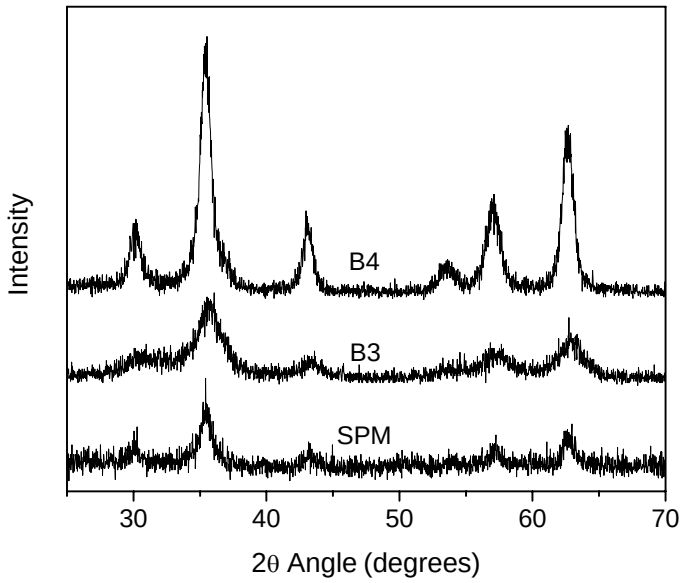

Figure 1.4: PXRD spectra for the synthesized iron oxide particles (B3, B4) and the commercial super-paramagnetic particles (SPM) used. By using the Debye-Scherer equation, an approximate crystallite diameter for each of the different batches of particles was evaluated.

Table 1.1 Summary of characteristics of the particles used.

Iron Oxide	M_R (emu/g)	M_S (emu/g)	H_C (Oe)	Average crystallite diameter PXRD (nm)	Particles diameter DLS (nm)	Color
B4	1 ± 0.2	65 ± 0.2	8.6 ± 2	23.6	314 ± 15	Black
B3	0.48 ± 0.1	49 ± 1.1	9.5 ± 0.1	14.8	449 ± 69	Black
SPM	~0			23.8		Light Brown

The magnetic field of a magnetite particle with 200 nm diameter and 1 emu/g permanent magnetic moment was calculated to be 0.67 G at 400 nm from the center of the particle using Equation 1.1. Since here only the magnitude of the field is of interest, the vector Equation 1.1 can be approximated with a scalar equation that returns the magnitude of the field in a distance x (see also Equation 1.2).

Equation 1.1: Equation calculating the magnetic field of a localized current distribution (in this case of the magnetic moment of a particle when treated as a point; for that x must be much larger than the radius of the particle for the equation to hold). B is the magnetic field at distance x from the center of the particle, n is the normal vector in the x direction, m is the magnetic moment of the particle and μ_0 is the magnetic permeability of vacuum.[39]

$$\vec{B}(\vec{x}) = \frac{\mu_0}{4\pi}\left[\frac{3\vec{n}(\vec{n}\cdot\vec{m}) - \vec{m}}{|\vec{x}|^3}\right]$$

Equation 1.2: Scalar form of Equation 1.1. The equation returns the magnitude of the magnetic field at a distance x from the center of a particle with magnetic moment m.

$$B(x) = \frac{\mu_0}{4\pi}\left[\frac{2m}{|x|^3}\right]$$

The average diameter of particles obtained by Dynamic Light Scattering was more than 10 times larger than the average crystallite size obtained from PXRD suggesting that the crystallinity of the samples is either poor or the DLS measures aggregates rather than individual particles.

Iron oxide particles and Horseradish Peroxidase

The catalytic activity of Horseradish Peroxidase increased when magnetite particles were present in the assay at low concentrations. These results were reproduced using different batches of enzyme and different vendors (Fisher, Pierce Biotechnology). In Figure 1.5 the activity of HRP, evaluated with the Phenol-Aminoantipyrine (AAP) chromogen system,[34] is plotted with various concentrations of particles in the assay. The activity of 0.4 nM HRP increased in the presence of B3 particles and reached a plateau at 1 μg/mL. The increase was about 5 times that of the native enzyme alone. The activity decreased back to the levels of the native enzyme when the concentration became 9 μg/mL. A similar behavior was observed for B4 particles but the maximum increase in activity was 30-fold. In contrast, the enzyme behavior was not altered when commercial super-paramagnetic particles with no permanent magnetic moment were present in the assay.

We examined various other redox enzymes with and without a heme group (Cytochrome C, Chloroperoxidase, Catalase, and Glucose oxidase) under the same limiting conditions but we were unable to observe any positive or negative effect on the activity when magnetic particles were present in the assay.

In Figure 1.6, two plates are shown with 12 wells and four repetitions in each. All wells in Figure 1.6 contain the same concentration of enzyme (0.4 nM) and the same concentration of hydrogen peroxide (5 mM) in each well. The 12 different rows of wells (1-12) have different concentrations of iron oxide.

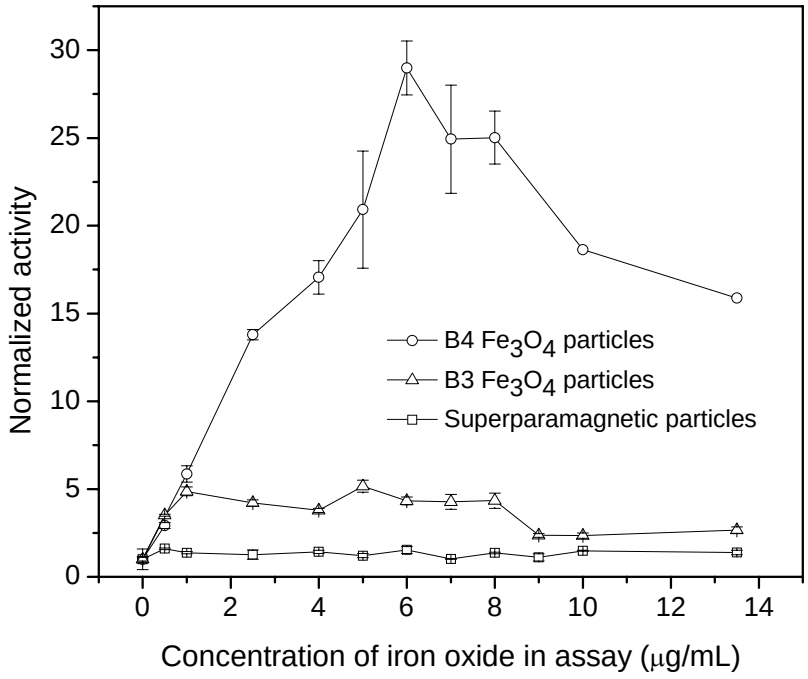

Figure 1.5: Activity of HRP when magnetic and super-paramagnetic iron oxide particles are present in the assay. The activity was measured with 5 mM of H_2O_2, 80 mM of phenol, 13 mM of 4-Aminoantipyrine and 0.4 nM of HRP in the assay. The error bars are the standard deviation of 4 repetitions.

The left plate contains super-paramagnetic particles in various concentrations. Row #1 is a blank row and there are no particles. The right plate contains B4 magnetite particles in various concentrations; in this case Row #2 is a blank row and there are no particles present. For both plates all other rows contain iron oxide particles with concentrations varying from 0.5 to 14 μg/mL. The intensity of the color is directly proportional to the activity of the enzyme.

The effect of B4 magnetite particles is evident (right plate). In contrast, the super-paramagnetic particles had no effect on the activity of the enzyme (left plate). The data extracted from these two plates were plotted in Figure 1.5.

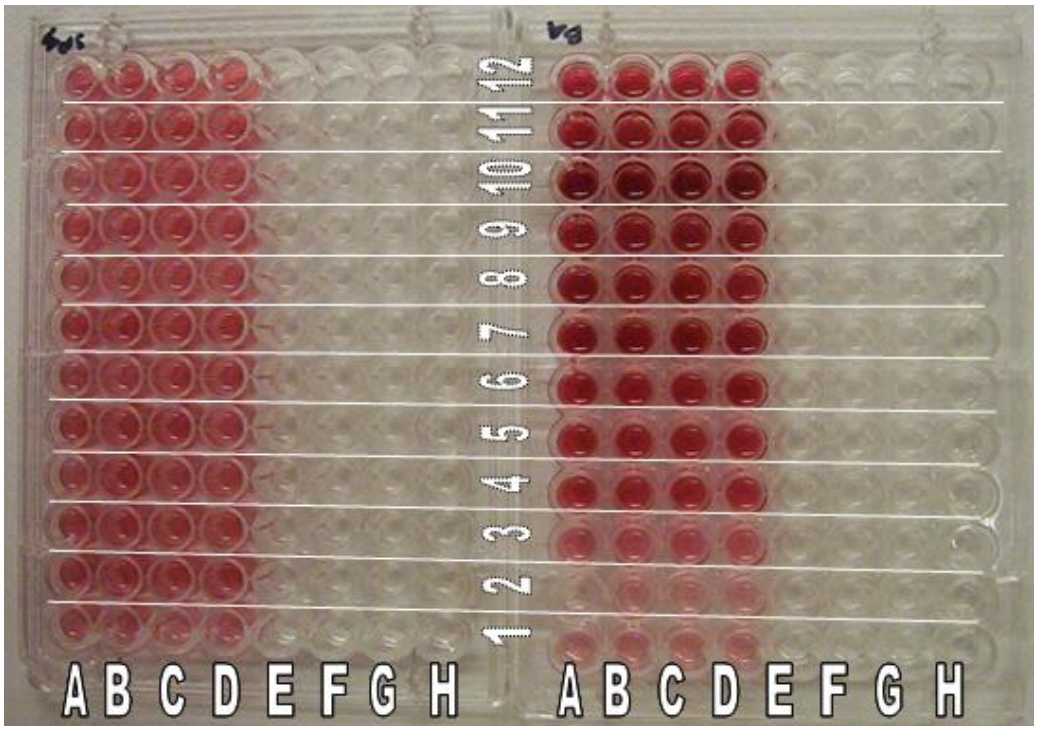

Figure 1.6: The two plates shown are assay runs with super-paramagnetic particles (left) and B4 iron oxide particles (right). The above picture is taken at the end of the data acquisition.

Iron oxide particles had no reducing or oxidizing effect on the substrates and no activity was found when the protocol was tested solely in the presence of iron oxide particles. In addition, the possibility of a redox process between the enzyme's active site and the particles was examined and the Soret band of the enzyme was probed in the presence of iron oxide particles and the enzyme alone. The characteristic peak of the heme group at 403 nm was not shifted nor was the intensity of the peak changed, when iron oxide particles were present (see Figure 1.7).

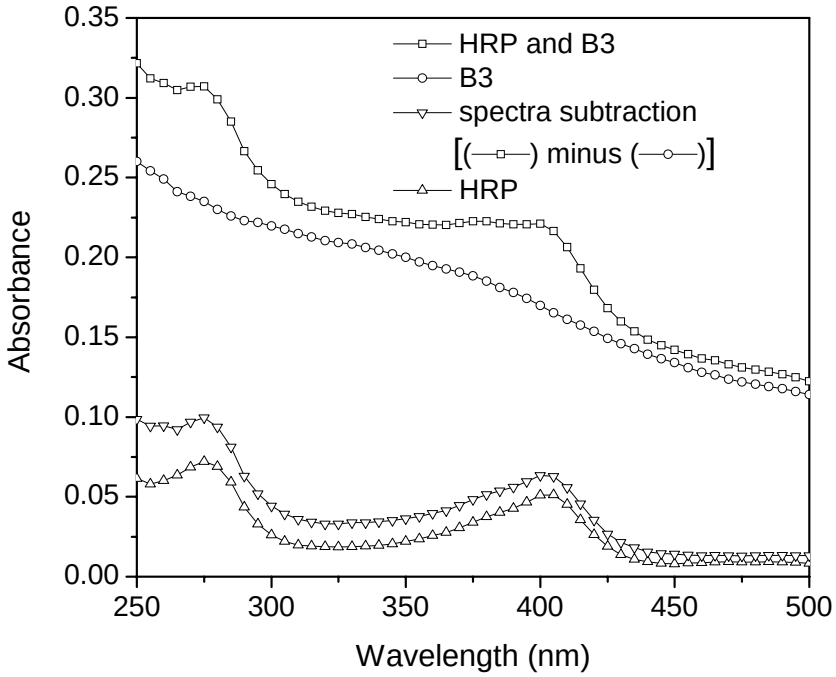

Figure 1.7: Absorption spectra of the native enzyme in water, Fe_3O_4 particles, and the combination of the two. The 403 nm peak, characteristic of the heme group, can be observed and neither the peak had shifted nor had the intensity of the peak changed when iron oxide particles were present. The small difference between the HRP spectrum and the subtracted spectrum of B3 from HRP is probably due to background absorption differences.

Reversibility of the effect of magnetic iron oxide particles on HRP

The effect of the particles in the assay was reversible, namely, the enzymatic activity returned to the original value once the particles were removed from the assay with a neodymium rare earth magnet. The reversibility was tested by measuring the activity of the same enzyme solution (3 nM of HRP) before and after adding particles, and finally after separating the particles with a neodymium magnet. The activity was initially 250 U/mg and after the particles were added, the measured activity was

approximately 3 times the initial value (706 U/mg). After the particles were removed the activity was measured close to the initial value at 240 U/mg. Thus we suggest that the activity increase is due solely to the presence of magnetic particles in the assay.

Origin of the activity increase

To obtain a better understanding of the enzyme behavior in the presence of magnetic particles, the apparent Michaelis-Menten kinetic parameters of the enzyme were measured with and without magnetic particles. The enzyme in the absence of particles had an activity maximum at 0.3 mM hydrogen peroxide and further increase of substrate in the assay resulted in a decrease of the catalytic activity. This last observation has been well documented for HRP where, at relatively high concentrations of peroxide, the enzyme undergoes substrate inhibition.[40-42]

The modified Michaelis-Menten equation for substrate inhibition[43] is presented in Equation 1.3. Figure 1.8 shows the Michaelis-Menten plots of the enzyme alone and in the presence of magnetic particles. Clearly the magnetic particles have an effect on the reaction kinetics. The activity of HRP with B4 particles reached a plateau at high peroxide concentrations, and substrate inhibition was registered only at concentrations close to 50 mM. Fitting the data to Equation 1.3, we obtained the apparent kinetic values V_{max}, K_m and the inactivation constant K_i.[27,44,45]

Equation 1.3 The modified Michaelis-Menten equation for substrate inhibition.[43]

$$V = \frac{V_{\max} \cdot [S]}{K_m + [S] + K_i \cdot [S]^2}$$

The data extracted from the fit are listed in Table 1.2. The largest effect of the particles on the apparent enzyme kinetics was a significant decrease of the substrate inhibition term K_i of close to 10-fold when magnetic particles were present.

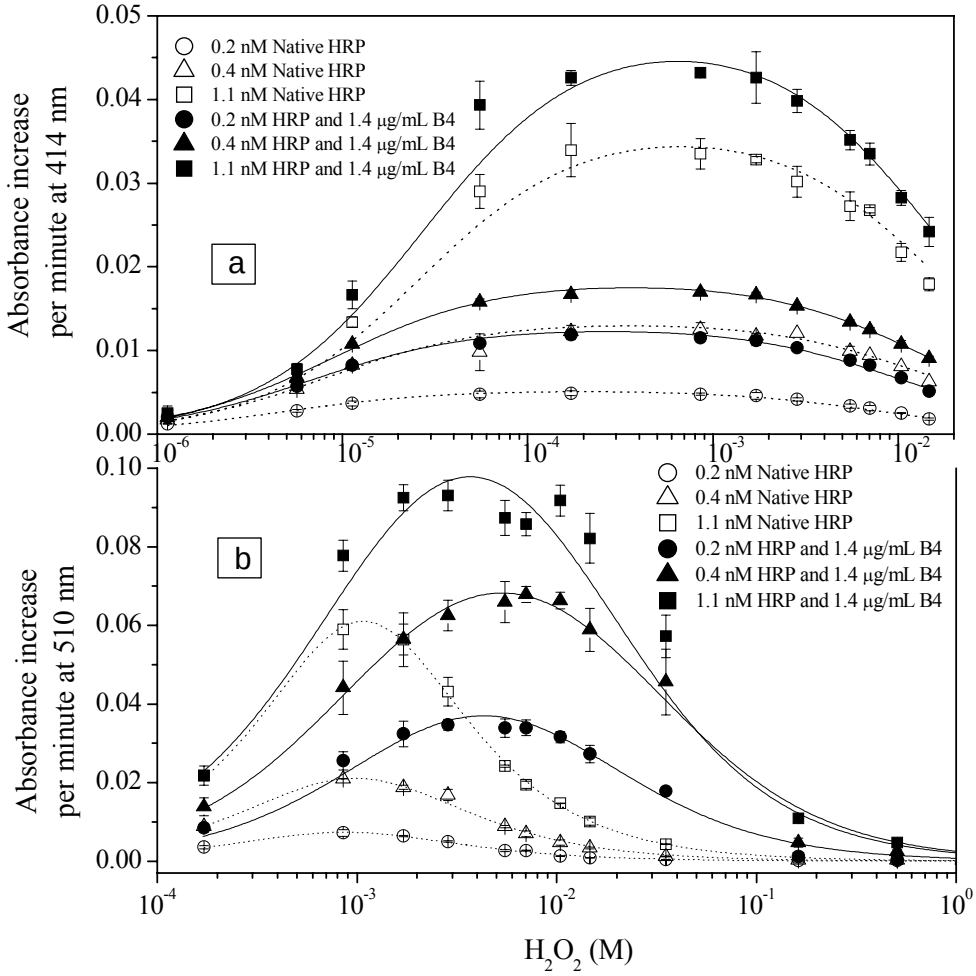

Figure 1.8: Dependence of enzymatic activity on H_2O_2 concentration. Various curves are shown with different molarities of HRP in the assay with and without 1.4 µg/mL of B4 particles. Figure 1.8a was obtained utilizing ABTS as chromogen and Figure 1.8b with phenol/AAP as the chromogen pair. Solid lines are relative to the HRP assay with particles. Dotted lines are relative to the assay with HRP alone. The error bars are the standard deviation of 4 repetitions.

The presence of particles in the assay had also a significant effect on the value of k_{cat}. k_{cat} is V_{max} normalized by the moles of enzyme in the assay (V_{max}/moles of enzyme), and is a measure of the rate at which the enzyme turns substrate into product (also known as turnover rate). The turnover rate was greatly increased in the presence of particles at low enzyme concentrations (at 0.2 nM of HRP the k_{cat} is almost three times larger for B3 particles and five times for B4 particles). At higher concentrations of enzyme in the assay the effect of the particles was decreased. Under these conditions the kinetics were probably dominated by the mass transfer of the substrate and product to and from the active center of the enzyme as this became the limiting step masking the effect of the particles.

A similar series of experiments was also conducted with 2,2´-Azino-di-(3-ethyl-benzthiazoline-6-sulphonic acid) (ABTS) as a secondary-chromogen substrate. The data extracted for the apparent Michaelis-Menten kinetic parameters through fitting Equation 1.3 are presented in Table 1.3. In this case, the k_{cat} of the enzyme was once again increased significantly in the presence of magnetic particles. However, contrary to the results with phenol/AAP, substrate inhibition was also observed in the presence of magnetic particles and the K_i remained unchanged. The V_{max}/K_m ratio increased in the presence of magnetic particles. This observation was consistent with the existence of a biradical enzyme-substrate complex which has been suspected to exist in the HRP catalytic cycle but has not yet confirmed.[15,32] The increase of V_{max}/K_m ratio was an indication that intersystem crossing occurred for a radical pair that decreased the probability of non-productive radical recombination, hence increasing the forward product formation.[23]

Table 1.2: Values of the apparent Michaelis-Menten parameters obtained through fitting Equation 1.3 to the data. The ± values are the standard deviation of the values resulting to the best fit. Data evaluated using the phenol/ AAP chromogen system.

	k_{cat} (s^{-1})	K_m (mM)	K_i (M^{-1})	Iron oxide in assay (μg/mL)	HRP in assay (nM)
HRP "alone"	164±5.8	0.1±0.06	204±48	0	0.2
	258.2±9.5	0.15±0.08	206±52	0	0.4
	362.7±52	0.31±0.08	344±46	0	1.1
	823±319	1.06±0.19	632±69.7	0	5.0
HRP and B4	1009±63	1.51±.020	81.1±0.7	1.4	0.2
	1112±89	1.04±0.24	36.7±8.6	1.4	0.4
	512±154	0.64±0.03	46±2.3	1.4	1.1
	845±9.5	1.42±0.13	577±35.8	1.4	5.0
HRP and B3	586±3.7	0.21±0.07	18.9±5.2	1.4	0.2
	645±8.5	0.46±0.02	85.2±0.7	1.4	0.4
	585±32	0.50±0.08	33±13	1.4	1.1
	523±17	0.78±0.1	176±70	1.4	5.0

Table 1.3: Values of the apparent Michaelis-Menten parameters obtained through fitting Equation 1.3 to the data. The ± values are the standard deviation of the values resulting to the best fit. Data evaluated using the ABTS chromogen system.

	k_{cat} (s^{-1})	K_m (μM)	K_i (M^{-1})	Iron oxide in assay (μg/mL)	HRP in assay (nM)
HRP "alone"	24.5±1.11	4.7±0.7	117±12	0	0.2
	31.2±0.5	8.2±0.4	63.5±4.4	0	0.4
	31.8±0.49	30±1.2	58.8±4	0	1.1
	37.6±0.79	70±3.7	24±2.2	0	5.0
HRP and B4	59.6±1.2	6.7±0.4	93.2±4.3	1.4	0.2
	42.5±0.46	9.0±0. 3	68.3±3.5	1.4	0.4
	40.9±0.51	30±0.9	63.9±3.2	1.4	1.1
	46.1±0.81	100±5.0	20.1±1.7	1.4	5.0
HRP and B3	82±1.3	6.7±0.4	68.3±7.3	1.4	0.2
	45±3.56	9.0±0.3	64.5±28	1.4	0.4
	61.4±1.9	29±0.9	68.2±14	1.4	1.1
	33.9±1.5	110±5	6.7±4	1.4	5.0

The difference between the apparent kinetic parameters obtained with the two chromogen assays was probably due to the differences of the two assays. We believe the parameters obtained from the ABTS chromogen are more reliable than those for phenol/AAP,[44] mainly because the latter depends on the combination of two radicals to generate a colored product.[45] Secondary side reactions exist for phenol radicals resulting in formation of biphenol products [35,45,46] that can generate various artifacts and errors in the evaluation of enzyme activity. It is also important to note that the kinetics and even the reaction mechanism of most enzymes strongly depend on the substrate utilized.[42,44,45] Nevertheless, the effect of the magnetic particles on enzymatic activity was similar and, with both protocols, an increased k_{cat} was evaluated.

Michaelis-Menten kinetics assays with B4 iron oxide particles

In Figure 1.9 the actual experimental plates used to generate Figures 1.8a and 1.8b can be seen. In addition, data shown in Tables 1.2 and 1.3 were obtained by fitting Equation 1.3 to the data extracted from Figure 1.9.

Figure 1.9 shows assay runs for HRP alone and HRP with B4 iron oxide particles using two different secondary substrate sets. The green colored wells (1 to 4) are the ABTS chromogen substrate assays and the red colored wells (5 to 8) are the phenol-aminoantipyrine assays.

All the wells in the same plate have the same concentration of enzyme. Plates 1 and 5 have 0.2 nM of HRP, plates 2 and 6 have 0.4 nM HRP, plates 3 and 7 have 1.1 nM and plates 4 and 8 have 5 nM of HRP.

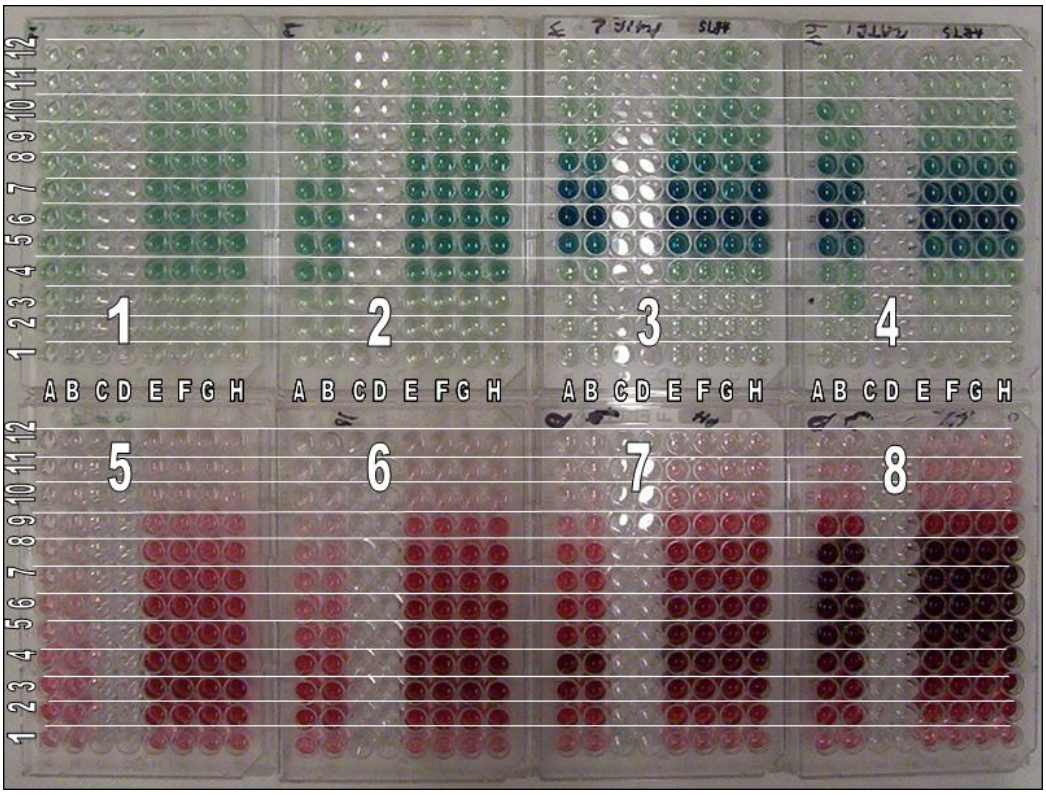

Figure 1.9: The actual eight 96-well plates from the experiments with B4 iron oxide particles at the end of the data acquisition.

In each plate, columns E, F, G and H are four repetitions of assays with the same concentration of B4 particles (i.e. wells E7, F7, G7 and H7 are identical assay runs). Columns A and B are 2 repetitions of HRP without particles (i.e. wells A2 and B2, A3 and B3 are identical). Furthermore, rows 1 to 12 have 12 different concentrations of hydrogen peroxide ranging from 10^{-6} to 10^{-1} M.

Michaelis-Menten kinetics assays with B3 iron oxide particles

Figure 1.10 shows assay runs for HRP alone and HRP with B3 iron oxide particles using two different secondary substrate sets. The data from these graphs were used to generate the values reported in Tables 1.2 and 1.3.

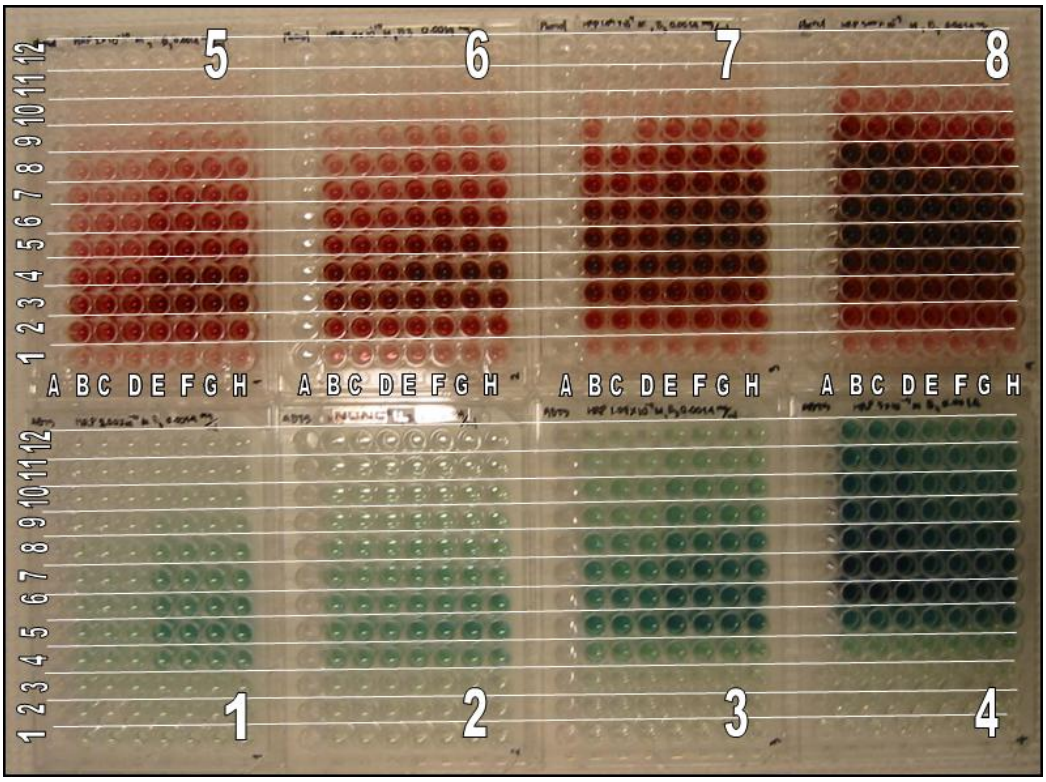

Figure 1.10: The actual eight 96-well plates from the experiments with B3 iron oxide particles at the end of the data acquisition.

The green-colored-well plates (1-4) are the ABTS substrate assays and the red-colored-well plates (5-8) are the phenol-aminoantipyrine assays. All the wells in the same plate have the same concentration of enzyme. In addition, plates 1 and 5 have 0.2 nM of HRP, plates 2 and 6 have 0.4 nM HRP, plates 3 and 7 have 1.1 nM and plates 4 and 8 have 5 nM of HRP.

In each plate, columns E, F, G and H are four repetitions of assays with the same concentration of B3 particles (i.e. wells E7, F7, G7 and H7 are identical assay runs). Columns A and B are 2 repetitions of HRP without particles (i.e. wells A2 and B2, A3 and B3 are identical). Rows 1 to 12 contain different hydrogen peroxide concentrations ranging from 10^{-6} to 10^{-1} M.

Extinction of ABTS radicals

From the data obtained using ABTS as the chromogen molecule, B3 particles appeared to have a larger effect on the turnover rate than the more magnetic B4 particles. This was counter-intuitive as we expected the more magnetic particles to have a larger effect. However, one possibility might be the increase of the recombination rate of the generated ABTS radicals which partially disproportionated back into ABTS due to the presence of magnetic particles.[36] To prove the above hypothesis and the assumption that magnetic particles can affect spin correlated radical pairs and their recombination rates, an experiment was designed that would track the evolution of a disproportionation reaction between two radicals when considered as Random Encounter Radical Pairs (RERP or F-pairs).[4]

A solution of HRP, hydrogen peroxide and excess ABTS was prepared so that all hydrogen peroxide was consumed to oxidize ABTS into ABTS radical cations (no further reaction could occur) and then the iron oxide particles were added. ABTS and ABTS radicals are spectrophotometrically distinct with an absorption peak at 340 nm for ABTS and 414 nm for the oxidized ABTS radical.[36] It is known that two ABTS radicals can disproportionate back into ABTS and an azodication product.[36] However, this step is very slow and, once formed, the ABTS radicals are very stable.[47] After the formation of radicals, iron oxide particles were added to the assay. The disproportionation rate of the diffusing radicals reacting back to ABTS was registered by tracking the changes of the characteristic absorption peaks at 340 and 414 nm. To avoid the error caused by light scattering of iron oxide particles, the particles were separated from the solution using a neodymium magnet every five to ten minutes. The spectrum of the solution in the absence of the particles was then obtained using a spectrophotometer registering the peaks of 340 and 414 nm. Figure 1.11 shows the percentage of the initially-formed radicals recombining to ABTS.

The raw data of the full spectra scans of the samples as a function of time are included in Figures 1.12, 1.13 and 1.14. Particles with increasing permanent magnetic moment had an increasingly beneficial role in the extent of disproportionation of radicals. A control solution was also made with the same concentration of ABTS radicals but with no iron oxide particles. In this case, no significant disproportionation was observed in the time scale of the experiment.

We believe the increase in the disproportionation rate is due to the presence of magnetic particles. In particular, the weak magnetic field of the randomly distributed particles increased the recombination rate of the diffusing ABTS radicals. The above observation is an indication that magnetic particles can play a significant role in reactions with spin correlated radical pairs and could possibly affect paramagnetic species, similar to the species formed during the HRP catalytic cycle (geminate pairs or diffusing RERPs)

In summary, our results indicated that low magnetic fields originating from randomly distributed magnetic particles had a profound increase on the catalytic activity of HRP. The above experiments may open a new area of investigation into the effects of very low magnetic fields on biological reactions. Further experiments with rapid-screening stopped-flow spectrophotometry could offer insight into the mechanism of the observed phenomenon. Additionally, a possible mechanistic explanation could have potential impact on other heme-containing proteins with radical intermediates and our understanding of magnetic field effects on the biological world.

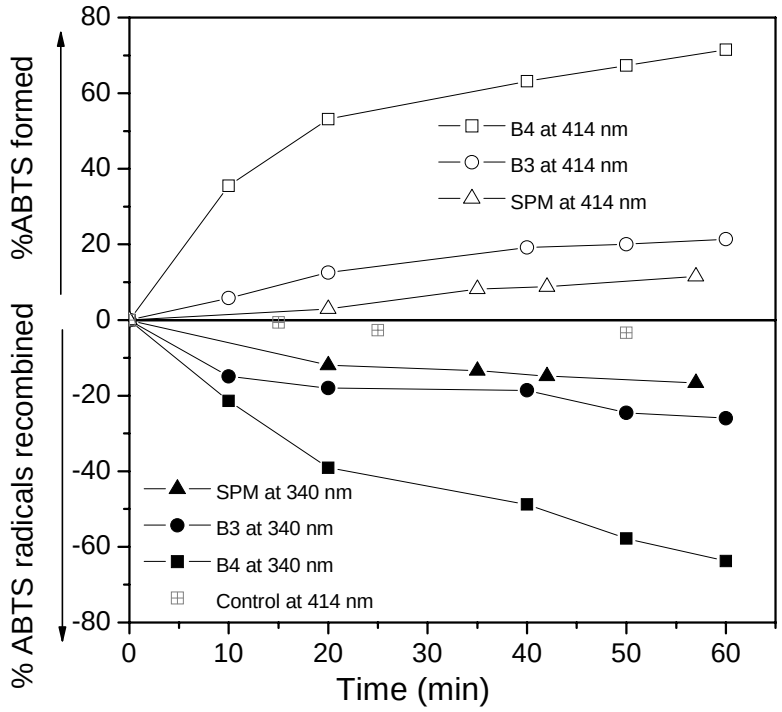

Figure 1.11: Extent of ABTS radicals recombination in the presence of iron oxide particles with increasing permanent magnetic moment.

(SPM=superparamagnetic ~0 emu/g, B3=magnetite 0.49 emu/g, B4= magnetite 1 emu/g)

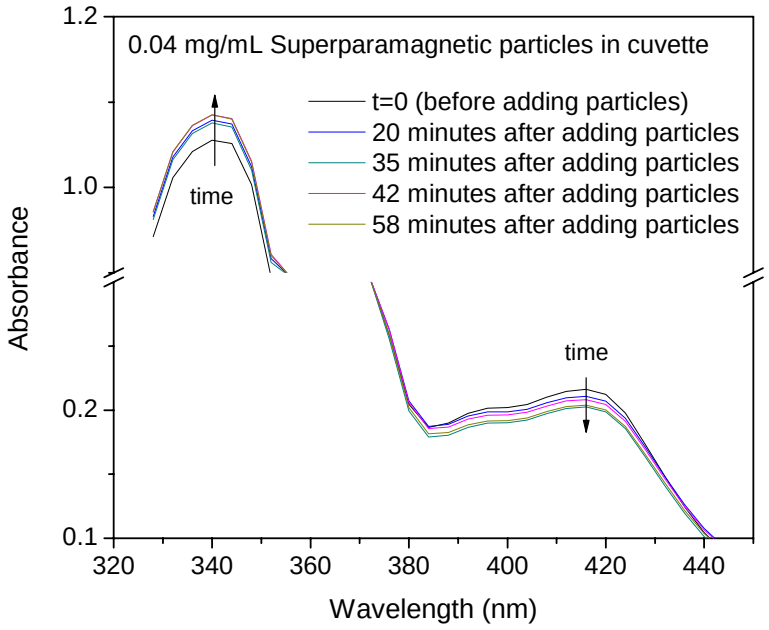

Figure 1.12: Spectra scans of a solution of radicals with 0.04 mg/mL SPM particles present in the assay.

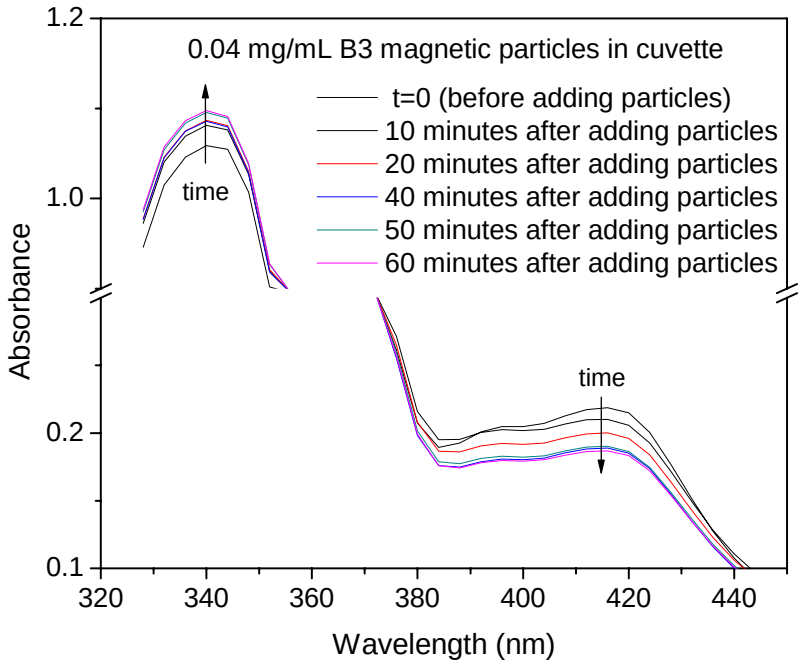

Figure 1.13: Spectra scans of a solution of radicals with 0.04 mg/mL B3 particles present in the assay.

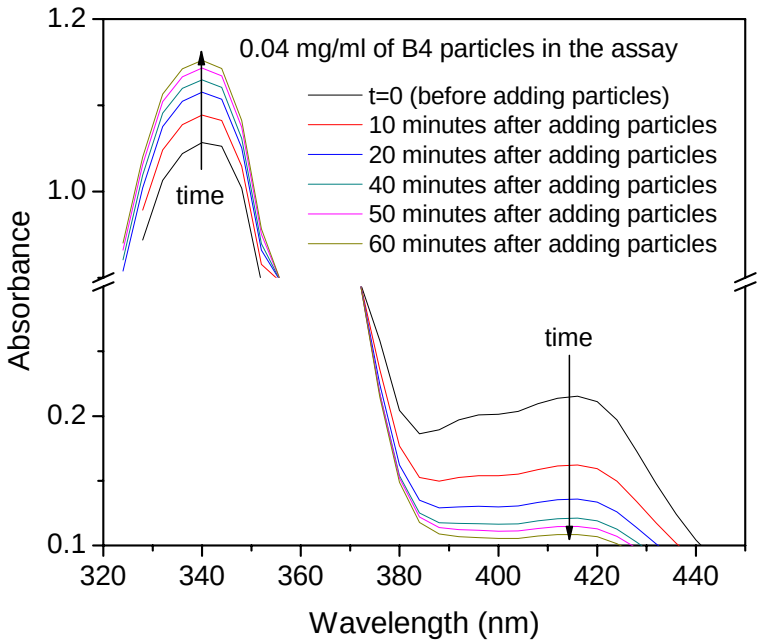

Figure 1.14: Spectra scans of a solution of radicals with 0.04 mg/mL B4 particles present in the assay.

REFERENCES

1. Ritz, T., Adem, S. & Schulten, K. A Model for Photoreceptor-Based Magnetoreception in Birds. *Biophysical Journal* **78**, 707-718 (2000).

2. Ritz, T., Thalau, P., Phillips, J. B., Wiltschko, R. & Wiltschko, W. Resonance Effects Indicate a Radical-Pair Mechanism for Avian Magnetic Compass. *Nature* **429**, 177-180 (2004).

3. Kirschvink, J. L. & Gould, J. L. Biogenic Magnetite as a Basis for Magnetic-Field Detection in Animals. *Biosystems* **13**, 181-201 (1981).

4. Salikhov, K. M., Molin, Y. N., Sagdeev, R. Z. & Buchachenko, A. L. *Spin Polarization and Magnetic Effects in Radical Reactions* (Elsevier; Akadémiai Kiadó, Amsterdam; New York; Budapest, Hungary, 1984).

5. Brocklehurst, B. Magnetic Fields and Radical Reactions: Recent Developments and Their Role in Nature. *Chemical Society Reviews* **31**, 301-311 (2002).

6. Grissom, C. B. Magnetic-Field Effects in Biology - a Survey of Possible Mechanisms with Emphasis on Radical-Pair Recombination. *Chemical Reviews* **95**, 3-24 (1995).

7. Maling, J. E., Weissblu.M & Jacobs, E. E. Enzyme Substrate Reactions in High Magnetic Fields. *Biophysical Journal* **5**, 767-& (1965).

8. Vanag, V. K., Kuznetsov, A. N. & Piruzyan, L. A. On the Influence of Magnetic-Field on H_2O_2 Decomposition by Catalase. *Biofizika* **28**, 18-23 (1983).

9. Rabinovi, B., Maling, J. E. & Weissblu, M. Enzyme-Substrate Reactions in Very High Magnetic Fields.2. *Biophysical Journal* **7**, 319-& (1967).

10. Rabinovi, B., Maling, J. E. & Weissblu, M. Enzyme-Substrate Reactions in Very High Magnetic Fields.1. *Biophysical Journal* **7**, 187-& (1967).

11. Vanag, V. K. & Kuznetsov, A. N. Magnetic Spin Effects in the Biological-Systems. *Izvestiya Akademii Nauk Sssr Seriya Biologicheskaya*, 215-228 (1988).

12. Steiner, U. E. & Ulrich, T. Magnetic-Field Effects in Chemical-Kinetics and Related Phenomena. *Chemical Reviews* **89**, 51-147 (1989).

13. Vanag, V. K. & Kuznetsov, A. N. Kinetic-Analysis of Possible Effects of a Constant Magnetic-Field on the Rate of Enzymic Reactions. *Biofizika* **29**, 23-29 (1984).

14. Anderson, M. A., Xu, Y. P. & Grissom, C. B. Electron Spin Catalysis by Xenon in an Enzyme. *Journal of the American Chemical Society* **123**, 6720-6721 (2001).

15. Taraban, M. B., Leshina, T. V., Anderson, M. A. & Grissom, C. B. Magnetic Field Dependence of Electron Transfer and the Role of Electron Spin in Heme Enzymes: Horseradish Peroxidase. *Journal of the American Chemical Society* **119**, 5768-5769 (1997).

16. Blank, M. & Soo, L. Enhancement of Cytochrome Oxidase Activity in 60 Hz Magnetic Fields. *Bioelectrochemistry and Bioenergetics* **45**, 253-259 (1998).

17. Blank, M. & Soo, L. Frequency Dependence of Cytochrome Oxidase Activity in Magnetic Fields. *Bioelectrochemistry and Bioenergetics* **46**, 139-143 (1998).

18. Eichwald, C. & Walleczek, J. Activation-Dependent and Biphasic Electromagnetic Field Effects: Model Based on Cooperative Enzyme Kinetics in Cellular Signaling. *Bioelectromagnetics* **17**, 427-435 (1996).

19. Eichwald, C. & Walleczek, J. Low-Frequency-Dependent Effects of Oscillating Magnetic Fields on Radical Pair Recombination in Enzyme Kinetics. *Journal of Chemical Physics* **107**, 4943-4950 (1997).

20. Kundla, E., Lippmaa, E. & Saluvere, T. *Magnetic Resonance and Related Phenomena: Proceedings of the XXth Congress Ampere, Tallinn, August 21-26, 1978* (Academy of Sciences of the Estonian SSR; sole distribution for all non-socialist countries by Springer-Verlag, [s.l.] Berlin; New York, 1979).

21. Harkins, T. T. & Grissom, C. B. B12 Ethanolamine Ammonia-Lyase - Magnetic-Field Dependence of Stopped-Flow Kinetic Rates. *Abstracts of Papers of the American Chemical Society* **208**, 21-Biol (1994).

22. Harkins, T. T. & Grissom, C. B. The Magnetic-Field Dependent Step in B12 Ethanolamine Ammonia-Lyase Is Radical-Pair Recombination. *Journal of the American Chemical Society* **117**, 566-567 (1995).

23. Harkins, T. T. & Grissom, C. B. Magnetic-Field Effects on B12 Ethanolamine Ammonia-Lyase - Evidence for a Radical Mechanism. *Science* **263**, 958-960 (1994).

24. Berglund, G. I., Carlsson, G. H., Smith, A. T., Szoke, H., Henriksen, A. & Hajdu, J. The Catalytic Pathway of Horseradish Peroxidase at High Resolution. *Nature* **417**, 463-468 (2002).

25. Jones, A., Scrutton, N. & Woodward, J. Magnetic Field Effects and Radical Pair Mechanisms in Enzymes: A Reappraisal of the Horseradish Peroxidase System. *Journal of the American Chemical Society* **128**, 8408-8409 (2006).

26. Poulos, T. L. & Kraut, J. The Stereochemistry of Peroxidase Catalysis. *Journal of Biological Chemistry* **255**, 8199-8205 (1980).

27. Rodriguez-Lopez, J. N., Lowe, D. J., Hernandez-Ruiz, J., Hiner, A. N. P., Garcia-Canovas, F. & Thorneley, R. N. F. Mechanism of Reaction of Hydrogen Peroxide with Horseradish Peroxidase: Identification of Intermediates in the Catalytic Cycle. *Journal of the American Chemical Society* **123**, 11838-11847 (2001).

28. Mulholland, A. J. Modelling Enzyme Reaction Mechanisms, Specificity and Catalysis. *Drug Discovery Today* **10**, 1393-1402 (2005).

29. Holliday, G. L., Bartlett, G. J., Almonacid, D. E., O'Boyle, N. M., Murray-Rust, P., Thornton, J. M. & Mitchell, J. B. O. Macie: A Database of Enzyme Reaction Mechanisms. *Bioinformatics* **21**, 4315-4316 (2005).

30. Moller, A. C., Lunding, A. & Olsen, L. F. Further Studies of the Effect of Magnetic Fields on the Oscillating Peroxidase-Oxidase Reaction. *Physical Chemistry Chemical Physics* **2**, 3443-3446 (2000).

31. Moller, A. C. & Olsen, L. F. Effect of Magnetic Fields on an Oscillating Enzyme Reaction. *Journal of the American Chemical Society* **121**, 6351-6354 (1999).

32. Afanasyeva, M., Taraban, M., Purtov, P., Leshina, T. & Grissom, C. Magnetic Spin Effects in Enzymatic Reactions: Radical Oxidation of Nadh by Horseradish Peroxidase. *Journal of the American Chemical Society* **128**, 8651-8658 (2006).

33. Dunford, H. B. Peroxidases and Mechanisms of Enzyme Action. *Abstracts of Papers of the American Chemical Society*, 332-332 (1979).

34. Worthington Biochemical Corporation. *Worthington Enzyme Manual: Enzymes, Enzyme Reagents, Related Biochemicals* (Worthington Biochemical Corp., Freehold, N.J., 1972).

35. Buchanan, I. D. & Nicell, J. A. Model Development for Horseradish Peroxidase Catalyzed Removal of Aqueous Phenol. *Biotechnology and Bioengineering* **54**, 251-261 (1997).

36. Childs, R. E. & Bardsley, W. G. Steady-State Kinetics of Peroxidase with 2,2'-Azino-Di-(3-Ethylbenzthiazoline-6-Sulphonic Acid) as Chromogen. *Biochemical Journal* **145**, 93-103 (1975).

37. Vink, C. B. & Woodward, J. R. Effect of a Weak Magnetic Field on the Reaction between Neutral Free Radicals in Isotropic Solution. *Journal of the American Chemical Society* **126**, 16730-16731 (2004).

38. Goya, G. F., Berquo, T. S., Fonseca, F. C. & Morales, M. P. Static and Dynamic Magnetic Properties of Spherical Magnetite Nanoparticles. *Journal of Applied Physics* **94**, 3520-3528 (2003).

39. Jackson, J. D. *Classical Electrodynamics* (Wiley, New York, 1999).

40. Hernandez-Ruiz, J., Arnao, M. B., Hiner, A. N. P., Garcia-Canovas, F. & Acosta, M. Catalase-Like Activity of Horseradish Peroxidase: Relationship to Enzyme Inactivation by H_2O_2. *Biochemical Journal* **354**, 107-114 (2001).

41. Weinryb, I. Behavior of Horseradish Peroxidase at High Hydrogen Peroxide Concentrations. *Biochemistry* **5**, 2003-& (1966).

42. Hiner, A. N. P., Hernandez-Ruiz, J., Arnao, M. B., Garcia-Canovas, F. & Acosta, M. A Comparative Study of the Purity, Enzyme Activity, and Inactivation by Hydrogen Peroxide of Commercially Available Horseradish Peroxidase Isoenzymes A and C. *Biotechnology and Bioengineering* **50**, 655-662 (1996).

43. Silverman, R. B. *The Organic Chemistry of Enzyme-Catalyzed Reactions* (Academic Press, San Diego, 2002).

44. Rodriguez-Lopez, J. N., Gilabert, M. A., Tudela, J., Thorneley, R. N. F. & Garcia-Canovas, F. Reactivity of Horseradish Peroxidase Compound II toward Substrates: Kinetic Evidence for a Two-Step Mechanism. *Biochemistry* **39**, 13201-13209 (2000).

45. Lebedeva, O. V. & Ugarova, N. N. Mechanism of Peroxidase-Catalyzed Oxidation. Substrate-Substrate Activation in Horseradish Peroxidase-Catalyzed Reactions. *Russian Chemical Bulletin* **45**, 18-25 (1996).

46. Yu, J., Taylor, K. E., Zou, H. X., Biswas, N. & Bewtra, J. K. Phenol Conversion and Dimeric Intermediates in Horseradish Peroxidase-Catalyzed Phenol Removal from Water. *Environmental Science & Technology* **28**, 2154-2160 (1994).

47. Wolfenden, B. S. & Willson, R. L. Radical-Cations as Reference Chromogens in Kinetic-Studies of One-Electron Transfer-Reactions-Pulse-Radiolysis Studies of 2,2'-Azinobis-(3-Ethylbenzthiazoline-6-Sulphonate). *Journal of the Chemical Society-Perkin Transactions 2*, 805-812 (1982).

CHAPTER 2: IMMOBILIZATION OF HORSERADISH PEROXIDASE ON MAGNETIC PARTICLES.

INTRODUCTION

Heme-peroxidases are present extensively in nature and they are found in plants, fungi, bacteria and mammals serving various biological functions.[1] In particular, Horseradish Peroxidase (HRP) utilizes hydrogen peroxide to oxidize a wide variety of organic and inorganic compounds. Horseradish is a hardy perennial herb cultivated in temperate regions and its roots are a rich source of the peroxidase enzyme. In the literature, numerous research papers have dealt with the reaction mechanism, properties and applications of HRP in the biological and analytical sciences.[1]

Currently, the production of Horseradish Peroxidase occurs on a relatively large scale because of its commercial use in clinical diagnostic kits, immunoassays, waste-water treatment and elsewhere.[2,3] However, the cost of HRP is relatively high (a few US dollars per mg) making the enzyme a costly reagent. As an example, the removal of phenol from wastewater using HRP is considered expensive and alternative routes have been suggested in the literature.[4] On the other hand, immobilization is a successful route to attain enzyme reusability with low cost and improved enzyme performance.[5,6] The immobilization of enzymes is accomplished mainly in four different ways including adsorption, cross linking, entrapment and covalent attachment on an insoluble moiety.[7]

Using the knowledge obtained from experiments in Chapter 1, we present an immobilization approach for HRP on magnetite particles which results in increased enzymatic activity and improved stability. This immobilization method falls in the "covalent attachment" category mentioned above, in which HRP binds to an insoluble

carrier in our case iron oxide (magnetite) particles. The benefit of using magnetic carriers for the immobilization of enzymes has been previously explored extensively due to the simplicity of magnetic field separation.[8-10]

MATERIALS AND METHODS

The deionized (DI) water used throughout the experiments was purified in a "Barnstead Nanopure RO" unit and had minimum resistivity of 18 MΩcm. Biotin, phenol, 4-aminoantipyrine (AAP), sulfuric acid and hydrogen peroxide (H_2O_2) were purchased from Sigma-Aldrich. Horseradish Peroxidase conjugate with Avidin (HRP-Avidin) was obtained from Pierce Biotechnology (2 moles of HRP per 1 mole of Avidin).

Fourier Transform Infra-Red (FTIR) spectroscopic measurements were performed on a Bruker Vertex 70 FTIR spectrometer equipped with a diamond crystal for attenuated total reflectance (ATR) IR scans.

Biotinylation of magnetite particles

Biotinylation of magnetite particles (Fe_3O_4) was realized through a condensation reaction in acidic conditions. 100 mg of biotin were dissolved in 5 mL of ethanol where previously 10 mg of B4 magnetite particles (see Chapter 1) were suspended. Finally, 0.5 mL of fuming sulfuric acid was added and the solution was stirred for 4 minutes in a 40 ºC water bath. Next, the particles were separated from the solution using a neodymium magnet and washed multiple times with deionized water until neutral pH was attained.

Activity measurements.

The Worthington protocol was followed to calculate the activity of the particle-immobilized enzymes as well as the residual activity in the washout solutions during

the immobilization process.[11] According to the protocol, a chromogen molecule was produced and the increase of absorbance at 510 nm was followed on a SpectraMax Plus spectrophotometer. The increase of absorbance at 510 nm was translated into enzyme activity through the specific absorptivity of the chromogen ($\varepsilon = 7100$ $M^{-1}cm^{-1}$).[12] The substrates used were 2.5 mM 4-aminoantipyrine with 0.17 M phenol and 1.7 mM H_2O_2. All measurements were in a phosphate buffer saline (PBS) with a pH of 7.2. Each experiment was repeated three times.

Immobilization of HRP-Avidin conjugate

In 2 mL of DI water, 0.3 mg of biotinylated magnetite particles and 1 nmole of HRP-Avidin conjugate were added. The suspension was stirred for 10 minutes and the particles with the attached enzyme were separated with the use of a neodymium magnet. The solution was named washout #1 and the particles were resuspended in 2 mL of DI water and separated once again. The process was repeated for a total of three times and produced three washout solutions.

To evaluate the extent of enzyme immobilization, the enzyme mass in the three washout solutions was estimated by measuring the enzymatic activity according to the Worthington protocol.[11] The measured activity was then translated to enzyme mass through a calibration curve generated previously. Finally, the mass of non-immobilized enzyme was subtracted from the initial amount and the enzyme bound to the biotinylated particles was estimated.

In addition, a protein concentration assay based on the absorption of the HRP heme group in the Soret band was employed ($\varepsilon = 102$ $mM^{-1}cm^{-1}$ at 403 nm).[13] Likewise, the moles of HRP in the washout solution #1 were estimated and the number of moles immobilized was calculated. The amount of enzyme in washout #2 and #3 was minimal.

RESULTS AND DISCUSSION

Biotin molecules were attached on magnetite particles via a condensation reaction as described in Materials and Methods section. A schematic of the process is shown in Figure 2.1.

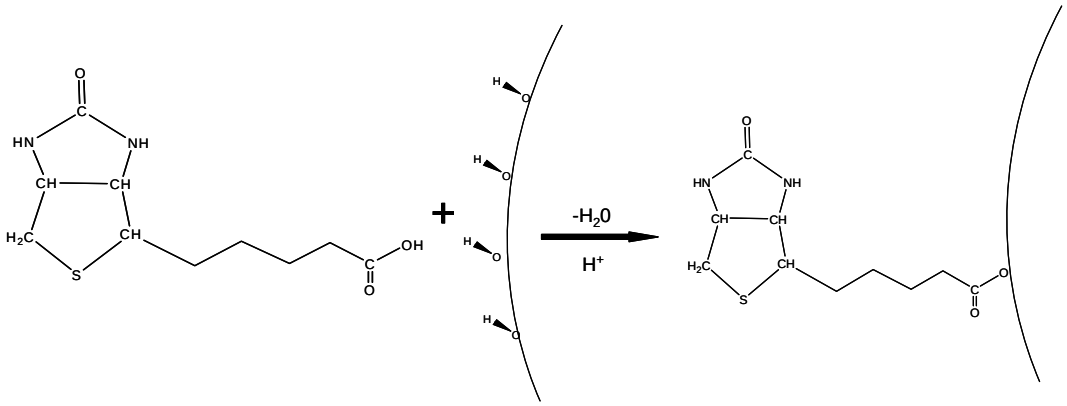

Figure 2.1: A schematic of the condensation reaction that was performed for the attachment of biotin molecules on the surface of iron oxide particles.

Successful synthesis was assessed using FTIR spectroscopy and in Figure 2.2 the IR spectra of biotin, biotinylated magnetite particles and magnetite particles are plotted. The existence of absorption peaks from alkyl groups was verified for the biotinylated particles even after multiple washes; these peaks were evidence of biotin attachment on the particles.

Immobilization of HRP on magnetite particles was realized using the strong interaction of biotin and Avidin. The process was a simple, one-step immobilization process that occurred under mild conditions of temperature (25 ºC) and pH 7. Since we were unable to measure directly the amount of enzyme immobilized (due to the presence of particles), we have calculated the amount of enzyme that was washed out during the process. Two different approaches were followed as described in Materials and Methods section. The first relied on the characteristic absorption of HRP enzyme at 403 nm [13] and the second was based on the residual activity measured in the washout solutions according to the Worthington protocol.[11] The estimated mass of

immobilized enzyme with the above methods was 28 and 15 μg of protein per 1 mg of magnetite particles or 0.18 nmoles and 0.096 nmoles per 1 mg of particles accordingly (Molecular weight of HRP-Avidin conjugate: 156 kDa).

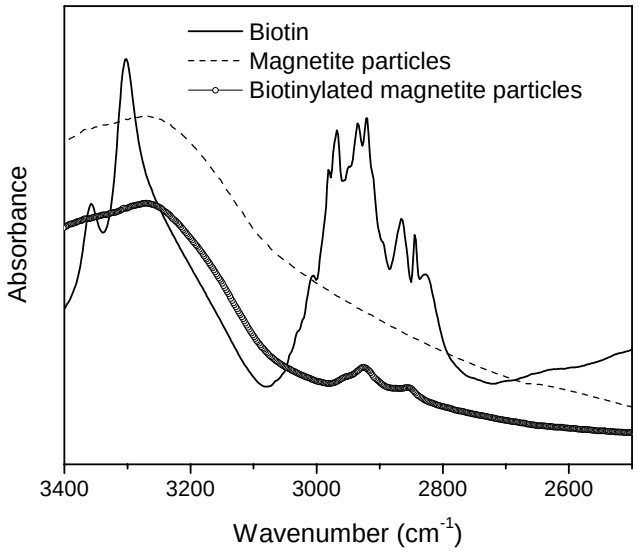

Figure 2.2: IR spectra of biotin and biotinylated magnetite particles. The characteristic peaks of the alkyl groups (2980-2850 cm^{-1}) can be observed in the spectrum of the biotinylated magnetite.

Based on the above calculated mass of immobilized enzyme, an increase of enzymatic activity per mg was observed, consistent with the results presented in Chapter 1. Following that, multiple experiments were realized with different amounts of hydrogen peroxide using the process described in Chapter 1. The above were accomplished using two forms of the same enzyme, the native HRP-Avidin conjugate and the immobilized conjugate on biotinylated particles. To make a valid comparison, the solutions needed to have identical enzyme masses. However, the exact moles of immobilized enzyme were measured indirectly and only estimates were available as

described previously. To obtain comparable results, the native enzyme solution contained the largest estimate for HRP mass per particles.

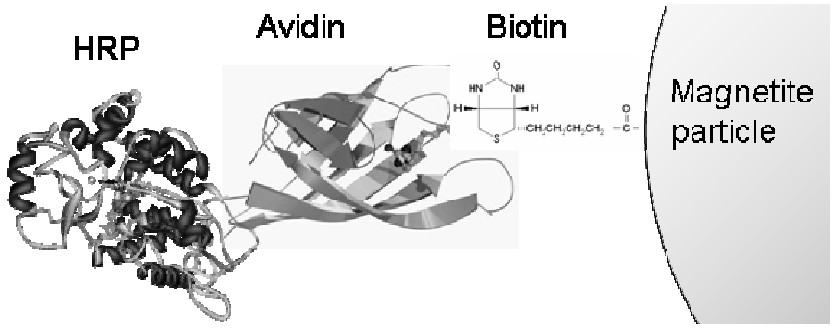

Figure 2.3: A schematic of an immobilized HRP-Avidin conjugate on a biotinylated magnetite particle (not in scale). Pictures for the protein structures where obtained through the protein databank PDB.[14]

Contrary to Chapter 1 where assays of HRP activity were performed in the presence of magnetite particles, the assays performed here had HRP attached on magnetite particles. Nevertheless, a similar beneficial effect on HRP kinetics was also observed. In Figure 2.4 the data of enzymatic activity for the immobilized HRP were consistent with the magnetic field effects observed in Chapter 1.

Furthermore, the storage stability of the immobilized enzyme was improved when compared to the native HRP-Avidin conjugate. The residual activity of the two enzyme solutions stored in 25 ºC is plotted in Figure 2.5. In a period of 15 days, the immobilized enzyme lost approximately 20 % of its initial activity where the native form had lost over 50 %.

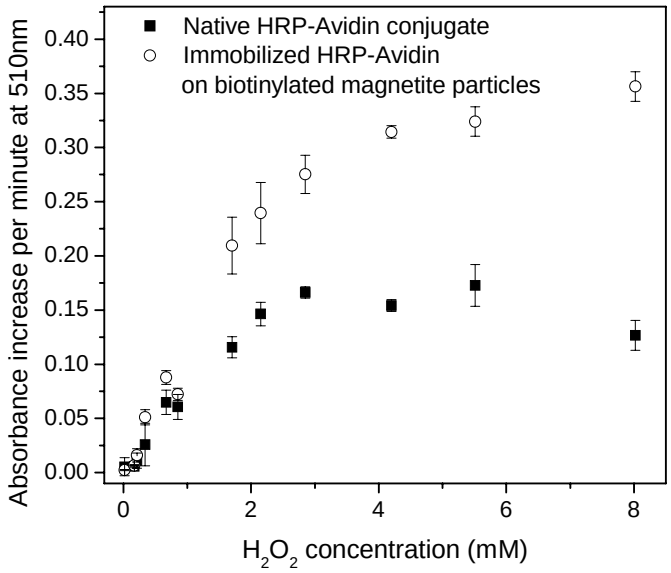

Figure 2.4: Dependence of enzymatic activity on H_2O_2 concentration for the native HRP-Avidin conjugate and the immobilized conjugate on biotinylated magnetite particles. The native enzyme assay contained 1.6 nM of HRP and the immobilized enzyme assay 1.6 nM of HRP and 5.3 µg/mL biotinylated magnetite particles.

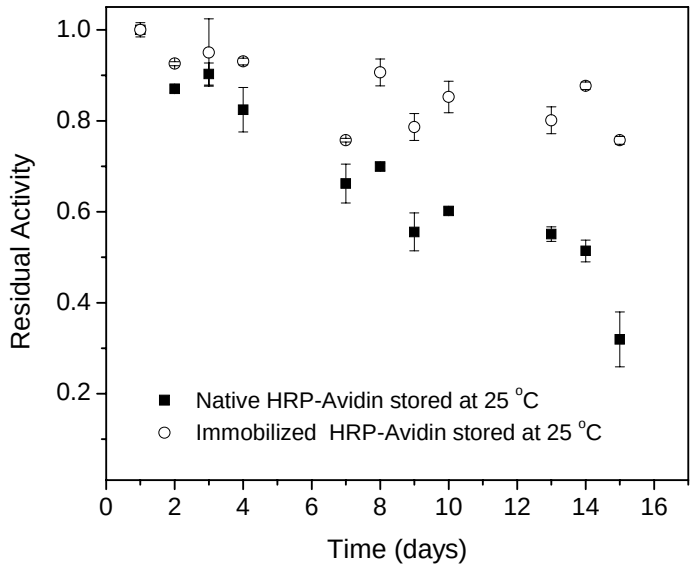

Figure 2.5: Residual activities for the native HRP-Avidin conjugate and its immobilized counterpart during two weeks of storage in room temperature. Both solutions had a concentration of 47 nM of enzyme in DI water.

CONCLUSIONS

Using the proposed immobilization method for HRP on biotinylated magnetite particles, we have achieved improved enzyme stability and higher enzymatic activity to the native counterpart. The immobilization process was a simple one-step process that was completed under mild conditions of temperature and pH using the strong affinity of biotin for Avidin. Moreover, the magnetic properties of the iron oxide particles had a significant effect in the kinetics of the immobilized HRP, which was consistent with the observations in Chapter 1. Further optimization could provide a measure for the application range of the proposed immobilization approach.

REFERENCES

1. Dunford, H. B. *Heme Peroxidases* (John Wiley, New York, 1999).

2. Klibanov, A. M., Tu, T. M. & Scott, K. P. Peroxidase-Catalyzed Removal of Phenols from Coal-Conversion Waste-Waters. *Science* **221**, 259-260 (1983).

3. Veitch, N. C. Horseradish Peroxidase: A Modern View of a Classic Enzyme. *Phytochemistry* **65**, 249-259 (2004).

4. Ambrosio, K., Rueda, E. & Ferreira, M. L. Magnetite-Supported Hematin as a Biomimetic of Horseradish Peroxidase in Phenol Removal by Polymerization. *Biocatalysis and Biotransformation* **22**, 35-44 (2004).

5. Bickerstaff, G. F. *Immobilization of Enzymes and Cells* (Humana Press, Totowa, N.J., 1997).

6. Bornscheuer, U. T. Immobilizing Enzymes: How to Create More Suitable Biocatalysts. *Angewandte Chemie-International Edition* **42**, 3336-3337 (2003).

7. Silman, I. H. & Katchals.E. Water-Insoluble Derivatives of Enzymes Antigens and Antibodies. *Annual Review of Biochemistry* **35**, 873-& (1966).

8. Dyal, A., Loos, K., Noto, M., Chang, S. W., Spagnoli, C., Shafi, K. V. P. M., Ulman, A., Cowman, M. & Gross, R. A. Activity of Candida Rugosa Lipase Immobilized on Gamma-Fe_2O_3 Magnetic Nanoparticles. *Journal of the American Chemical Society* **125**, 1684-1685 (2003).

9. Liao, M. H. & Chen, D. H. Immobilization of Yeast Alcohol Dehydrogenase on Magnetic Nanoparticles for Improving Its Stability. *Biotechnology Letters* **23**, 1723-1727 (2001).

10. Yang, H. H., Zhang, S. Q., Chen, X. L., Zhuang, Z. X., Xu, J. G. & Wang, X. R. Magnetite-Containing Spherical Silica Nanoparticles for Biocatalysis and Bioseparations. *Analytical Chemistry* **76**, 1316-1321 (2004).

11. Worthington Biochemical Corporation. *Worthington Enzyme Manual: Enzymes, Enzyme Reagents, Related Biochemicals* (Worthington Biochemical Corp., Freehold, N.J., 1972).

12. Buchanan, I. D. & Nicell, J. A. Model Development for Horseradish Peroxidase Catalyzed Removal of Aqueous Phenol. *Biotechnology and Bioengineering* **54**, 251-261 (1997).

13. Dunford, H. B. Peroxidases and Mechanisms of Enzyme Action. *Abstracts of Papers of the American Chemical Society*, 332-332 (1979).

14. Berman, H. M., Westbrook, J., Feng, Z., Gilliland, G., Bhat, T. N., Weissig, H., Shindyalov, I. N. & Bourne, P. E. The Protein Data Bank. *Nucleic Acids Research* **28**, 235-242 (2000).

CHAPTER 3: AN AVIDIN-BIOTIN IMMOBILIZATION APPROACH FOR HORSERADISH PEROXIDASE AND GLUCOSE OXIDASE ON LAYERED SILICATES WITH HIGH CATALYTIC ACTIVITY RETENTION AND IMPROVED THERMAL BEHAVIOR.

INTRODUCTION

During the last decades of the 20th century, enzymatic reactions found an increasing number of applications due to their versatility and specificity. A broad array of technologies ranging from organic synthesis, biosensors, green energy applications and many other fields are now depended on biological catalysis.[1] This strengthened the need for better and improved enzymatic properties and led to numerous efforts for the development of insoluble enzymes with tailored properties.[2-5] Immobilized enzymes have various advantages compared to their soluble counterparts, including enhanced stability, repeated or continuous use, easy separation and possible modulation of their catalytic properties.[6] Successful control of all the above can result in a lower production cost or improved process control in an industrial scale.

Currently, there is a growing number of publications investigating new enzyme immobilization approaches or improving existing methods.[7-12] Most immobilization techniques fall into four categories of non-covalent adsorption, covalent attachment, entrapment, and crosslinking. However, one of the drawbacks of enzyme immobilization is the alteration of the enzyme's three dimensional conformation. In this context, the advantages of immobilization are often accompanied with partial loss of the catalytic activity. To obtain optimum immobilization conditions, one has to balance between a number of conditions that are not always well understood.

In the recent past, there has been an increasing number of publications investigating immobilization approaches with minimal activity loss[10,13,14] and

improved performance.[15,16] In that direction, an immobilization approach with high retention of catalytic activity and improved thermal behavior is presented for two frequently used enzymes, namely Horseradish Peroxidase (HRP) and Glucose Oxidase (GOx). The immobilization support was a synthetic layered silicate. Layered silicates are stable inorganic materials with interesting properties such as excellent dispersability in water, large surface area per mass and tunable surface chemistry via simple ion-exchange and surface chemistry reactions. Layered silicate-enzyme complexes have appeared in literature before and various immobilization methods and applications were realized.[17-25] In this work, a new approach of enzyme immobilization on layered silicates is presented, utilizing the edge hydroxyl groups on their surface. Using this approach, the large surface area of the silicates remained available for functionalization, leaving open the possibility of various modifications of the surface area present in the galleries between the layers of the silicates. As an example, modification of the layered silicates with surfactants[26-28] can render the silicates highly hydrophobic. Suspension of the immobilized enzymes in hydrophobic organic solvents and non aqueous enzymatic catalysis could be possible.[29-32]

MATERIALS AND METHODS

UV/Vis spectra were obtained on a Perkin-Elmer® model Lambda 10 instrument, connected serially on a PC running Windows® 2000 and controlled through UVWinlab software provided by Perkin Elmer.

Fourier Transform Infra-Red (FTIR) spectroscopic measurements were performed on a Bruker Vertex 70 FTIR spectrometer equipped with a diamond crystal for attenuated total reflectance (ATR) setup.

Several buffer solutions of different pH were employed. The pH 7 buffer was a 0.05 M potassium phosphate monobasic solution, the pH 10 buffer was a 0.05 M

Potassium Carbonate/Potassium Tetraborate/Potassium Hydroxide/Disodium EDTA Dihydrate solution. The pH 4 and pH 5 were 0.01 M sodium acetate solutions. The pH 7.4 was a 0.05 M potassium phosphate solution and the pH 8 was a 0.01 M Tris-HCl solution.

The deionized water (DI) used throughout the experiments was purified in a "Barnstead Nanopure RO" unit and had minimum resistivity of 18 MΩcm. Phenol, 4-aminoantipyrine, hydrochloric acid and hydrogen peroxide were purchased from Sigma-Aldrich, and the temperature controller was a Mirak Thermolyne 49 by Barnstead Corporation.

Biotinylation of layered silicates

A synthetic layered silicate, Somasif ME-100 (Na^+-Fluoromica or FM) with a cation exchange capacity of 120 mequiv/100 g was obtained from CO-OP Chemical LTD. Biotin was obtained from Sigma Aldrich as a lyophilized powder. Functionalization of layered silicates with biotin was accomplished through a condensation reaction between the carboxyl group of biotin and the hydroxyl groups located at the edges of the silicate. 100 mg of fluoromica and 370 mg of biotin were added in 20 mL of ethanol with 0.5 mL of hydrochloric acid (12 N). After stirring the mixture for 5 minutes at 40 ºC the solid product was washed and centrifuged multiple times with deionized water until neutral pH was reached.

Enzyme Immobilization.

The high affinity between Avidin and biotin was utilized to immobilize enzyme-Avidin conjugates on biotin functionalized silicates (biotinylated silicates). Horseradish Peroxidase (HRP) conjugate with Avidin and Glucose Oxidase (GOx) conjugate with Avidin were obtained from Pierce Biotechnology and Rockland Immunochemicals as lyophilized powders. The immobilization of the enzyme

conjugates was accomplished in a simple one-step process. An excess amount of an enzyme-Avidin conjugate with biotinylated silicates were added in an aqueous solution. After stirring for 3 minutes, the solution was centrifuged at 11,000 rpm for 10 minutes. The resulting pellet was resuspended and centrifuged three times in order to remove any unbound enzyme. The activity of the washouts was evaluated in order to calculate the amount of enzyme lost during the process and thus, the extent of immobilization.

Evaluation of the enzymatic activity

The activity of HRP was measured spectrophotometrically according to the Worthington protocol.[33] The protocol involves the production of a colored product with maximum absorbance at 510 nm. According to the Worthington protocol, 1.5 mL of buffered hydrogen peroxide (1.7 mM) was added in a quartz cuvette to 1.4 mL phenol (0.17 M) and 4-aminoantipyrine solution (2.5 mM). The pH during the assay was kept constant using a potassium phosphate monobasic buffer (pH 7). After temperature equilibration, 0.1 mL of an unknown activity HRP solution was added. From the increase of absorbance at 510 nm with time, the activity of the unknown solution was calculated. Likewise the activity of GOx was evaluated using a similar protocol described in the Worthington manual.[33]

The enzymatic activity at various temperatures was measured using the above protocol. A temperature controlled digital stirrer and a water bath were used during the measurements. The accuracy of the temperature controller was ±1 ºC. The cuvette containing all reagents was immersed into the bath and after temperature equilibration, it was inserted into the spectrophotometer where the enzyme solution was finally added.

For the thermal stability experiments, 2 mL of the enzyme solution (in a sealed container to avoid evaporation of the solvent) were placed in a temperature controlled oven and at various times 0.1 mL of the sample were removed and tested (at 25 ºC) for residual enzymatic activity.

RESULTS AND DISCUSSION

Successful functionalization of the silicates with biotin was assessed using FTIR spectroscopy. The functionalized silicates showed the characteristic absorbance peaks of biotin's aliphatic groups after extensive washing and decantation through centrifugation (see Figure 3.1).

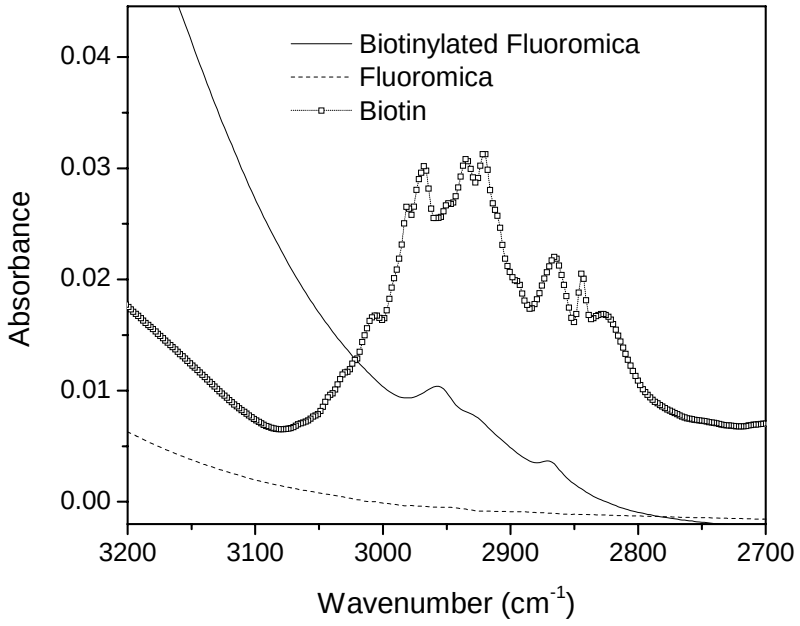

Figure 3.1: IR spectra for pristine silicate (fluoromica), biotin, and biotinylated fluoromica. The characteristic absorption peaks of alkyl groups can be seen in the biotinylated fluoromica between 2980 and 2850 cm^{-1}.

The maximum loading of enzyme on the support was approximately 1 wt.%. A sketch of the immobilized enzyme on a biotinylated silicate is shown in Figure 3.2.

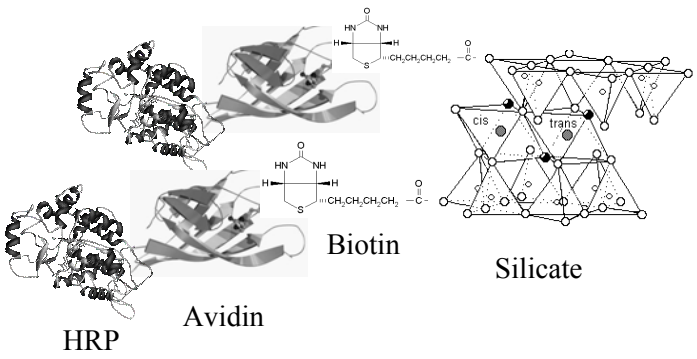

Figure 3.2: A schematic of the HRP-Avidin conjugate immobilized on a biotinylated silicate (not in scale). The pictures for the protein structures where obtained through the protein databank PDB.[34]

In the case of Horseradish Peroxidase-Avidin conjugate (HRP), the activity retention for the immobilized enzyme was close to 95 % when compared to the native enzyme. All data presented for the native enzyme are based on the Avidin conjugate of HRP. However, the activities of commercial HRP enzymes with or without Avidin conjugation are comparable (a few hundreds of units per mg of enzyme). In Figure 3.3, the storage stability at room temperature of the immobilized HRP is presented. The results were almost identical when compared to the native enzyme conjugate after 34 days. Furthermore, the pH behavior of the immobilized and native enzyme followed the same bell-curve behavior with an optimal value of pH 7 (see Figure 3.4). However, the immobilized HRP and GOx appeared to have improved thermal behavior at elevated temperatures when compared to their native forms.

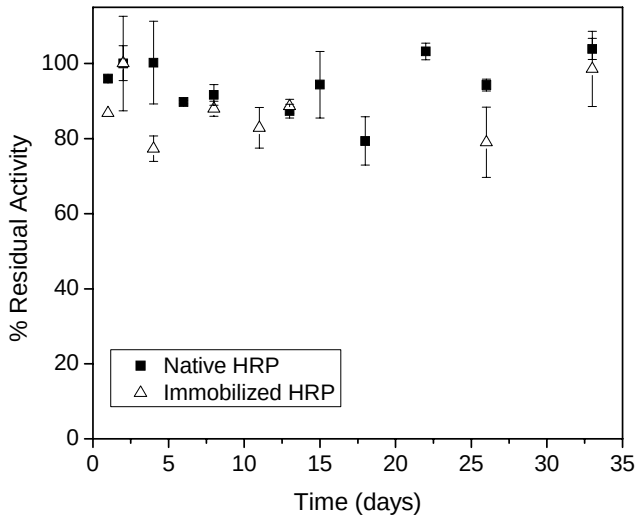

Figure 3.3: Storage stability at room temperature for the native and immobilized HRP-Avidin conjugate.

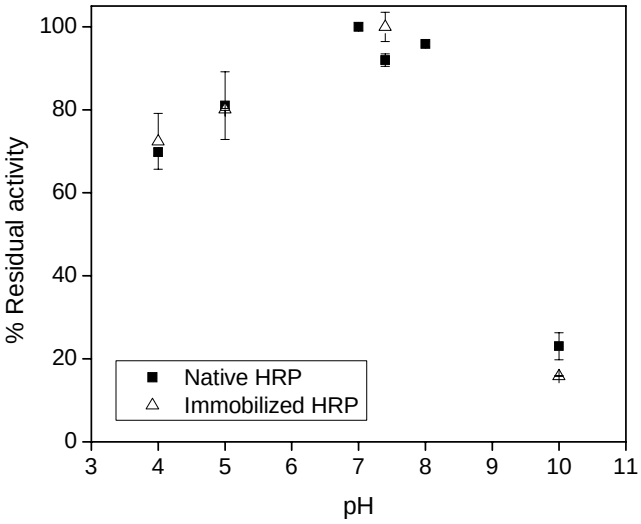

Figure 3.4: Enzymatic activity at different pH environments for immobilized HRP on biotinylated silicates and native HRP.

Horseradish Peroxidase

Horseradish Peroxidase is a heat-stable enzyme that denatures at temperatures over 76 ºC. The enzyme retains most of its catalytic activity for temperatures below 70 ºC [35,36] and due to enzyme's thermal stability, its apparent activity increases with increasing temperature. This is a well-documented phenomenon and chemical reaction rates approximately double for every 10 ºC increase. The behavior of HRP is illustrated in Figure 3.5, where the normalized activities of the native and immobilized enzymes are plotted as a function of temperature.

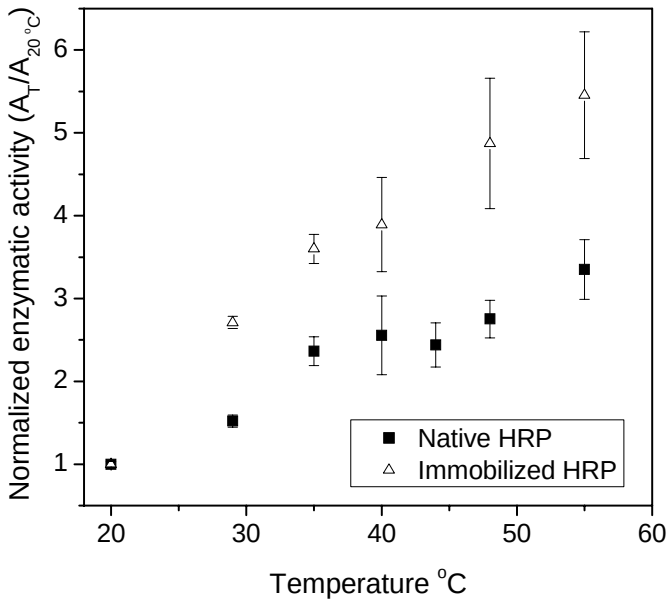

Figure 3.5: Apparent activity increase with temperature for native and immobilized HRP. The enzymatic activity was normalized with the activity at 20 ºC and was plotted as a function of temperature. The activity of native HRP at 20 ºC is 142 U/mg and of the immobilized HRP under the same conditions, 137 U/mg.

In Figure 3.5, the activity increase for the immobilized enzyme with temperature is more pronounced when compared to the native enzyme. We suspected that the temperature dependence was due to the improved stability of the immobilized HRP. To investigate the above hypothesis, the evolution of the residual activity of the two forms of HRP at elevated temperatures was plotted. The residual activity of both enzymes in a period of 70 minutes is plotted in Figure 3.6. The residual activity of both native and immobilized enzymes was found to be almost identical when heated at 66 ºC and measured again at 25 ºC.

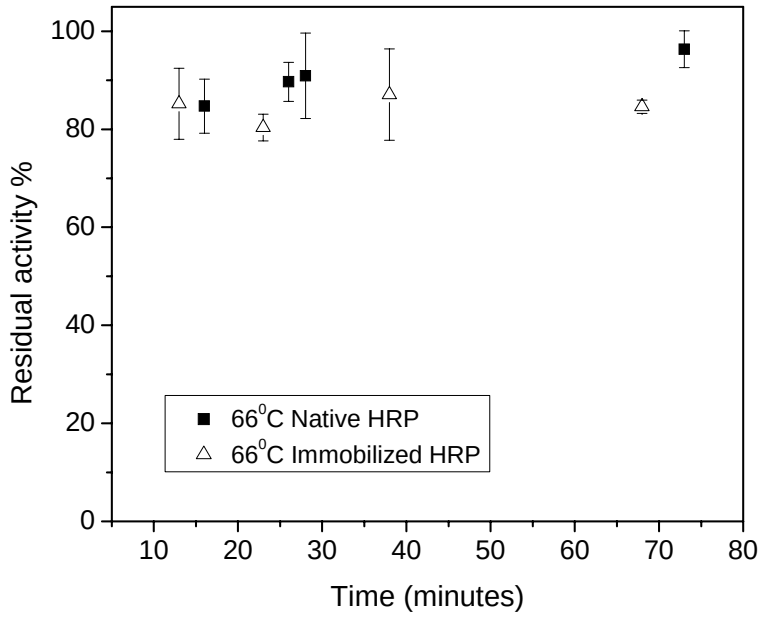

Figure 3.6: Residual activity of native and immobilized HRP at 66 ºC during a period of 70 minutes.

The above results prompted further investigation for the apparent enhanced performance and further study of the enzymatic mechanism was undertaken. Michaelis-Menten kinetics were assumed for both native and immobilized enzymes. Multiple experiments with different substrate concentrations were performed at

different temperatures in order to obtain Michaelis-Menten kinetics plots (see Figure 3.7). Through linear fitting, we obtained values for the kinetic parameters of the native and immobilized enzymes. The kinetic data calculated from the Lineweaver-Burk graphs were also in agreement with the values calculated from fitting the data in the classical exponential form.

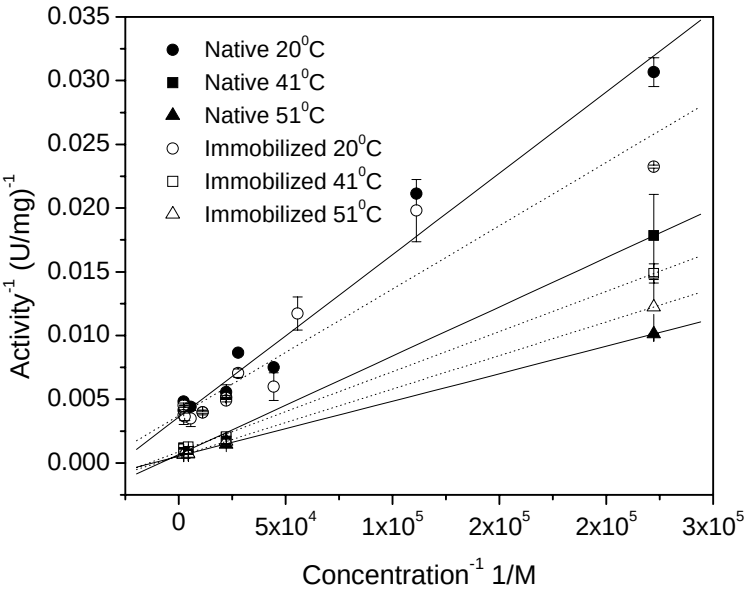

Figure 3.7: Lineweaver-Burk activity representations for the native and immobilized enzyme at 20 ºC, 41 ºC and 51 ºC. The kinetic parameters K_m and V_{max} can be extracted by fitting the data to a line.

Assuming Arrhenius behavior, the logarithm of K_m as a function of the inverse of temperature was plotted as shown in Figure 3.8, in order for the values of the pre-exponential factor, A, and the activation energy, E_A, to be obtained. A summary of these values and parameters are listed in Table 3.1. The activation energy for the immobilized enzyme is doubled but the pre-exponential factor increases significantly compared to the native HRP.

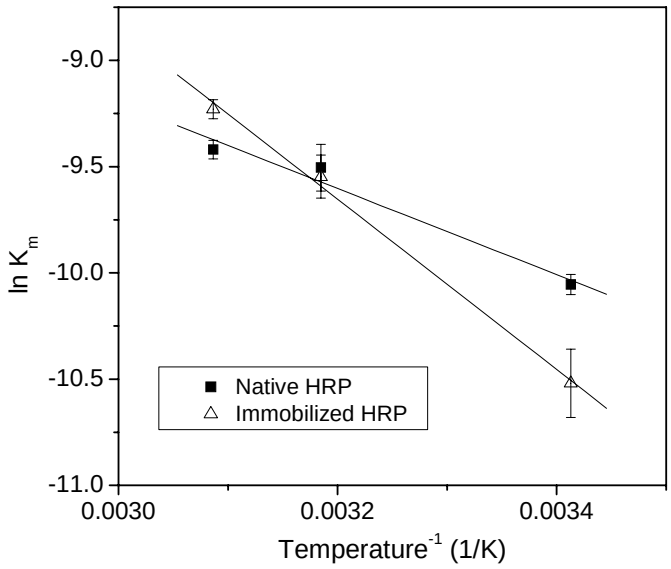

Figure 3.8: Arrhenius behavior of the experimental kinetic parameters for the immobilized and native enzyme conjugates

The above results suggest that the immobilized enzyme was altered in a way that, even though the activation energy for the reaction was larger by a factor of two, the pre-exponential factor increased more. This resulted in higher activity for the immobilized enzyme at higher temperatures compared to the native enzyme.

Glucose Oxidase

Avidin-Glucose Oxidase conjugate was also immobilized on biotin functionalized layered silicates. The activity retention in the case of immobilized glucose oxidase (GOx) was almost 70 % at 20 ºC and pH 7 when compared to the native GOx (GOx-Avidin conjugate).

Table 3.1: Summary of experimental kinetic parameters for the immobilized and native HRP-Avidin conjugate. Calculated activation energies and pre-exponential factors, assuming Arrhenius behavior, are also listed.

	K_m (M) at 20 ºC	K_m (M) at 41 ºC	K_m (M) at 51 ºC	A (M)	E_a (KJ/mol)
Native HRP	$4.3 \cdot 10^{-5} \pm 2.1 \cdot 10^{-6}$	$7.4 \cdot 10^{-5} \pm 8.2 \cdot 10^{-6}$	$8.1 \cdot 10^{-5} \pm 3.2 \cdot 10^{-6}$	0.04 ± 0.03	16.8 ± 2.9
Immobilized HRP	$2.7 \cdot 10^{-5} \pm 4.3 \cdot 10^{-6}$	$7.1 \cdot 10^{-5} \pm 7.2 \cdot 10^{-6}$	$9.8 \cdot 10^{-5} \pm 4.4 \cdot 10^{-6}$	23 ± 2.9	33.3 ± 1.9

Similarly to HRP, an improved catalytic behavior at higher temperatures was observed for GOx. In Figure 3.9, the immobilized GOx retained 65 % of its activity at 58 ºC while in the case of the native enzyme only 20 % of the enzymatic activity was still present under the same conditions.

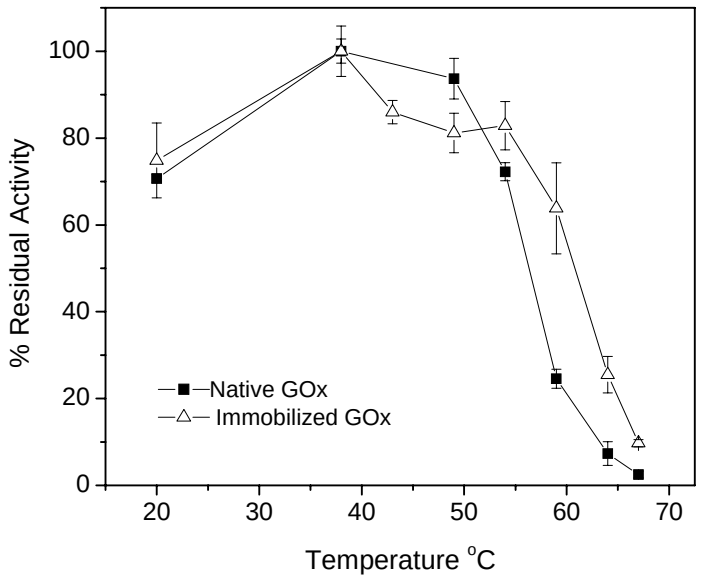

Figure 3.9: Residual activity of the immobilized and native GOx-Avidin conjugate at pH 7 as a function of temperature.

Improved catalytic behavior of the immobilized GOx enzyme was also observed at different pH environments. In particular, the immobilized GOx retained 35 % of its activity compared to 15 % for the native enzyme at 20 ºC and pH 4. Furthermore, in a basic environment (pH 10) the immobilized GOx retained 20 % of its activity where the native enzyme under the same conditions retained only 5 % of its initial enzymatic activity.

CONCLUSIONS

We have presented a versatile immobilization approach for avidinylated enzymes on biotin modified layered silicates with the biotin-Avidin moiety serving as the spacer between the inorganic particles and enzyme. The immobilized enzymes retained high levels of activity compared to the native enzymes and showed improved thermal behavior. In addition, immobilized GOx at various pH environments showed enhanced activity when compared to the native form. This simple one-step immobilization approach could find applications (such as non aqueous enzymatic catalysis) in various fields.

REFERENCES

1. Kirk, O., Borchert, T. V. & Fuglsang, C. C. Industrial Enzyme Applications. *Current Opinion in Biotechnology* **13**, 345-351 (2002).

2. Kim, J., Grate, J. W. & Wang, P. Nanostructures for Enzyme Stabilization. *Chemical Engineering Science* **61**, 1017-1026 (2006).

3. Clark, D. S. Can Immobilization Be Exploited to Modify Enzyme-Activity. *Trends in Biotechnology* **12**, 439-443 (1994).

4. Torrey, S. *Enzyme Technology, Preparation, Purification, Stabilization, Immobilization: Recent Advances* (Noyes Data Corp., Park Ridge, N.J., 1983).

5. Bickerstaff, G. F. *Immobilization of Enzymes and Cells* (Humana Press, Totowa, N.J., 1997).

6. Bornscheuer, U. T. Immobilizing Enzymes: How to Create More Suitable Biocatalysts. *Angewandte Chemie-International Edition* **42**, 3336-3337 (2003).

7. Katz, E. & Willner, I. Integrated Nanoparticle-Biomolecule Hybrid Systems: Synthesis, Properties, and Applications. *Angewandte Chemie-International Edition* **43**, 6042-6108 (2004).

8. Niemeyer, C. M. Nanoparticles, Proteins, and Nucleic Acids: Biotechnology Meets Materials Science. *Angewandte Chemie-International Edition* **40**, 4128-4158 (2001).

9. Patil, A. J., Muthusamy, E. & Mann, S. Synthesis and Self-Assembly of Organoclay-Wrapped Biomolecules. *Angewandte Chemie-International Edition* **43**, 4928-4933 (2004).

10. Luckarift, H. R., Spain, J. C., Naik, R. R. & Stone, M. O. Enzyme Immobilization in a Biomimetic Silica Support. *Nature Biotechnology* **22**, 211-213 (2004).

11. Shen, S. Y. & Tu, S. I. Immobilization of Horseradish Peroxidase in Cross-Linked Phyllosilicates: Conditions and Characterizations. *Biotechnology and Applied Biochemistry* **29**, 185-189 (1999).

12. Cao, L. *Carrier-Bound Immobilized Enzymes: Principles, Applications and Design* (Wiley-VCH, Weinheim, 2005).

13. Lei, C. H., Shin, Y. S., Liu, J. & Ackerman, E. J. Entrapping Enzyme in a Functionalized Nanoporous Support. *Journal of the American Chemical Society* **124**, 11242-11243 (2002).

14. Dyal, A., Loos, K., Noto, M., Chang, S. W., Spagnoli, C., Shafi, K. V. P. M., Ulman, A., Cowman, M. & Gross, R. A. Activity of Candida Rugosa Lipase Immobilized on Gamma-Fe_2O_3 Magnetic Nanoparticles. *Journal of the American Chemical Society* **125**, 1684-1685 (2003).

15. Reetz, M. T., Zonta, A. & Simpelkamp, J. Efficient Heterogeneous Biocatalysts by Entrapment of Lipases in Hydrophobic Sol-Gel Materials. *Angewandte Chemie-International Edition in English* **34**, 301-303 (1995).

16. Liao, M. H. & Chen, D. H. Immobilization of Yeast Alcohol Dehydrogenase on Magnetic Nanoparticles for Improving Its Stability. *Biotechnology Letters* **23**, 1723-1727 (2001).

17. Dick, W. A. & Tabatabai, M. A. Kinetics and Activities of Phosphatase-Clay Complexes. *Soil Science* **143**, 5-15 (1987).

18. Sarkar, J. M., Leonowicz, A. & Bollag, J. M. Immobilization of Enzymes on Clays and Soils. *Soil Biology & Biochemistry* **21**, 223-230 (1989).

19. Garwood, G., Mortland, M. M. & Pinnavaia, T. J. Enzyme Intercalation and Catalytic Activity in Layered Silicates-Glucose Oxidase. *Abstracts of Papers of the American Chemical Society* **175**, 133-133 (1978).

20. Morgan, H. W. & Corke, C. T. Release of Flavine Adenine-Dinucleotide on Adsorption of Enzyme Glucose Oxidase to Clays. *Canadian Journal of Microbiology* **23**, 1109-1117 (1977).

21. Morgan, H. W. & Corke, C. T. Adsorption, Desorption, and Activity of Glucose Oxidase on Selected Clay Species. *Canadian Journal of Microbiology* **22**, 684-693 (1976).

22. Cosnier, S., Lambert, F. & Stoytcheva, M. A Composite Clay Glucose Biosensor Based on an Electrically Connected Hrp. *Electroanalysis* **12**, 356-360 (2000).

23. Huang, Q. Y., Shindo, H. & Goh, T. B. Adsorption, Activities and Kinetics of Acid-Phosphatase as Influenced by Montmorillonite with Different Interlayer Material. *Soil Science* **159**, 271-278 (1995).

24. Chhonkar, P. K. & Tarafdar, J. C. Degradation of Clay-Enzyme Complexes by Soil-Microorganisms. *Zentralblatt Fur Mikrobiologie* **140**, 471-474 (1985).

25. Boyd, S. A. & Mortland, M. M. Urease Activity on a Clay-Organic Complex. *Soil Science Society of America Journal* **49**, 619-622 (1985).

26. Giannelis, E. P. Polymer Layered Silicate Nanocomposites. *Advanced Materials* **8**, 29-& (1996).

27. Bergaya, F. & Lagaly, G. Surface Modification of Clay Minerals. *Applied Clay Science* **19**, 1-3 (2001).

28. Hackett, E., Manias, E. & Giannelis, E. P. Molecular Dynamics Simulations of Organically Modified Layered Silicates. *Journal of Chemical Physics* **108**, 7410-7415 (1998).

29. Bindhu, L. V. & Abraham, T. E. Preparation and Kinetic Studies of Surfactant-Horseradish Peroxidase Ion Paired Complex in Organic Media. *Biochemical Engineering Journal* **15**, 47-57 (2003).

30. Kamyshny, A., Trofimova, D., Magdassi, S. & Levashov, A. Native and Modified Glucose Oxidase in Reversed Micelles. *Colloids and Surfaces B-Biointerfaces* **24**, 177-183 (2002).

31. Klibanov, A. M. Improving Enzymes by Using Them in Organic Solvents. *Nature* **409**, 241-246 (2001).

32. Hou, C. T. *Handbook of Industrial Biocatalysis* (Taylor & Francis/CRC, Boca Raton, FL, 2005).

33. Worthington Biochemical Corporation. *Worthington Enzyme Manual: Enzymes, Enzyme Reagents, Related Biochemicals* (Worthington Biochemical Corp., Freehold, N.J., 1972).

34. Berman, H. M., Westbrook, J., Feng, Z., Gilliland, G., Bhat, T. N., Weissig, H., Shindyalov, I. N. & Bourne, P. E. The Protein Data Bank. *Nucleic Acids Research* **28**, 235-242 (2000).

35. Chattopadhyay, K. & Mazumdar, S. Structural and Conformational Stability of Horseradish Peroxidase: Effect of Temperature and pH. *Biochemistry* **39**, 263-270 (2000).

36. Veitch, N. C. Horseradish Peroxidase: A Modern View of a Classic Enzyme. *Phytochemistry* **65**, 249-259 (2004).

CHAPTER 4: A NANOHYBRID MEMBRANE WITH LIPID BILAYER-LIKE PROPERTIES UTILIZED AS A CONDUCTIMETRIC SACCHARIN SENSOR.

INTRODUCTION

In the last few years, there has been an unprecedented interest in the development of analytical devices for the detection and monitoring of various biological and chemical analytes. For several decades analytical chemists were inspired from the biological sciences. One of the most important models was the cell, whose specificity and sensitivity made it the ideal sensor. All of the communications of the cell with the outside world materialize on its surface consisting of the cell lipid bilayer and integrated proteins. Inspired by the above example, the number of publications related to lipid films as sensors and biosensors has grown considerably.[1] A review article in 2001 listed 122 articles using Bilayer Lipid Membranes (BLMs) in analytical applications[2] and in 2000 the first book focused on biomimetic sensor technologies was published.[3]

One of the major disadvantages in adopting this technology is that freely suspended BLMs are mechanically fragile and unsuitable for most practical applications. However, in the last few years supported BLMs were used on metal surfaces (solid-supported), in polymer matrices (gel-supported) or deposited on porous membranes (filter-supported).[1,2,4] Even though the above modifications improved the stability of BLMs, they didn't resolve the problem and most of these had a lifetime of only hours or days.

There are two distinct areas of sensing applications based on either modified or unmodified BLMs. The term "modified" signifies a BLM where an enzyme, antibody, receptor protein or DNA probe were immobilized while "unmodified" describes a

BLM "as-is", where the sensing ability originates from the interaction of the analyte with the lipid bilayer alone, and no specific binding or chemical reaction is taking place. In literature, various molecules were reported to interact with unmodified BLMs and sensing devices have been realized.[4-12] On the other hand, layered silicates have been utilized in numerous applications and their versatile properties[13,14] were exploited by a large number of researchers in the fields of materials science, environmental applications and elsewhere.[15-21]

In this work, we utilized an alternative approach to a more stable nanohybrid membrane that served as a robust and fast sensor. Modeling the lipid bilayer structure, an inorganic layered silicate and amphiphilic molecules were combined to obtain a nanohybrid membrane with BLM-like structure. To evaluate the membrane's sensing capability we developed a sensing platform that utilized the nanohybrid membrane as the recognition element. The sensing capability was evaluated using saccharin as the analyte, a suspected carcinogen molecule already proven to interact with unmodified BLMs in a sensor setup.[12,22] Impedance Spectroscopy (IS) was employed to monitor the electrical properties changes of the membrane due to analyte exposure and microfabricated Interdigitated Electrodes (IDEs) were utilized to enhance the sensitivity of the device.

MATERIALS AND METHODS

A synthetic layered silicate, Somasif ME-100 (Na+-Fluoromica or FM), with a cation exchange capacity (CEC) of 120 mequiv/100 g was obtained from CO-OP Chemical LTD. Dihexadecyl-dimethylammonium bromide and didodecyl-dimethylammonium bromide were obtained from Sigma-Aldrich. Deionized water was used throughout the measurements (Barnstead Nanopure RO, 18 MΩcm resistivity). Saccharin, glucose and sucrose (>98 %) were obtained from Sigma-

Aldrich. The buffer solution was obtained from Fisher Scientific and was a pH 7, 10 mM potassium phosphate monobasic and sodium hydroxide solution. All other materials and solvents were ACS grade.

Powder X-Ray Diffraction (PXRD) spectra were collected on a Scintag Inc θ-θ diffractometer using CuK_{α} source radiation and a germanium detector. Modulated differential scanning calorimetry (MDSC) was performed under nitrogen on a TA instruments DSC Q1000 series, with a scanning rate of 3 ºC/min and modulation of ±1 ºC/min. The percent of organic content in the material was estimated Thermo-Gravimetrically (TGA) from the weight loss associated with decomposition. The latter analyses were carried out under an 80 mL/min flow of nitrogen on a TG/DTA 320 S.I. instrument at 10 ºC/min rate. Contact angle measurements were performed on an apparatus equipped with an x-y-z controlled stage and a microscope positioned parallel to the stage plane. The angle was read through the microscope by a scale built inside the optical tube. The measurements were realized by adding 2.5 mL of a solution with different concentrations on a previously cast nanohybrid membrane. Scanning electron microscopy (SEM) was performed on a LEICA 440 SEM instrument. An Energy Dispersive X-Ray Spectrometer (SEM-EDS) JEOL 8900 EPMA Microprobe was utilized for quantitative elemental analysis. The utilized beam ranged from 15 KV to 25 KV. Fourier Transform Infra-Red (FTIR) spectroscopy was performed in a Mattson Galaxy 2020 IR spectrometer. The samples were prepared by mixing and grinding with potassium bromide in a mortar and pestle, and finally pressed into a pellet using a hydraulic press. The FTIR spectra were obtained under a nitrogen flow in the sample chamber.

Interdigitated Electrodes (IDEs) microfabrication.

Multiple sensors/IDEs with Pt electrodes were fabricated on silicon using facilities at the Cornell Nanoscale Science and Technology Facility (CNF). The design was done in CAD and a mask was patterned on a GCA/Mann 3600F Pattern Generator. On a 4" silicon substrate wafer, 10 μm SiO_2 layer was deposited using a GSI PECVD tool, and UV resist, Shipley 1813, was patterned on a GCA-6300 5x g-line stepper. A stack of 5 nm of Cr and 50 nm of Pt layers were deposited in an e-beam evaporator CVC SC4500. An array of fourteen IDEs/sensors was deposited on a single wafer and was cut into fourteen single sensors using a diamond knife. The IDE's characteristic lengths were 20 μm wide Pt electrodes with 20 μm inter-electrode spacing. The electrode fingers were 3.8 mm long and each sensor had 100 fingers. The scanning area was 0.076 cm^2. The contact pads were part of the design and contact for electrical measurements was realized through copper clips.

Synthesis of the nanohybrid membrane.

The nanohybrid membrane was synthesized by a cation exchange reaction between the layered host and excess alkylammonium cations (1.5 times the cation exchange capacity). The quaternary ammonium cations were dissolved in a 1:1 mixture of ethanol and deionized water at 60-70 ºC. A 1 wt.% aqueous suspension of the host was added to the alkylammonium solution and the mixture was stirred for 24 hours at 60-70 ºC. The modified silicate was collected by filtration and was subsequently washed with a mixture of hot ethanol and deionized water three times. In addition, the filter cake was washed in a soxhlet apparatus with ethanol overnight to remove any remaining alkylammonium salt. Once the filter cake was dried overnight under vacuum and 60 ºC, the white solid was grinded at 14000 rpm using an 80 μm mesh in a Glen Mills Inc centrifugal grinder. 2C12FM and 2C18FM correspond to

didodecyldimethylammonium and dihexadecyldimethylammonium exchanged silicate respectively.

Sensing experimental setup

To evaluate the sensing capability of the nanohybrid membrane, thin films were formed on IDEs by evaporating 20 μL of 4 wt.% modified silicate suspensions in toluene. The cast membranes were dried at room temperature for several hours. The thickness of the membranes measured by SEM was 7±1 μm. The IDEs/membranes were immersed in a beaker of 100 mL pH 7 buffered stirred solutions. The response of different analyte concentrations was measured by standard addition of aliquots of analyte to the beaker. The temperature during the experiments was kept at room temperature unless otherwise specified. To evaluate the electrical properties of the membrane, an Impedance Spectrometer HP 4192A controlled by a PC and Labview® software was used. Measurements were done using a two-electrode setup applying a 10 mV amplitude AC voltage while measuring the current passing through the IDE and the phase angle. The Spectrometer had an option of measuring the impedance modulus and the phase angle while sweeping frequencies from 5 Hz to 13 MHz or evaluating conductance at a set frequency and registering the changes with time. The latter was used extensively for all the sensing measurements; however, frequency sweeps were also obtained to identify the equivalent circuit of our setup and to decide the value of the optimum frequency where all further experiments were performed.

Equivalent circuit investigation

The equivalent circuit investigation of the IDEs and IDEs with deposited membranes were based on previously published work.[23,24] The equivalent circuit suggested in literature and adopted in this work is shown in Figure 4.1. The capacitor C_{di} is the dielectric capacitance over the plane of the electrodes, the capacitors C_{DL} are

the double layer capacitances formed in the vicinity of the electrodes and R_{sol} is the resistance of the solution over the plane of the electrodes. To validate the circuit proposed and estimate the values of the circuit elements, impedance spectra were obtained and fitted by LEVMW v.8 software using complex nonlinear least squares. The software was made available by Prof R. Macdonald and Solarton Group ltd. To obtain a calibration curve various concentrations of KCl solutions were used and the R_{sol} was measured. The result was a conductivity-conductance calibration graph for the IDEs (see Figure 4.2). The calibration curve was in agreement with an analogous curve presented in literature using a two-electrode technique and an IDE with similar geometry.[25]

The spectra of IDEs with the membranes deposited were similar and the equivalent circuit already discussed held where the R_{sol} of the circuit was the resistance of the hydrated membrane. Based on impedance spectra, the frequency of 1 KHz was chosen for the sensing experiments in order to minimize the noise and achieve a relatively large magnitude component for the real vector on the Nyquist plot complex plane.

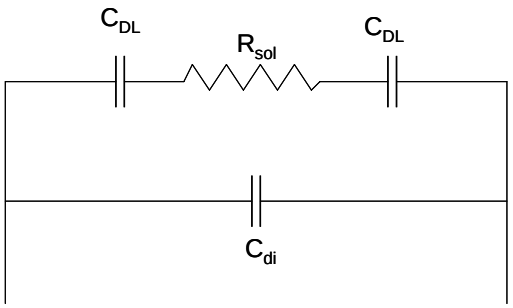

Figure 4.1: Equivalent circuit for the IDEs utilized in this work.

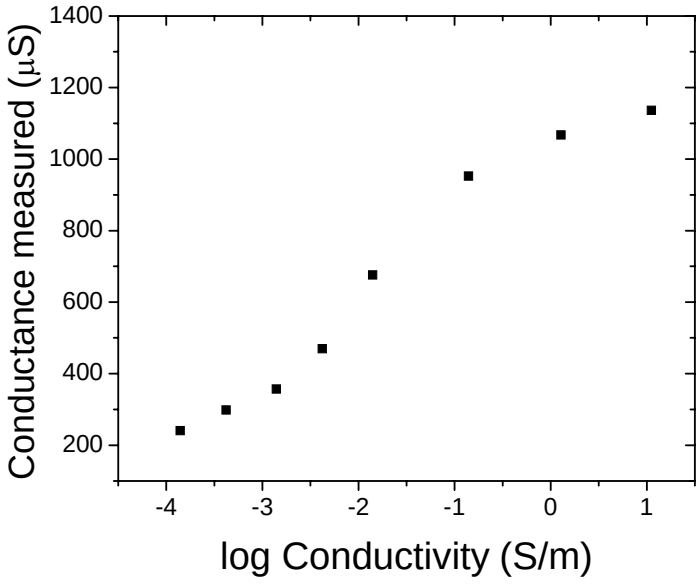

Figure 4.2: Calibration curve of the IDEs utilizing various concentrations of KCl of known conductivities. This graph was utilized to transform the conductance values of the experimental setup into conductivity values.

RESULTS AND DISCUSSION

Characterization of the Nanohybrid Membrane.

Didodecyldimethylammonium bromide modified fluoromica (2C12FM) and dihexadecyldimethylammonium bromide modified fluoromica (2C18FM) were fine, white, highly hydrophobic powders, dispersable in solvents like toluene and chloroform. To evaluate the modification success, Powder X-ray diffraction (PXRD) was employed and the results are plotted in Figure 4.3. The pristine silicate had a gallery d-spacing of 0.9 nm, this peak disappeared in the 2C18FM and 2C12FM modified silicate, whose galleries d-spacings became 3.3 and 2.4 nm accordingly (Figure 4.3).

Energy dispersive scanning electron (SEM-EDS) microscopy was used to calculate the extent of ion–exchange and intercalation in the nanohybrids. The results showed 72 % for 2C18FM and 69 % for 2C12FM based on the CEC value (120 mequiv/100 g) which corresponded to a calculated 38 % and 27 % organic content, respectively. The presence of unexchanged salt in the nanohybrid was less than 2 wt.% and Thermo-Gravimetric Analysis revealed an organic content of 41 % for 2C18FM and 32 % for 2C12FM, which were consistent with the above SEM-EDS results. The nanohybrids were suspended in toluene at 4 or 2 wt.% concentrations and cast to produce thin multi-bilayered membranes.

Nanohybrid Membranes: Analogies to Bilayer Membranes

Films formed by solvent casting consisted of a multi-bilayered membrane of several (hundreds) stacks of a few nanometer thick bilayers (see Figure 4.4). The resulting artificial membrane had many similarities with the two-leafed structure of the cell membrane. The membrane consisted of bilayers with defined hydrophobic and hydrophilic areas and overall thickness that varied between 1.5 and 3 nm depending on the amphiphile utilized. The silicate served as host and template for the bilayer formation of the amphiphilic molecules inside the inter-layer gallery. The amphiphiles simulate the phospholipids (Figure 4.4 and 4.3) with the hydrophobic alkyl chains and the charged head groups (the ammonium group in this case). The result was a very stable and robust membrane that withstood large variations of pH and temperature up to 200 ºC without losing its properties.

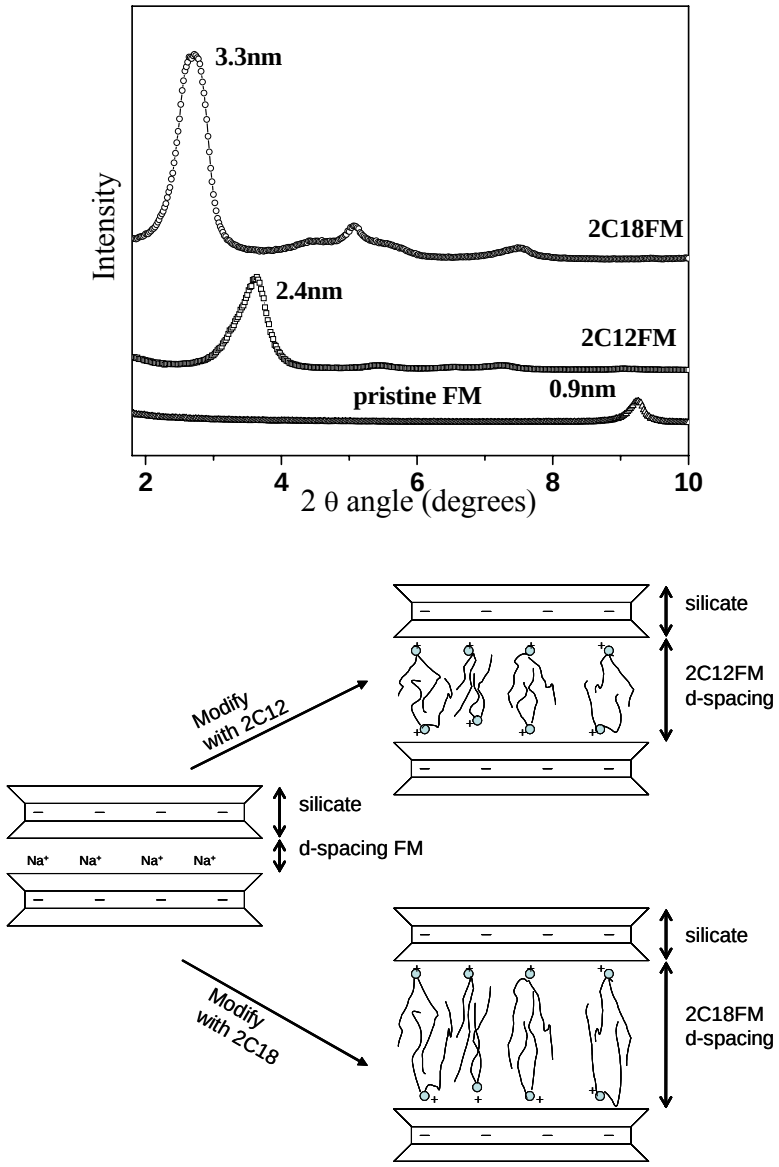

Figure 4.3: X-ray diffraction spectra of the pristine and the ion-exchanged silicate host with two different amphiphiles. Also a schematic of the modification is shown.

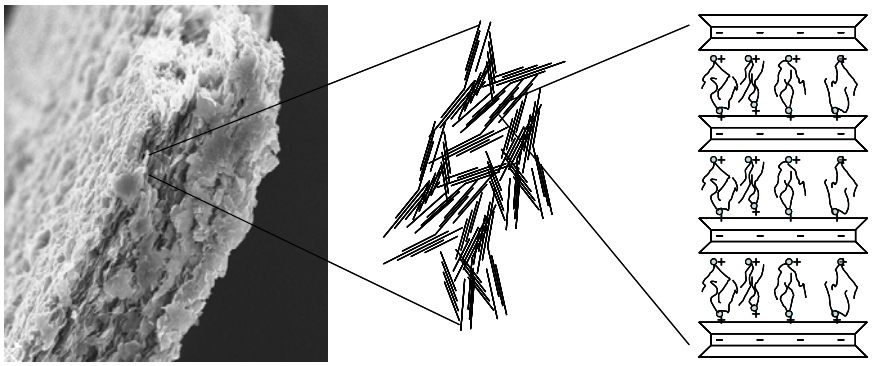

Figure 4.4: SEM picture of a nanohybrid membrane. Also a sketch of three bilayers is displayed; multi-stacks of these bilayers form the nanohybrid membrane. In the sketch, the beads represent the hydrophilic groups and the long lines the hydrophobic alkyl chains. The planes represent the silicate layers.

Lipid bilayer membranes are known to have three major thermotropic phases: the L_β phase, where the alkyl chains are in a rather ordered state also called the 'gel' phase, the L_α phase, where the alkyl chains adopt a more fluid-like character, also called the 'liquid crystalline' phase, and an in-between L_o phase, which rises from the presence of cholesterol in the lipid bilayer membrane.[26-30] A phase diagram of these three phases was reported in the phosphatidylcholine-cholesterol system.[29] Similarly, the nanohybrid membrane exhibited 1st order thermal transitions that correspond to the "melting" of an ordered gel phase to a more disordered liquid crystalline phase.

Furthermore, cholesterol was integrated in the nanohybrid membrane by mixing a suspension of 2C18FM or 2C12FM in toluene with a cholesterol-chloroform solution. After casting of the membrane, we expected cholesterol integration in the gallery and alignment with the ammonium ions due to the amphiphilic character of cholesterol. Evidence of cholesterol integration was obtained by FTIR and PXRD. In Figure 4.5 the d-spacing expansion of the interlayer gallery due to the integration of cholesterol is plotted. Similar data were reported previously in the dipalmitoyl-L-lecithin, cholesterol and water system.[31]

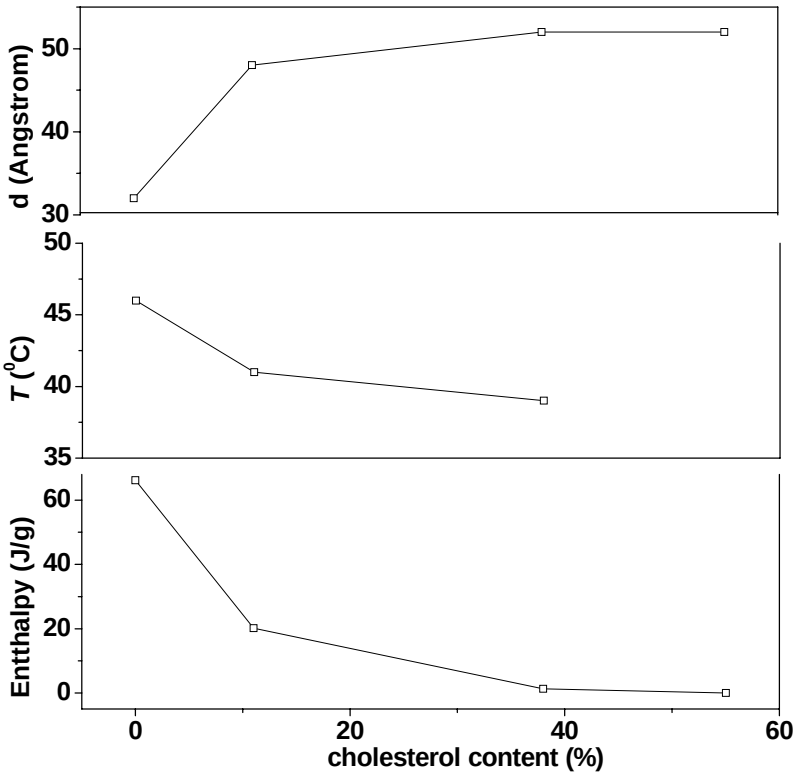

Figure 4.5: Summary of the results utilizing PXRD and MDSC to probe the effect of cholesterol on the nanohybrid membrane. The top graph is the d-spacing of the silicate interlayer gallery (note that in the values reported the 9 Å of the silicate thickness is included). The middle graph is the temperature where the transition peak is observed and finally, the bottom is the integration value of the peak corresponding to the enthalpy of the 1st order transition. The data are in agreement with previous results.[28]

To obtain an 11, 38 and 55 wt.% cholesterol content membranes, modified silicate and cholesterol solutions were made with 20:1, 4:1 and 2:1 weight ratios. MDSC investigations of the above cholesterol containing samples revealed similar decrease on the thermal transitions as with conventional lipid bilayer membranes and liposomes.[29-31] The MDSC curve for 55 wt.% cholesterol was identical with the 38 wt.% with no transition observed. It is important to note that beyond 38 wt.% (44 % mole) concentration, the presence of cholesterol crystals was verified by PXRD, suggesting that the membrane was saturated with cholesterol and the lipid bilayers were all in the L_o phase. The saturation concentration was previously reported at 34 wt.% (50 % mole) for the 1,2-dipalmitoyl-L-lecithin–cholesterol system.[28] Figure 4.5 summarizes results from several techniques to further characterize the effect of cholesterol on the nanohybrid membrane. MDSC experiments verified the shift of the transition temperature as well as the enthalpic magnitude of the transition with different cholesterol concentration (see Figure 4.6).

The nanohybrid membrane as a sensor.

In Figure 4.7 the response of 2C12FM membrane to saccharin is plotted. The response plot for 2C18FM is shown in Figure 4.8 with the main difference between the two the limit of detection and sensitivity that are lower in the latter. For all the experimental points used to produce the response graph, a new IDE and a newly cast nanohybrid membrane was employed. The structure of the analyte molecule is illustrated as an inset in Figure 4.7.

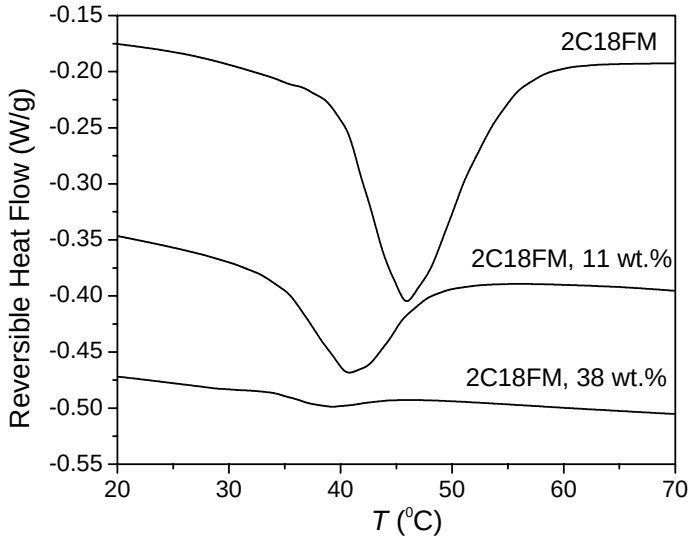

Figure 4.6: MDSC reversible heat fluxes of 2C18FM, containing 0 wt.%, 11 wt.% and 38 wt.% cholesterol with respect to the total organic content of the nanohybrid membrane.

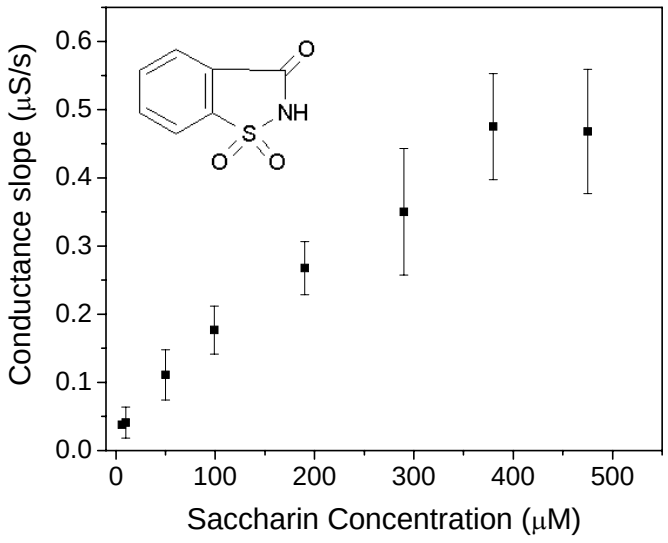

Figure 4.7: Sensing response of the 2C12FM nanohybrid membrane to the analyte. (Inset: the saccharin molecule)

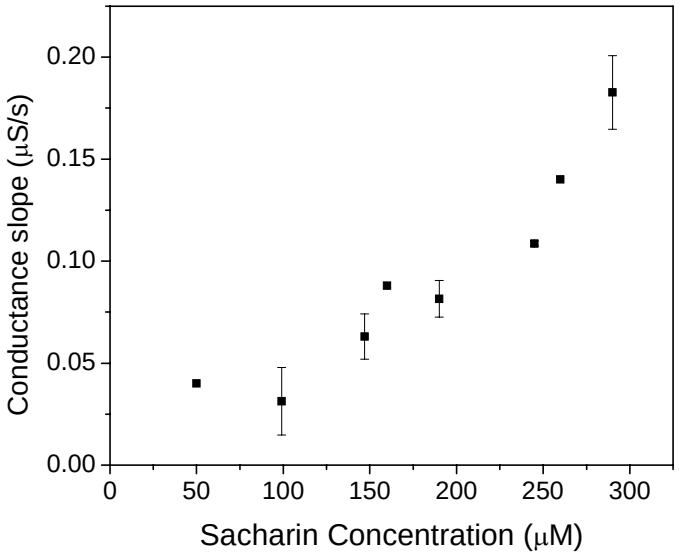

Figure 4.8: 2C18FM membrane response to saccharin.

The y-axis in Figures 4.7 and 4.8 are conductance slope μS/s and the justification of that selection is shown in Figure 4.9 where raw data of various

experiments are plotted. The dynamic range of the sensor was 20 μM to 400 μM and the lower limit of detection was 6 μM. The sensitivity of the sensor was 12 $nS \cdot s^{-1}$ per 10 μM of analyte and the error was ±16 μM. A summary of the specifications of our sensor together with properties of other reported saccharin sensors are included in Table 4.1 for comparison.[12,32,33]

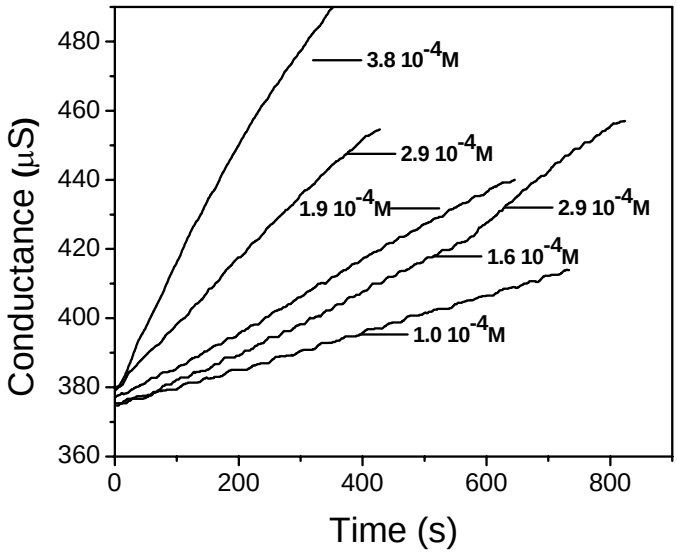

Figure 4.9: Response of the sensing setup to various saccharin concentrations. The second curve from the bottom had two slopes due to a second consecutive addition of analyte at t~550 sec.

Table 4.1: Summary of the characteristics of the sensor presented here with saccharin sensors reported in literature.

	Nanohybrid Membrane sensor	Capitan-Vallvey et al, [33]	Elmosallamy et al, [32]	Nikolelis et al, [12]
Transduction method	Conductimetric	Spectrophotometric	Potentiometric	Electrochemical
Recognition element	Artificial BLM	Sephadex G-25 solid column	Aliquat 336S-saccharinate ion pair in a PVC membrane	Surface stabilized BLM
Lower limit of detection	6 μM	5.5 μM	30 μM	0.3 μM
Dynamic Range	20 - 400 μM	5.5 - 1000 μM	50 μM - 0.1 M	0.4 -7 μM

To evaluate the selectivity of the sensor, the response of the setup to glucose and sucrose was investigated. Interference studies were done in a competitive study where both analyte and interference molecules were present at the same solution; no significant interference was observed. To further ensure the specificity of the response, a blank buffered solution was examined; glucose was consecutively added up to 250 μM following an addition of a saccharin aliquot that resulted to a membrane response as if glucose was absent.

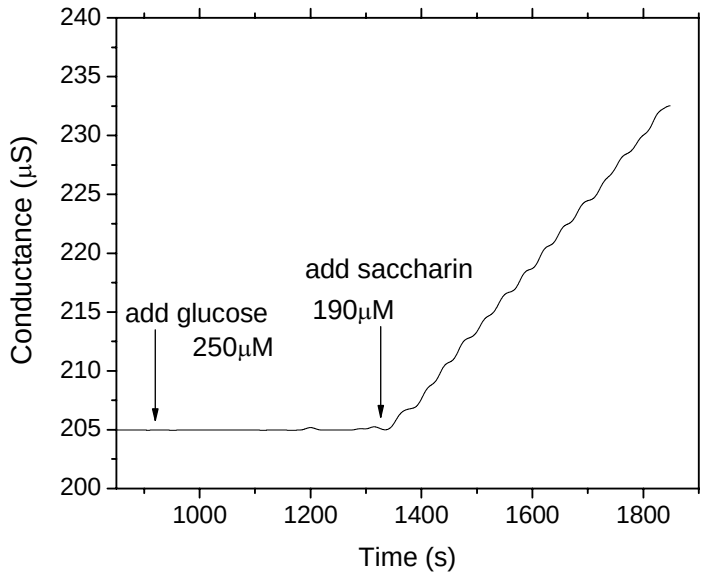

Figure 4.10: Data recording from an interference experiment showed no response to glucose. The addition of saccharin gave rise to the anticipated response.

Investigating the origin of the response.

To determine the mechanism of the response, we focused on the structural changes of the membrane caused by analyte exposure. MDSC, FTIR, PXRD and Contact Angle measurements were utilized to probe the origin of the response. Previous studies on supported BLMs found that exposure of a BLM to saccharin caused an increase to the hydrophilicity of the membrane; consequently more water

molecules could integrate and associate with the polar head groups of the membrane. An increase in hydrophilicity, apart from increasing permeation of ions, can also change the "effective area" of the head group of the amphiphile and the orientation/association of water; therefore, the electrostatic field at the surface of a membrane.[3,12,34-38]

Measurements with nanohybrid membranes revealed a decrease in the contact angle with increasing saccharin content. At 0.1 mM of saccharin the contact angle was 93 degrees, at 1 mM it was 77 and at 10 mM was 65. The decrease of the contact angle supported the suggestion that the membrane became more hydrophilic with increasing saccharin concentration exposure. A control experiment on an inert surface (Teflon) showed no dependence of the contact angle with different concentrations of saccharin.

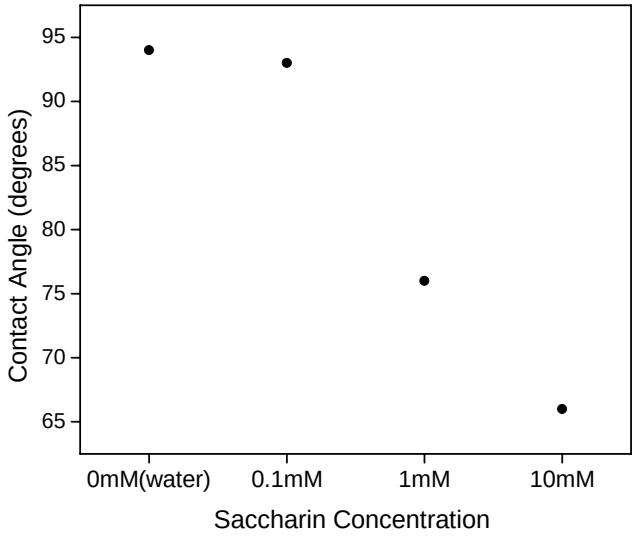

Figure 4.11: Contact angles of different concentration solutions of saccharin on a nanohybrid membrane.

To further examine the mechanism, four different samples were prepared to evaluate the changes of the membrane structure due to saccharin exposure.

Nanohybrid membranes were cast on a glass slide from a 4 wt.% toluene solution. After drying overnight at room temperature the membranes were exposed to a different saccharin concentration solution for 15 minutes. Finally, the membranes were dried and removed from the glass substrate for further analysis. PXRD scans showed that when exposed to a saccharin solution, the d-spacing of the bilayer increased by 5.7 Å (see Figure 4.12a).

The extent of this expansion was proportional to the concentration of the analyte. Given that the Van der Waals average diameter of a water molecule is approximately 2.8 Å the expansion came from the integration of water molecules in the lipid bilayer into the layered host justifying the 5.6 Å (2·2.8 Å) expansion.[39,40] From MDSC and FTIR investigations larger water content in samples C and D than samples A and B, were also observed.

To ensure that Saccharin entered the nanohybrid membrane and it was responsible for the observed signal, we employed FTIR spectroscopy to track the saccharin signature peaks in samples A, B, C and D. The spectra of the samples described above were obtained and plotted in Figure 4.12b. As it was expected the characteristic peaks of saccharin at 1580 and 1270 cm^{-1} were gradually appearing with increasing intensity for the membranes exposed to increasing analyte concentration. The ratio of the intensity at 1580 cm^{-1} over the intensity at 1469 cm^{-1} (1469 cm^{-1} is a characteristic peak of the membrane modifier C12) it was larger for samples C and D indicating that saccharin was present at higher concentrations in the membranes with increased exposure to saccharin. Furthermore, the characteristic peak of water at 1643 cm^{-1} also increased in intensity, an observation consistent with the hypothesis of water integration in the interlayer gallery of the nanohybrid membrane.

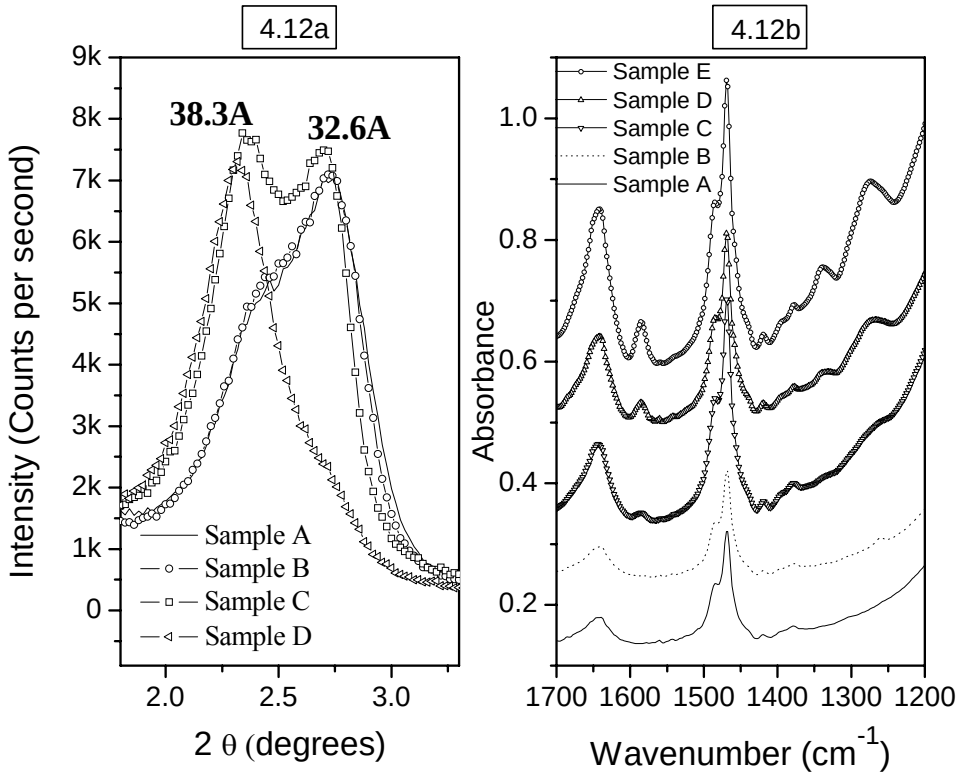

Figure 4.12: In Figure 4.12a, X-ray diffraction profiles are plotted for membranes exposed to increasing concentrations of analyte. In Figure 4.12b, FTIR spectra of the same membranes are shown. Sample A was exposed to water. Sample B was exposed to 0.1 mM of saccharin. Sample C was exposed to 1 mM of saccharin. Sample D was exposed to 10 mM of saccharin. All 4 samples were exposed to the above solutions for 15 minutes. Sample E is exposed to 10 mM of saccharin for 12 hours.

From the above observations, we concluded that the saccharin molecule entered the bilayers of the membrane, interacting with the polar groups of the lipid bilayers allowing water molecules to integrate into the nanohybrid membrane. These changes in membrane's hydrophilicity lead to the observed conductimetric response.

CONCLUSIONS

A stable artificial membrane and a sensor mimicking a lipid bilayer using a nanohybrid of an inorganic host and amphiphilic organic molecules were presented. The nanohybrid membrane exhibited two thermotropic phases corresponding to the L_α and L_β phases that lipid bilayer membranes are known to adopt. Integration of cholesterol molecules into the nanohybrid membrane lead to the same qualitative effect as in lipid bilayers, including expansion of the bilayer spacing and decrease of the L_α to L_β transition enthalpy. The nanohybrid membrane was used as a conductimetric sensor and its ability to sense saccharin molecules was evaluated. The lower limit of detection of the sensor was 6 μM and the dynamic range was from 20 μM to 400 μM. Our mimetic approach offers high stability, robustness and simple synthesis compared to other artificial membranes.

REFERENCES

1. Sackmann, E. Supported Membranes: Scientific and Practical Applications. *Science* **271**, 43-48 (1996).

2. Trojanowicz, M. Miniaturized Biochemical Sensing Devices Based on Planar Bilayer Lipid Membranes. *Fresenius Journal of Analytical Chemistry* **371**, 246-260 (2001).

3. Toko, K. *Biomimetic Sensor Technology* (Cambridge University Press, Cambridge, UK; New York, 2000).

4. Nikolelis, D. P., Hianik, T. & Krull, U. J. Biosensors Based on Thin Lipid Films and Liposomes. *Electroanalysis* **11**, 7-15 (1999).

5. Kumazawa, T., Nomura, T. & Kurihara, K. Liposomes as Model for Taste Cells - Receptor-Sites for Bitter Substances Including N-C=S Substances and Mechanism of Membrane-Potential Changes. *Biochemistry* **27**, 1239-1244 (1988).

6. Kumazawa, T., Sasaki, K., Nomura, T. & Kurihara, K. Receptor Mechanism of Bitter Substances - Characterization of Receptor-Sites and Mechanism of the Receptor Potential. *Chemical Senses* **12**, 509-509 (1987).

7. Nomura, T. & Kurihara, K. Effects of Changed Lipid-Composition on Responses of Liposomes to Various Odorants - Possible Mechanism of Odor Discrimination. *Biochemistry* **26**, 6141-6145 (1987).

8. Nomura, T., Sato, T. & Kurihara, K. Lipid Bilayer-Membrane as a Model for Olfactory Receptor Membrane - a New Model for Odor Discrimination. *Chemical Senses* **12**, 507-507 (1987).

9. Nomura, T. & Kurihara, K. Liposomes as a Model for Olfactory Cells - Changes in Membrane-Potential in Response to Various Odorants. *Biochemistry* **26**, 6135-6140 (1987).

10. Nomura, T. & Kurihara, K. Liposomes as a Model for Olfactory Cells and a Possible Mechanism of Odor Discrimination. *Journal of Pharmaceutical Sciences* **76**, S54-S54 (1987).

11. Nikolelis, D. P. & Krull, U. J. Direct Electrochemical Sensing of Insecticides by Bilayer-Lipid Membranes. *Analytica Chimica Acta* **288**, 187-192 (1994).

12. Nikolelis, D. P. & Pantoulias, S. A Minisensor for the Rapid Screening of Acesulfame-K, Cyclamate, and Saccharin Based on Surface-Stabilized Bilayer Lipid Membranes. *Electroanalysis* **12**, 786-790 (2000).

13. Bergaya, F. & Lagaly, G. Surface Modification of Clay Minerals. *Applied Clay Science* **19**, 1-3 (2001).

14. Lagaly, G. & Malberg, R. Disaggregation of Alkylammonium Montmorillonites in Organic-Solvents. *Colloids and Surfaces* **49**, 11-27 (1990).

15. Ozsoz, M., Erdem, A., Ozkan, D., Kerman, K. & Pinnavaia, T. J. Clay/Sol-Gel-Modified Electrodes for the Selective Electrochemical Monitoring of 2,4-Dichlorophenol. *Langmuir* **19**, 4728-4732 (2003).

16. Ozkan, D., Kerman, K., Meric, B., Kara, P., Demirkan, H., Polverejan, M., Pinnavaia, T. J. & Ozsoz, M. Heterostructured Fluorohectorite Clay as an Electrochemical Sensor for the Detection of 2,4-Dichlorophenol and the Herbicide 2,4-D. *Chemistry of Materials* **14**, 1755-1761 (2002).

17. Nennemann, A., Kulbach, S. & Lagaly, G. Entrapping Pesticides by Coagulating Smectites. *Applied Clay Science* **18**, 285-298 (2001).

18. Malberg, R., Dekany, I. & Lagaly, G. Short-Chain Alkylammonium Montmorillonites and Alcohols-Gas-Adsorption and Immersional Wetting. *Clay Minerals* **24**, 631-647 (1989).

19. Lagaly, G. Pesticide-Clay Interactions and Formulations. *Applied Clay Science* **18**, 205-209 (2001).

20. El-Nahhal, Y. Z. & Lagaly, G. Salt Effects on the Adsorption of a Pesticide on Modified Bentonites. *Colloid and Polymer Science* **283**, 968-974 (2005).

21. Billinge, S. J. L., McKimmy, E. J., Shatnawi, M., Kim, H. J., Petkov, V., Wermeille, D. & Pinnavaia, T. J. Mercury Binding Sites in Thiol-Functionalized Mesostructured Silica. *Journal of the American Chemical Society* **127**, 8492-8498 (2005).

22. Budavari, S. *The Merck Index: An Encyclopedia of Chemicals, Drugs, and Biologicals* (Merck, Whitehouse Station, NJ, 1996).

23. Van Gerwen, P., Laureyn, W., Laureys, W., Huyberechts, G., De Beeck, M. O., Baert, K., Suls, J., Sansen, W., Jacobs, P., Hermans, L. & Mertens, R. Nanoscaled Interdigitated Electrode Arrays for Biochemical Sensors. *Sensors and Actuators B-Chemical* **49**, 73-80 (1998).

24. Laureyn, W., Nelis, D., Van Gerwen, P., Baert, K., Hermans, L., Magnee, R., Pireaux, J. J. & Maes, G. Nanoscaled Interdigitated Titanium Electrodes for Impedimetric Biosensing. *Sensors and Actuators B-Chemical* **68**, 360-370 (2000).

25. Steinschaden, A., Adamovic, D., Jobst, G., Glatz, R. & Urban, G. Miniaturised Thin Film Conductometric Biosensors with High Dynamic Range and High Sensitivity. *Sensors and Actuators B-Chemical* **44**, 365-369 (1997).

26. Bender, J., Michaelis, W. & Schubert, R. Morphological and Thermal Properties of Vesicular Phospholipid Gels Studied by DSC, Rheometry and Electron Microscopy. *Journal of Thermal Analysis and Calorimetry* **68**, 603-612 (2002).

27. Ghosh, Y. K., Indi, S. S. & Bhattacharya, S. Thermal Lipid Order-Disorder Transitions in Mixtures of Cationic Cholesteryl Lipid Analogues and Dipalmitoyl Phosphatidylcholine Membranes. *Journal of Physical Chemistry B* **105**, 10257-10265 (2001).

28. Ladbrook, B., Williams, R. M. & Chapman, D. Studies on Lecithin-Cholesterol-Water Interactions by Differential Scanning Calorimetry and X-Ray Diffraction. *Biochimica Et Biophysica Acta* **150**, 333-& (1968).

29. Ipsen, J. H., Karlstrom, G., Mouritsen, O. G., Wennerstrom, H. & Zuckermann, M. J. Phase-Equilibria in the Phosphatidylcholine-Cholesterol System. *Biochimica Et Biophysica Acta* **905**, 162-172 (1987).

30. Yeagle, P. *The Structure of Biological Membranes* (CRC Press, Boca Raton, 1992).

31. Ladbrook.Bd, Williams, R. M. & Chapman, D. Studies on Lecithin-Cholesterol-Water Interactions by Differential Scanning Calorimetry and X-Ray Diffraction. *Biochimica Et Biophysica Acta* **150**, 333-& (1968).

32. Elmosallamy, M. A. F., Ghoneim, M. M., Killa, H. M. A. & Saber, A. L. Potentiometric Membrane Sensor for Determination of Saccharin. *Microchimica Acta* **151**, 109-113 (2005).

33. Capitan-Vallvey, F., Valencia, M. C. & Nicolas, E. A. Flow-through Spectrophotometric Sensor for the Determination of Aspartame in Low-Calorie and Dietary Products. *Analytical Sciences* **20**, 1437-1442 (2004).

34. Akiyama, H., Toko, K. & Yamafuji, K. Detection of Taste Substances Using Impedance Change of Phospholipid Langmuir-Blodgett Membrane. *Japanese Journal of Applied Physics Part 1-Regular Papers Short Notes & Review Papers* **35**, 5516-5521 (1996).

35. Oohira, K. & Toko, K. Theory of Electric Characteristics of the Lipid/PVC/DOPP Membrane and PVC/DOPP Membrane in Response to Taste Stimuli. *Biophysical Chemistry* **61**, 29-35 (1996).

36. Oohira, K., Toko, K., Akiyama, H., Yoshihara, H. & Yamafuji, K. Electric Characteristics of Hybrid Polymer Membranes Composed of 2 Lipid Species. *Journal of the Physical Society of Japan* **64**, 3554-3561 (1995).

37. Toko, K., Akiyama, H., Chishaki, K., Ezaki, S., Iyota, T. & Yamafuji, K. Detection of Taste Substances Using Impedance Change in Lipid/Polymer Membranes. *Sensors and Materials* **9**, 321-329 (1997).

38. Nikolelis, D. P., Pantoulias, S., Krull, U. J. & Zeng, J. Electrochemical Transduction of the Interactions of the Sweeteners Acesulfame-K, Saccharin and Cyclamate with Bilayer Lipid Membranes (BLMs). *Electrochimica Acta* **46**, 1025-1031 (2001).

39. Franks, F. & Royal Society of Chemistry (Great Britain). *Water: A Matrix of Life* (Royal Society of Chemistry, Cambridge, 2000).

40. Finney, J. L. The Water Molecule and Its Interactions: The Interaction between Theory, Modelling, and Experiment. *Journal of Molecular Liquids* **90**, 303-312 (2001).

CHAPTER 5: SYNTHESIS, CHARACTERIZATION AND DELIVERY OF A MODIFIED FLUORESCENT SILICATE TO 9L GLIOMA CELLS

INTRODUCTION

During the last decades, the field of drug delivery has generated a number of novel delivery techniques and numerous researchers have focused on the complex challenges. As an example, there is an increasing need to enhance delivery of therapeutic proteins to the brain for treating neurodegenerative disorders.[1,2] However, delivery of therapeutic proteins greatly depends on the penetration of proteins through the cell membrane[3] and the biggest challenge often encountered is the translocation of water soluble proteins across the hydrophobic core of the membrane. Post-translational modification of proteins is a method used by cells to transport proteins to their final destination after synthesis in vivo.[4-6]

In 1987 Kabanov et al. were successful in modifying a water soluble protein with fatty acids. The modified protein could translocate through a lipid membrane and penetrate intact cells.[7,8] The lipid modifier served the role of the anchoring moiety for the protein onto the outer lipid cell membrane. Finally, the anchored protein was uptaken by the cell through endocytosis. This approach was employed in a number of different delivery experiments. For example, fatty acid acylated peroxidase was able to cross the cell membrane of hamster ovary fibroblastic cells and reside in endocytic vesicles.[9] Fatty acid acylated antibodies were successfully used for virus suppression on a madin darby canine kidney (MDCK) cell line.[10] Inspired by the above experiments, we used a layered silicate modified with amphiphilic molecules, to deliver a fluorescent protein to 9L Glioma cells, namely Avidin Fluorescein Isothiocyanate (Avidin-FITC).

MATERIALS AND METHODS

Biotin was obtained from Sigma-Aldrich and deionized (DI) water (Barnstead Nanopure RO) was used throughout the measurements.

Fourier Transform Infra-Red (FTIR) spectroscopic measurements were performed on a Bruker Vertex 70 FTIR spectrometer equipped with a diamond crystal for attenuated total reflectance (ATR) setup.

Modification of a layered silicate

Functionalization of a layered silicate (Montmorillonite or MMT) with biotin was accomplished through a condensation reaction between the carboxyl group of biotin and the hydroxyl groups at the silicate edges. 100 mg of MMT and 370 mg biotin were added in 20 mL of ethanol with 0.5 mL hydrochloric acid (12 N). After stirring for 5 minutes at 40 ºC the solid product was washed and centrifuged multiple times with DI water until neutral pH was reached.

MMT had cation exchange capacity of 80 mequiv/100 g. The MMT silicate was modified with dodecyl-dimethylammonium surfactants (abbreviated as C12) via an ion-exchange reaction between the pristine sodium ions of the silicate and the ammonium salts. The product of the modification was a relatively hydrophobic dispersion of C12 modified silicate in water that was centrifuged at 11,000 rpm and resuspended in water multiple times to remove unexchanged C12 surfactants. The C12 modified and biotinylated MMT was abbreviated as C12MB.

Avidin-FITC attachment to the biotinylated silicate.

The high affinity between Avidin and biotin was utilized to attach Avidin-FITC conjugate on the biotin functionalized silicate. The immobilization was accomplished in a simple one-step process. An excess amount of Avidin-FITC conjugate and biotinylated silicates were added in a container. After stirring for 3

minutes, the solution was centrifuged at 11,000 rpm for 10 minutes. The resulting pellet was resuspended and centrifuged three times to remove the unbound Avidin.

9L Glioma cell line

9L Glioma cells were cultured in Dulbecco's Modified Eagle Medium (DMEM) with high glucose and supplemented with 10 % Fetal Bovine Serum (FBS) and 1 % Penicillin-Streptomycin. At 70-80 % confluence, cells were trypsinized and plated on glass coverslips. An amount of biotinylated silicates with immobilized Avidin-FITC was added and the cells were incubated at 37 ºC and a humid atmosphere with 5 % CO_2 for 24 hrs. The media was then removed and replaced with fresh media; this was repeated 3 times to ensure all silicates previously suspended in the media were removed from the flask. The coverslips were washed with phosphate-buffered saline (PBS pH 7.2), fixed in 4 % formaldehyde for 30 minutes and rinsed with PBS. The fixed cells were then stained consecutively with 2 fluorescent dyes. First the cells were stained with propidium iodide (PI), a red fluorescent dye staining primarily the nucleic acid of the nucleus. Secondly, and after the coverslips were rinsed with PBS, the fixed cells were also stained with Alexa Fluor® 568 phalloidin, a red fluorescent dye that formed a complex with F-actin. After two more rinses with PBS, the coverslips were sealed onto glass slides using Cytoseal. Slides were analyzed with confocal microscopy using a 488, 568 nm dual excitation filter on a Bio-Rad Confocal Microscope, or on an Inverted Fluoresence Microscope (Olympus IX71).

RESULTS AND DISCUSSION

Successful functionalization of the layered silicate with biotin was assessed using FTIR spectroscopy. The functionalized silicate had the characteristic absorbance-peaks of biotin's aliphatic groups even after extensive washing and

centrifugation. The FTIR Spectra of the modified and unmodified MMT silicate are plotted in Figure 5.1.

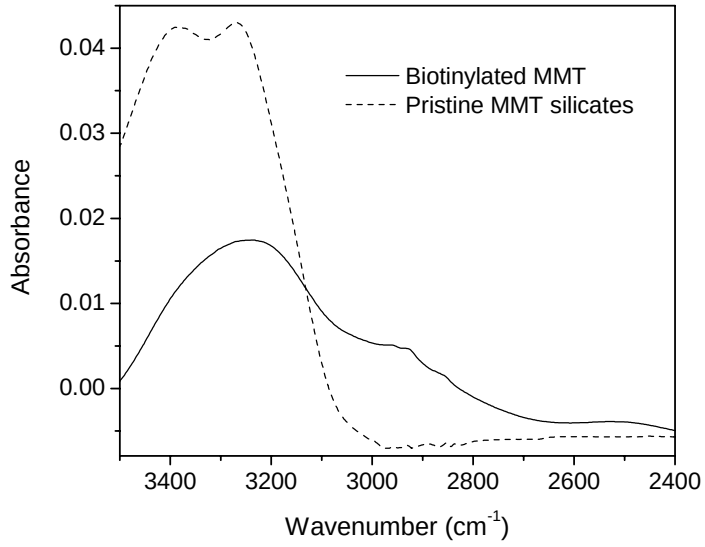

Figure 5.1: IR spectra for pristine and biotinylated MMT silicate. The characteristic absorption peaks of biotin's alkyl groups appear in the biotinylated MMT spectrum between 2980 and 2850 cm^{-1}.

9L Glioma cells were incubated in the presence of modified fluorescent montmorillonite layered silicate (C12MB-Avidin-FITC) for 24 hrs. In Figure 5.2 the images obtained indicated that fluorescent modified silicate was uptaken by the cells.

The C12MB-Avidin-FITC particles appeared to have no significant lethal effect on the cell culture. The surfactant modified silicate served the role of the delivery moiety. The hydrophobic alkyl chains were the anchoring molecules to the lipid bilayer in the same manner that Kabanov et al. used fatty acid alkyl chains for proteins. The biotin molecules were the connectors for the Avidin-FITC conjugate and the layered silicate. We suggest that the hydrophobic C12 modifiers of the silicate anchor the particles onto the cell membrane and with time endocytosis of the particle and protein occurred.

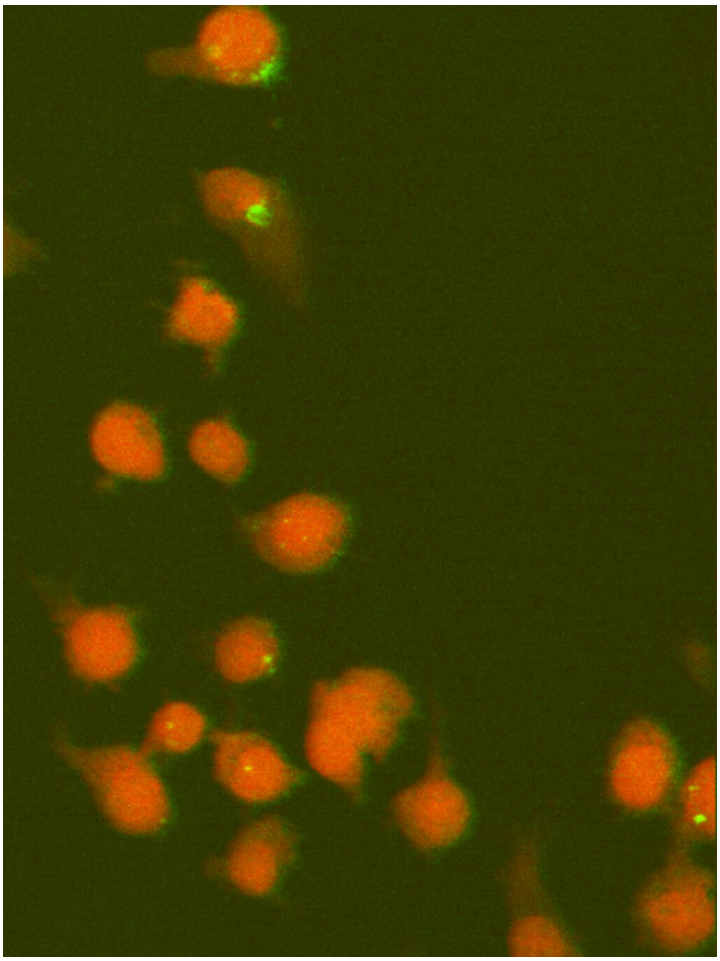

Figure 5.2: Image showing a number of fixed cells with green patches indicative of Avidin-FITC protein uptake. The cells are stained red with two fluorescent dyes, one targeting the nucleus and another, the membrane protein F-actin.

The MMT particles had a size distribution that ranged from a few hundred nm to 1 μm, and the smaller particles of the population were possibly uptaken by the cells. In this context, optimization of size distribution could improve greatly this delivery approach. As an example, lucentite silicate particles with average size around 300 nm or smaller could be another choice for this delivery approach. In the literature, the diameter of spherical particles uptaken through endocytosis ranges from tens to hundreds of nanometers with the optimal size at 50 nm.[11]

To determine the location of the green fluorescent particles, we utilized two red fluorescent staining molecules. Propidium Iodide (PI) stained the cell nucleus and Alexa Fluor®-Phalloidin formed a complex with F-actin. F-actin is a protein located on the cell membrane and serves as the backbone of the lipid bilayer as well as the regulator of the cell shape.[12] The confocal images revealed a distribution of particles onto and into cells. The smallest particles were located under the membrane and inside the cell, when for larger particles it was not conclusive if they were fully uptaken or residing on the surface of the cells (Figures 5.2 and 5.3).

As a control, 9L Glioma cells were incubated in the presence of MMT silicate particles with no C12 surfactant modification. The result of this experiment was different from when the silicate was modified. The presence of the unmodified silicate had resulted either in the death of the cells or the detachment of the cells from the glass surface. We were not able to distinguish between the above two cases because 24 hrs after the incubation, no cells could be seen anchored on the bottom of the incubation well and only a suspension of agglomerates could be seen (possibly cells and silicate particles). The layered silicate is inherently negatively charged and sodium cations exist on the surface balancing the charge. This negative surface charge of the silicate could be the reason that the anchorage-dependent 9L Glioma cells attach to the silicate; the same property is used by cells to attach on the glass coverslip surface.[13]

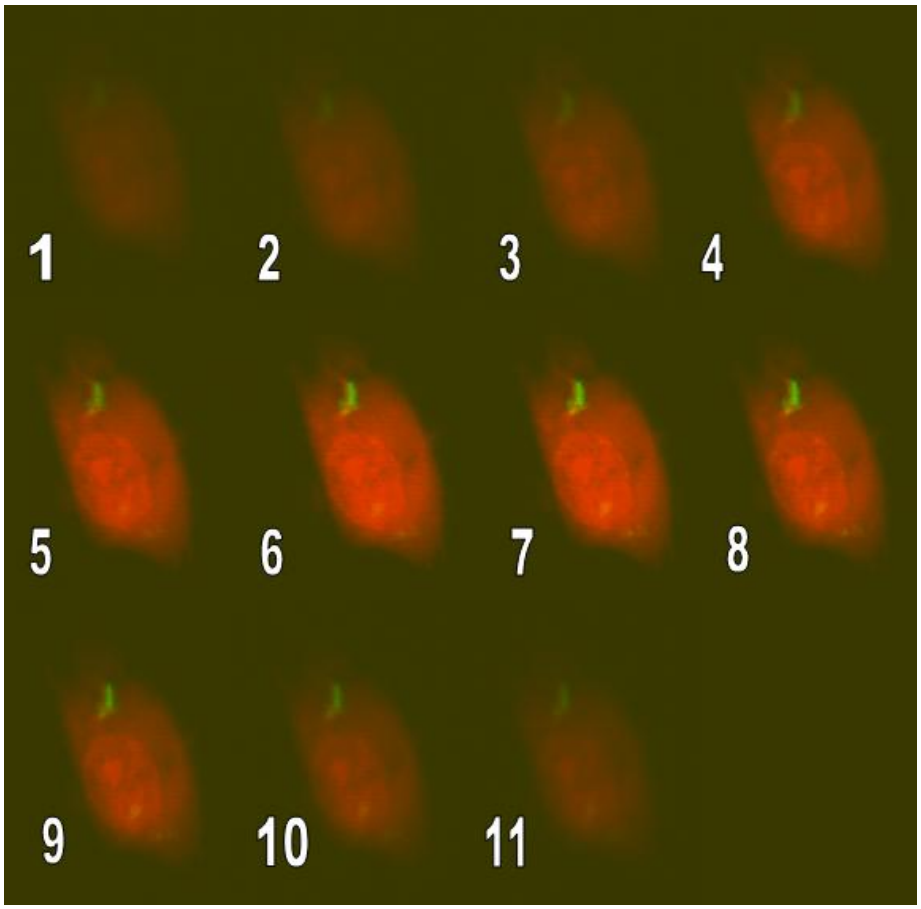

Figure 5.3: Eleven consecutive confocal images showing a single cell (nucleus and cell membrane stained red) with a clear green particle. The location of the green particle indicated that the particle was located under the cell membrane and endocytosis had occurred.

In light of the above encouraging results for the uptake of fluorescent modified silicate particles by 9L Glioma cells, we have decided that a flow cytometry experiment was needed to evaluate the extent of transfection. In the process of obtaining these data, we tested a blank experiment for possible uptake of the fluorescent protein (Avidin-FITC) alone by the 9L Glioma cells. The conditions of the control experiment were identical with the above experiment performed with 9L Glioma cells and modified silicate. The cells were incubated for 24 hours in the

presence of the fluorescent protein alone and fluorescence microscopy images were obtained.

By using an Inverted Fluorescence Microscope we have obtained images suggesting the transfection of a number of cells with the fluorescent protein alone. The images obtained can be seen in Figure 5.4.

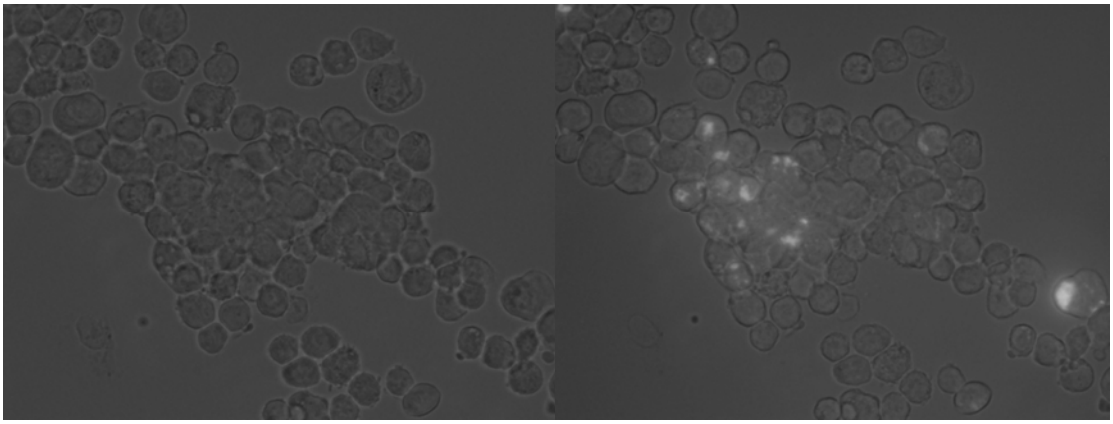

Figure 5.4: These two images were taken with an inverted fluorescence microscope. The cells were incubated 24 hrs with Avidin-FITC and washed multiple times with PBS. The left picture is the bright field image. The right image is the same area with a Hg lamp on, along with a bright field lamp. The fluorescent areas on the cells can be seen clearly.

CONCLUSIONS

The effect of the protein uptake from the cells was initially not examined and it was assumed that the transfection of the cells by the fluorescent protein was due to the uptake of a modified fluorescent silicate. Furthermore, no reference was found for Avidin uptake by the cell line in literature. However, the results of the above control experiment raised doubts on the above presented data using a modified silicate.

The data obtained with the control experiment did not dismiss the presented results with the modified silicate, since the protein in that case was immobilized on the

silicate. Nevertheless, the control experiment left open the possibility of the protein being detached from the silicate and being uptaken by the cells. That could be possible if a hydration reaction occurred between the carboxyl group of biotin and the hydroxyl group of the silicate. However, this reaction, in principle, is very slow in the environment that the experiments were realized (pH 7.2). Furthermore, the results from Figure 5.4 could also signify that the uptake of the modified particles, if successful, was due to the protein uptake by the cells and not the other way around.

The above methodology, if proven successful, could be utilized for delivering various therapeutic proteins to cell cultures in vitro and potentially in vivo applications. As an example, the protein to be delivered could be attached to the delivery moiety (the modified layered silicate) via a different chemistry approach that would include a sulfur-sulfur bond. This bond is known to be easily cleaved by intracellular reductase (i.e. protein disulfide isomerase).[14] This sulfur-sulfur dissociation delivery approach was successful for the delivery of a biotinylated DNA transferin conjugate by Sato et al.[15]

REFERENCES

1. Gozes, I. Neuroprotective Peptide Drug Delivery and Development: Potential New Therapeutics. *Trends in Neurosciences* **24**, 700-705 (2001).

2. Kabanov, A. V. & Batrakova, E. V. New Technologies for Drug Delivery across the Blood Brain Barrier. *Current Pharmaceutical Design* **10**, 1355-1363 (2004).

3. Mindell, J. A. Swimming through the Hydrophobic Sea: New Insights in Protein Translocation. *Proceedings of the National Academy of Sciences of the United States of America* **95**, 4081-4083 (1998).

4. Magee, A. I. Lipid Modification of Proteins and Its Relevance to Protein Targeting. *Journal of Cell Science* **97**, 581-584 (1990).

5. Chow, M., Der, C. J. & Buss, J. E. *Structure and Biological Effects of Lipid Modifications on Proteins* (1992).

6. Resh, M. D. Fatty Acylation of Proteins: New Insights into Membrane Targeting of Myristoylated and Palmitoylated Proteins. *Biochimica Et Biophysica Acta-Molecular Cell Research* **1451**, 1-16 (1999).

7. Kabanov, A. V., Levashov, A. V. & Martinek, K. Transformation of Water-Soluble Enzymes into Membrane Active Form by Chemical Modification. *Annals of the New York Academy of Sciences* **501**, 63-66 (1987).

8. Kabanov, A. V., Levashov, A. V. & Alakhov, V. Y. Lipid Modification of Proteins and Their Membrane-Transport. *Protein Engineering* **3**, 39-42 (1989).

9. Slepnev, V. I., Phalente, L., Labrousse, H., Meliknubarov, N. S., Mayau, V., Goud, B., Buttin, G. & Kabanov, A. V. Fatty-Acid Acylated Peroxidase as a Model for the Study of Interactions of Hydrophobically-Modified Proteins with Mammalian-Cells. *Bioconjugate Chemistry* **6**, 608-615 (1995).

10. Kabanov, A. V., Ovcharenko, A. V., Melikhubarov, N. S., Bannikov, A. I., Alakhov, V. Y., Kiselev, V. I., Sveshnikov, P. G., Kiselev, O. I., Levashov, A. V. & Severin, E. S. Fatty-Acid Acylated Antibodies against Virus Suppress Its Reproduction in Cells. *Febs Letters* **250**, 238-240 (1989).

11. Gao, H. J., Shi, W. D. & Freund, L. B. Mechanics of Receptor-Mediated Endocytosis. *Proceedings of the National Academy of Sciences of the United States of America* **102**, 9469-9474 (2005).

12. Rivero, F., Koppel, B., Peracino, B., Bozzaro, S., Siegert, F., Weijer, C. J., Schleicher, M., Albrecht, R. & Noegel, A. A. The Role of the Cortical Cytoskeleton: F-Actin Crosslinking Proteins Protect against Osmotic Stress,

Ensure Cell Size, Cell Shape and Motility, and Contribute to Phagocytosis and Development. *Journal of Cell Science* **109**, 2679-2691 (1996).

13. Freshney, R. I. *Culture of Animal Cells: A Manual of Basic Technique* (Wiley-Liss, Hoboken, N.J., 2005).

14. Kuan, C. T. & Pastan, I. Recombinant Immunotoxin Containing a Disulfide-Stabilized Fv Directed at Erbb2 That Does Not Require Proteolytic Activation. *Biochemistry* **35**, 2872-2877 (1996).

15. Sato, Y., Yamauchi, N., Takahashi, M., Sasaki, K., Fukaura, J., Neda, H., Fujii, S., Hirayama, M., Itoh, Y., Koshita, Y., Kogawa, K., Kato, J., Sakamaki, S. & Niitsu, Y. In Vivo Gene Delivery to Tumor Cells by Transferrin-Streptavidin-DNA Conjugate. *Faseb Journal* **14**, 2108-2118 (2000).

CHAPTER 6: SYNTHESIS, CHARACTERIZATION AND APPLICATIONS OF NANOHYBRIDS WITH HIGH LOADINGS OF GRAMICIDIN

INTRODUCTION

Gramicidin is a polypeptide antibiotic from *Bacillus Brevis* with a molecular weight of 1880 Dalton. Gramicidin's unique properties lie in the primary structure of the protein which is: HCO–L-Val–Gly–L-Ala–D-Leu–L-Ala–D-Val–L-Val–D-Val–L-Try–D-Leu–L-Try–D-Leu–L-Try–D-Leu–L-Try–$NHCH_2CH_2OH$.[1] Due to the alternating L- and D- amino acid residues, the polypeptide forms β-type helices.[1] In these β-helices, the carbonyl moieties of the residues are located in the interior of the helix.[2] The above unique property results in a helical molecule with a hydrophilic core and a hydrophobic outer shell as shown in Figure 6.1.

Gramicidin is known to form membrane-spanning ion channels in lipid bilayers that are selective to alkali metals and protons.[3] The property of channeling monovalent cations through a lipid bilayer is the key property for gramicidin's antibiotic action. The protein can be integrated in the lipid bilayer and form ion channels that disrupt the ionic balance of a cell. In literature, various applications have been realized using gramicidin's ability to form ion channels selective to alkali metals.[3-5]

Utilizing the concept of a biomimetic membrane presented in Chapter 4, we have integrated gramicidin into a layered host (fluoromica) to form a nanohybrid of an inorganic host and a protein. This resulted to multibilayered particles with high loadings of gramicidin that could form membranes according to the same process described in Chapter 4. In addition, the synthesized nanohybrid particles were also

examined as delivery vehicles of gramicidin to *E. coli* bacteria and the protein's antibiotic ability was evaluated.

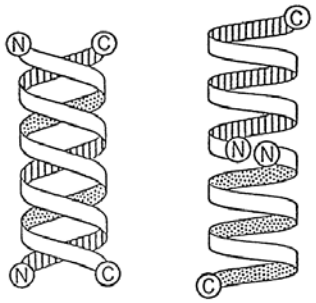

Figure 6.1: Schematic diagram of gramicidin showing the polypeptide backbone as double helical [left] and as a helical dimer [right].[6]

MATERIALS AND MATERIALS

A synthetic layered silicate, Somasif ME-100 (Na+-Fluoromica or FM), with a cation exchange capacity (CEC) of 120 mequiv/100 g was obtained from CO-OP Chemical LTD. Dodecyl-dimethylammonium bromide was obtained from Sigma-Aldrich and deionized (DI) water was used throughout the measurements (Barnstead Nanopure RO).

Fourier Transform Infra-Red (FTIR) spectroscopic measurements were performed in a Mattson Galaxy 2020 IR spectrometer. The samples were prepared by mixing and grinding with potassium bromide in a mortar and pestle and pressed into a pellet using a hydraulic press. The FTIR spectra were obtained under a nitrogen flow in the sample chamber.

Powder X-Ray Diffraction (PXRD) spectra were collected on a Scintag Inc θ-θ diffractometer using CuK_{α} source radiation and a germanium detector.

Nanohybrids synthesis

In a vial with 4 mL dodecyl-dimethylammonium bromide (C12) of 15.5 mM concentration (critical micelle concentration 15 mM), 13 mg of gramicidin were

introduced under stirring. Gramicidin due to its hydrophobic character did not dissolve in water and was incorporated into the micelles. After stirring for 5 minutes, 2.5 mL of a 2 w.t.% Na^+ Fluoromica aqueous solution was added and the mixture was left on a shaker table for 15 minutes. An ion exchange reaction occurred with the ammonium groups of the surfactants taking the place of Na^+ ions on the surface of the silicate. Flocculation was immediately observed rendering the layered silicate slightly hydrophobic due to their modification with the amphiphilic surfactants.

The product of the reaction was centrifuged at 12,000 rpm for 10 minutes and separated from any unexchanged C12 surfactants. The gramicidin-containing modified layered silicate (nanohybrids) were washed multiple times with water and centrifuged. To evaluate the amount of protein immobilized on the nanohybrid, we quantified the absorbance peak at 280 nm of the washout solutions. The majority of proteins absorb around the above wavelength due to the presence of aromatic moieties in three amino acids, namely tryptophan, tyrosine and phenylalanine. Gramicidin also such residues and absorbs at 280nm wavelength ($\varepsilon \sim 11000\ M^{-1}cm^{-1}$);[7] by calculating the amount of gramicidin lost in the washout solutions, we were able to estimate the amount of gramicidin integrated into the layered silicate.

RESULTS AND DISCUSSION

Integration of gramicidin on a layered silicate (fluoromica in this case) was realized through an ion exchange reaction between cationic surfactant micelles and the layered silicate. The micelles were formed in a solution with concentration higher of the critical micelle concentration (CMC) and gramicidin was then added to the micelle solution. Due to the highly hydrophobic character of the molecule, gramicidin was incorporated into the micelles. The synthetic process is summarized in Figure 6.2 and 6.3.

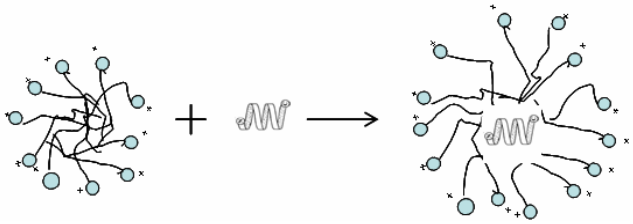

Figure 6.2: Integration of gramicidin into dodecyldimethylammonium surfactant micelles. The circles signify the hydrophilic group (ammonium) and the lines the hydrophobic alkyl chains of the surfactant.

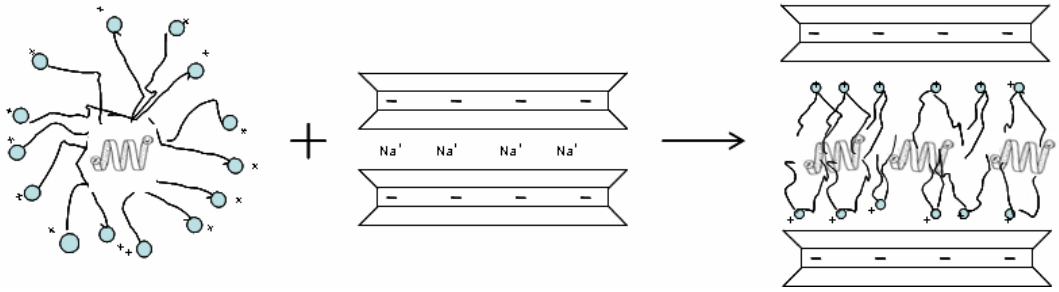

Figure 6.3: Ion exchange reaction between the gramicidin-containing micelles and the layered silicate. A sketch of the gramicidin-nanohybrid as the product is also shown.

Successful synthesis of gramicidin-nanohybrids was verified through FTIR spectroscopy. Proteins have multiple characteristic absorption peaks in the IR region that rise from the existence of amide bonds between aminoacids. The amide A (3225-3280 cm^{-1}) and amide II (1510-1580 cm^{-1}) absorption peaks, as they are referred in literature,[8] were identified in the IR spectra of the gramicidin nanohybrid (see Figure 6.4). We were unable to distinguish amide I peak (around 1650 cm^{-1}) since the peak coincided with the absorption peak of the ammonium group of the C12 modifier. However, the intensity of the peak when compared to the 1480 cm^{-1} peak (signature peak for the alkyl groups of the modifier) increased in the spectrum of the nanohybrid indicating that the amide I peak was contributing to that absorption.

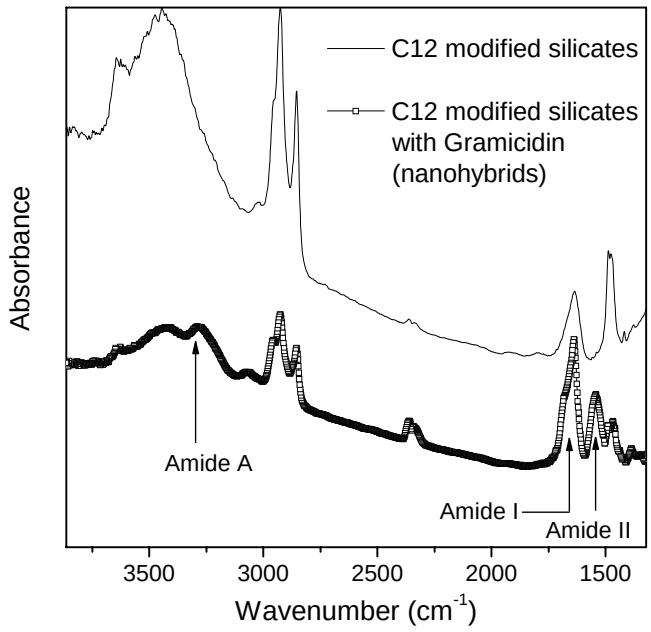

Figure 6.4: IR spectra of C12 modified fluoromica and gramicidin nanohybrid (nanohybrid: C12 modified fluoromica containing gramicidin).

The integration of gramicidin on a layered silicate with the above method resulted in high loading of protein on silicate (20 mg of protein per 100 mg of unmodified silicate).

The high loading of gramicidin into the interlayer gallery of the layered silicate had also an effect on the d-spacing of the gallery. The above phenomenon was verified through PXRD. In Figure 6.5 the PXRD spectrum of a modified silicate with C12 surfactants is plotted together with the spectrum of the same material with gramicidin integrated between the galleries (see Figure 6.3).

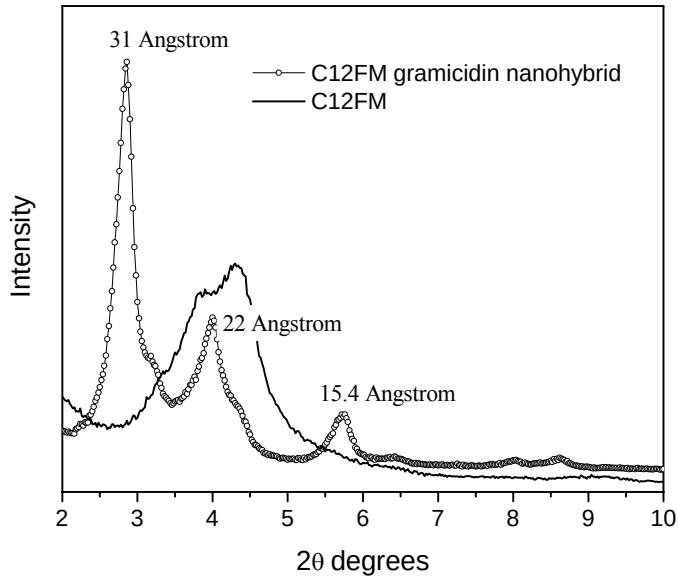

Figure 6.5: PXRD spectra of C12 modified layered silicate with and without gramicidin integration in the interlayer galleries. The 31 Å peak appears in the gramicidin nanohybrid spectrum. Protein integration resulted to the swelling of the interlayer gallery. The 22 Å peak can still be seen, probably due to the co-existence of layered silicate modified with C12 surfactants only.

Formation of ion channels in a nanohybrid membrane

The synthesized gramicidin-containing nanohybrid was examined for two possible applications, which are described below. Taking advantage of the channel forming property of gramicidin, a setup was realized to test the nanohybrid membrane as an ion selective membrane. The membrane was cast on a paper mesh and separated two aqueous solutions (see Figure 6.6); the two solutions had the same amounts of two different salts, namely $CaCl_2$ and NaCl. Since gramicidin is selective to monovalent cations we anticipated that Na^+ could cross the membrane and establish a small ΔV between the two sides of the membrane. Two Ag/AgCl reference electrodes and a

voltmeter were utilized to measure possible potential differences between the two sides of the membrane. The above phenomenon is the basic principle behind the technology used in manufacturing ion selective electrodes.[9] However, from the above experiment we were unable to document reproducible potential differences resulting from the integration of gramicidin in the nanohybrid membrane.

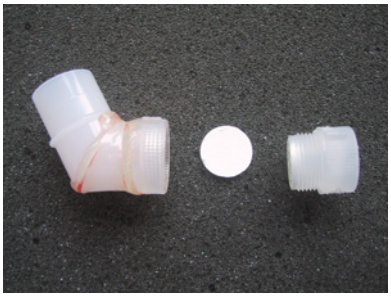

Figure 6.6: A picture of the setup used for the ion permeability experiment. The tube was filled with a NaCl solution and later inserted into a beaker with a $CaCl_2$ solution. The paper mesh with the cast nanohybrid membrane was screwed onto the tube.

Antibiotic action of gramicidin.

Gramicidin has antibiotic properties and, in order to function, the protein needs first to be dissolved in an aqueous media for the targeted host to uptake it. However, the solubility of gramicidin in water is very small. To resolve this, we examined the possibility of suspending the protein, rather than dissolving it, into an aqueous solution using the synthesized nanohybrids.

To examine this, *E. coli* bacteria (ATCC 12407) were exposed to gramicidin and gramicidin nanohybrids. Initially, we utilized Luria-Bertani (LB) Agar plates with integrated gramicidin and gramicidin nanohybrids in the gel, yet from multiple platings, we saw no effect on the number of *E. coli* colonies (see Figure 6.7) in either case. We ascribed the lack of gramicidin's antibiotic effect to the solid substrate used

(LB Agar gels) that prevented diffusion of species. In an effort to improve the availability of gramicidin, we have repeated the experiments in a liquid media.

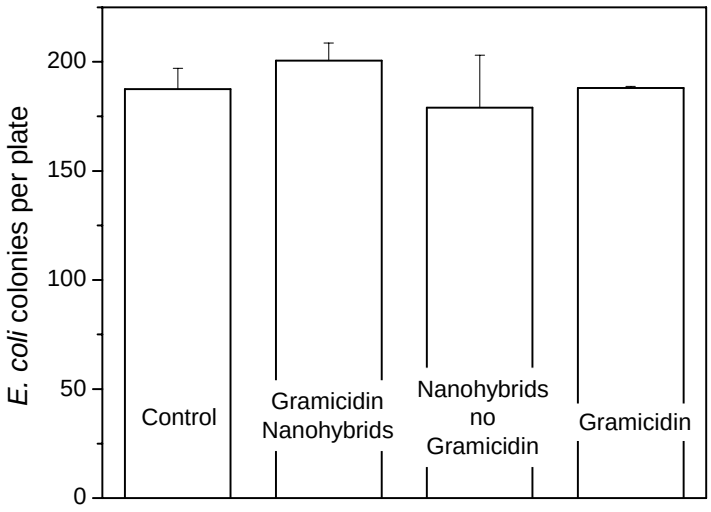

Figure 6.7: Number of colonies measured after 24 hrs on LB Agar plates inoculated with *E. coli* bacteria. The experiment with nanohybrids is shown along with 3 control experiments. "Control" column is a blank LB Agar plate, "gramicidin" is an LB Agar plate with the same amount of gramicidin as in the nanohybrid experiment, and the "nanohybrid with no gramicidin" column has the same amount of the modified layered silicate (C12FM) but no gramicidin.

E. coli were used to inoculate an LB broth where gramicidin and gramicidin nanohybrids were previously added. The growth of the bacteria was monitored by measuring the optical density of the culture media. As has been well documented, bacteria scatter light in the same way as particles scatter light, and the extent of the scattering is proportional to the population of bacteria. In a UV/Vis spectrophotometer, light scattering is registered as absorption (or optical density, OD), so the OD of the culture media is a proportional measure of bacteria population.

From Figure 6.8 it is evident that addition of gramicidin to the media had no effect on the growth of the bacteria, while the gramicidin nanohybrid had a significant antibiotic effect. The data plotted in Figure 6.8 shows that all cultures tested were into the log phase after 5-6 hours, something that was not observed with the gramicidin nanohybrid culture. Even though nanohybrids without gramicidin (C12FM) had a small effect on the bacteria population, this cannot be accounted for the large effect registered in the case of gramicidin nanohybrids.

The presented delivery approach of gramicidin to *E. coli* bacteria was based on integrating the hydrophobic gramicidin molecule into the modified silicate. The nanohybrid particles were suspended in an aqueous solution and through the modifiers' alkyl chains anchored the particles onto the lipid bilayer in a similar mechanism as described in Chapter 5.[10,11] Since gramicidin's antibiotic action rises from the formation of ion channels in the lipid bilayers of bacteria, it is possible that the proximity of nanohybrid particles to bacteria enhanced the delivery and the antibiotic action of gramicidin.

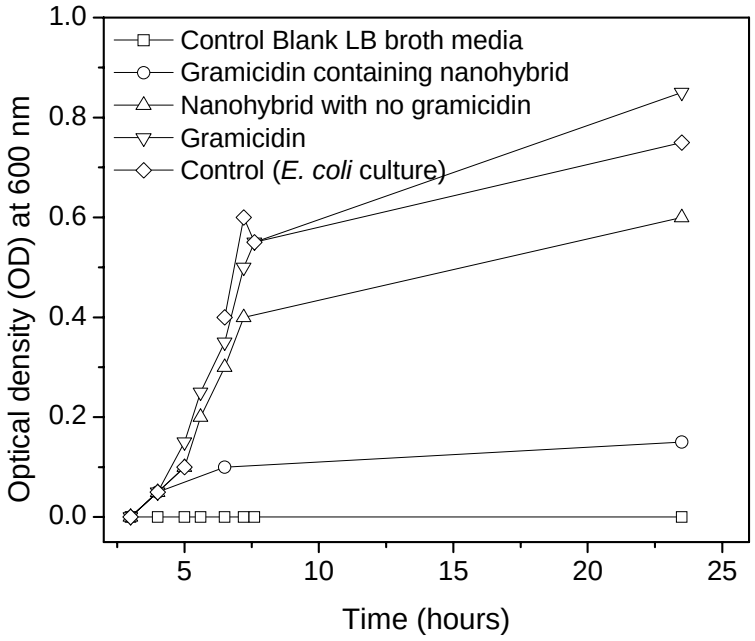

Figure 6.8: Optical density of *E. coli* culture media with time and various additions. Where applicable, the cultures had the same amount of gramicidin (0.05 mg/mL) and silicate.

REFERENCES

1. Urry, D. W. Gramicidin-A Transmembrane Channel - Proposed Pi(L,D) Helix. *Proceedings of the National Academy of Sciences of the United States of America* **68**, 672-& (1971).

2. Bransburg-Zabary, S., Kessel, A., Gutman, M. & Ben-Tal, N. Stability of an Ion Channel in Lipid Bilayers: Implicit Solvent Model Calculations with Gramicidin. *Biochemistry* **41**, 6946-6954 (2002).

3. Vallejo, A. E. & Gervasi, C. A. Impedance Analysis of Ion Transport through Gramicidin Channels in Supported Lipid Bilayers. *Bioelectrochemistry* **57**, 1-7 (2002).

4. Nikolelis, D. P., Siontorou, C. G., Krull, U. J. & Katrivanos, P. L. Ammonium Ion Minisensors from Self-Assembled Bilayer Lipid Membranes Using Gramicidin as an Ionophore. Modulation of Ammonium Selectivity by Platelet-Activating Factor. *Analytical Chemistry* **68**, 1735-1741 (1996).

5. Zein, M. & Winter, R. Effect of Temperature, Pressure and Lipid Acyl Chain Length on the Structure and Phase Behaviour of Phospholipid-Gramicidin Bilayers. *Physical Chemistry Chemical Physics* **2**, 4545-4551 (2000).

6. Wallace, B. A. Recent Advances in the High Resolution Structures of Bacterial Channels: Gramicidin A. *Journal of Structural Biology* **121**, 123-141 (1998).

7. Tombs, M. P., Souter, F. & Maclagan, N. F. Spectrophotometric Determination of Protein at 210 M-Mu. *Biochemical Journal* **73**, 167-171 (1959).

8. Ulrich, W. P. & Vogel, H. Polarization-Modulated FTIR Spectroscopy of Lipid/Gramicidin Monolayers at the Water Interface. *Biophysical Journal* **76**, 1639-1647 (1999).

9. Zýka, J. Instrumentation in Analytical Chemistry (Horwood, New York, 1991).

10. Kabanov, A. V., Levashov, A. V. & Alakhov, V. Y. Lipid Modification of Proteins and Their Membrane-Transport. *Protein Engineering* **3**, 39-42 (1989).

11. Kabanov, A. V., Levashov, A. V. & Martinek, K. Transformation of Water-Soluble Enzymes into Membrane Active Form by Chemical Modification. *Annals of the New York Academy of Sciences* **501**, 63-66 (1987).